



HAL
open science

Tracing the ancestry of modern bread wheats

Caroline Pont, Thibault Leroy, Michael Seidel, Alessandro Tondelli, Wandrille Duchemin, David Armisen, Daniel Lang, Daniela Bustos-Korts, Nadia Goué, François Balfourier, et al.

► **To cite this version:**

Caroline Pont, Thibault Leroy, Michael Seidel, Alessandro Tondelli, Wandrille Duchemin, et al.. Tracing the ancestry of modern bread wheats. *Nature Genetics*, 2019, 51 (5), pp.905-911. 10.1038/s41588-019-0393-z . hal-02154676

HAL Id: hal-02154676

<https://hal.science/hal-02154676>

Submitted on 22 Nov 2021

HAL is a multi-disciplinary open access archive for the deposit and dissemination of scientific research documents, whether they are published or not. The documents may come from teaching and research institutions in France or abroad, or from public or private research centers.

L'archive ouverte pluridisciplinaire **HAL**, est destinée au dépôt et à la diffusion de documents scientifiques de niveau recherche, publiés ou non, émanant des établissements d'enseignement et de recherche français ou étrangers, des laboratoires publics ou privés.



University of Dundee

Tracing the ancestry of modern bread wheats

Pont, Caroline; Leroy, Thibault; Seidel, Michael; Tondelli, Alessandro; Duchemin, Wandrille

Published in:
Nature Genetics

DOI:
[10.1038/s41588-019-0393-z](https://doi.org/10.1038/s41588-019-0393-z)

Publication date:
2019

Document Version
Peer reviewed version

[Link to publication in Discovery Research Portal](#)

Citation for published version (APA):

, Pont, C., Leroy, T., Seidel, M., Tondelli, A., Duchemin, W., Armisen, D., Lang, D., Bustos-Korts, D., Goué, N., Balfourier, F., Molnár-Láng, M., Lage, J., Kilian, B., Özkan, H., Waite, D., Dyer, S., Letellier, T., Alaux, M., ... Salse, J. (2019). Tracing the ancestry of modern bread wheats. *Nature Genetics*, 51(5), 905-911. <https://doi.org/10.1038/s41588-019-0393-z>

General rights

Copyright and moral rights for the publications made accessible in Discovery Research Portal are retained by the authors and/or other copyright owners and it is a condition of accessing publications that users recognise and abide by the legal requirements associated with these rights.

- Users may download and print one copy of any publication from Discovery Research Portal for the purpose of private study or research.
- You may not further distribute the material or use it for any profit-making activity or commercial gain.
- You may freely distribute the URL identifying the publication in the public portal.

Take down policy

If you believe that this document breaches copyright please contact us providing details, and we will remove access to the work immediately and investigate your claim.

Tracing the ancestry of modern bread wheats.

Caroline Pont^{1*}, Thibault Leroy^{2,3*}, Michael Seidel^{4*}, Alessandro Tondelli^{5*}, Wandrille Duchemin^{1*}, David Armisen^{1*}, Daniel Lang^{4*}, Daniela Bustos-Korts^{6*}, Nadia Goué¹, François Balfourier¹, Marta Molnar-Lang⁷, Jacob Lage⁸, Benjamin Kilian^{9,10}, Hakan Özkan¹¹, Darren Waite¹², Sarah Dyer¹³, Thomas Letellier¹⁴, Michael Alaux¹⁴, WHEALBI consortium¹⁵, IWGSC¹⁶, Joanne Russell¹⁷, Beat Keller¹⁸, Fred van Eeuwijk⁶, Manuel Spannagl⁴, Klaus F.X. Mayer^{4,19}, Robbie Waugh^{17,20,21}, Nils Stein¹⁰, Luigi Cattiveli^{5§}, Georg Haberer^{4§}, Gilles Charmet^{1§}, Jerome Salse^{1§†}

1. INRA-Université Clermont-Auvergne, UMR 1095 GDEC, 5 Chemin de Beaulieu, 63000 Clermont-Ferrand, France.
2. INRA-Université de Bordeaux, UMR 1202 BIOGECO, 69 Route d'Arcachon, 33612 Cestas, France.
3. ISEM, Université de Montpellier, CNRS, IRD, EPHE, Place Eugène Bataillon, 34095 Montpellier, France
4. PGSB, Helmholtz Center Munich, Ingolstädter Landstraße 1 · D-85764 Neuherberg, Germany.
5. Council for Agricultural Research and Economics (CREA), Research Centre for Genomics and Bioinformatics, via S. Protaso, 302. I -29017 Fiorenzuola d'Arda PC, Italy.
6. Wageningen University, Droevendaalsesteeg 4, 6708 PB, Wageningen, Netherlands.
7. Agricultural Institute, Centre for Agricultural Research, Hungarian Academy of Sciences, Martonvásár, Brunszvik u. 2, 2462, Hungary.
8. KWS UK Ltd, 56 Church St, Thriplow, Royston SG8 7RE, United Kingdom.
9. Global Crop Diversity Trust, 53113 Bonn, Germany.
10. Leibniz Institute of Plant Genetics and Crop Plant Research (IPK), Corrensstraße 3, 06466 Gatersleben, Germany.
11. University of Çukurova, Faculty of Agriculture, Department of Field Crops, 01330 Adana, Turkey.
12. Earlham Institute, Norwich Research Park, Norwich NR4 7UZ, United Kingdom.
13. NIAB, Huntingdon Road, Cambridge CB3 0LE, United Kingdom.
14. URGI, INRA, Université Paris-Saclay, 78026, Versailles, France.
15. WHEAt and barley Legacy for Breeding Improvement (WHEALBI) consortium, <https://www.whealbi.eu/project/partners/>. *Coordinator*, Gilles Charmet (gilles.charmet@inra.fr), INRA UMR 1095 GDEC, France.
16. International Wheat Genome Sequencing Consortium (IWGSC), <http://www.wheatgenome.org>. *Executive Director*, Kellye Eversole (eversole@eversoleassociates.com), 2841 NE Marywood Ct Lee's Summit, MO 64086, United States.
17. The James Hutton Institute, Invergowrie Dundee DD2 5DA, Scotland.
18. Department of Plant and Microbial Biology, University of Zurich, Zollikerstrasse 107, 8008 Zürich, Switzerland.
19. School of Life Sciences, Technical University Munich, Weihenstephan, Germany.
20. The University of Dundee, Division of Plant Sciences, School of Life Sciences, Dundee, DD1 4HN, Scotland.
21. School of Agriculture, Food and Wine, University of Adelaide, Adelaide, South Australia, Australia.

* These authors contributed equally to this work.

§ These authors jointly supervised this work.

† Corresponding author.

ABSTRACT - For more than 10,000 years, the selection of plant and animal traits that are better tailored for human use has shaped the development of civilizations. During this period, bread wheat (*Triticum aestivum*) emerged as one of the world's most important crops. **We used exome sequencing of a world-wide panel of almost 500 genotypes selected from across the geographical range of the wheat species complex to explore how 10,000 years of hybridization, selection, adaptation and plant breeding shaped the genetic makeup of modern bread wheats. We observed considerable genetic variations at the genic, chromosomal and subgenomic levels deciphering the likely origins of modern day wheats, the consequences of range expansion and allelic variants selected since its domestication.** Our data supports a reconciled model of wheat evolution and provides novel avenues for future breeding improvement.

INTRODUCTION - Bread wheat has an allo-hexaploid genome consisting of three closely related subgenomes (AABBDD). It is proposed to have originated from two polyploidization events, (i) a tetraploidization some 0.5 million years before present (ybp) from the hybridization between wild *Triticum urartu* Tumanian ex Gandilvan (AA) and an undiscovered species of the *Aegilops speltoides* Tausch lineage (BB), followed by (ii) a hexaploidization some 10,000 ybp as a result of hybridization between a descendant of this original tetraploid hybrid (AABB) and the wild diploid *Aegilops tauschii* (Coss) (DD)¹. Archaeobotanical evidence suggests that the

resulting allo-hexaploid wheats were domesticated in the Fertile Crescent, a region extending from Israel, Jordan, Lebanon, Syria to South-East Turkey, to northern Iraq and western Iran²⁻⁵. Modern cultivated bread wheats are therefore the product of at least 10,000 years of human selection during domestication and cultivation (improvement and breeding). Today they comprise high-yielding varieties adapted to a wide range of environments ranging from low humidity regions in Nigeria, Australia, India, and Egypt to high humidity regions like South America⁶.

RESULTS - In order to explore the origins and patterns of genetic diversity that exist within the currently accessible wheat gene pool, we assembled a worldwide panel of 487 genotypes that included wild diploid and tetraploid relatives, domesticated tetraploid and hexaploid landraces, old cultivars and modern elite cultivars (Table S1). Mapping exome capture sequence data⁷ from these lines onto the ‘Chinese Spring’ reference genome sequence (IWGSC⁸) revealed 620,158 genetic variants (including 595,939 SNPs and InDels between hexaploid genotypes) distributed across 41,032 physically ordered wheat genes (Table S2). Equivalent sequence coverage at the chromosome and homoeologous gene/region levels (medians within one standard deviation) excluded bias in the detection and calling of structural variants (Figure S1). Furthermore, correlation between gene and structural variant distribution ($r > 82\%$) across the three subgenomes, expected from exome capture experiment, supports the lack of bias in genic variants detection at the chromosome level with a visible gradient from distal gene-rich regions to pericentromeric gene-poor regions (Figure S2). Both individual subgenomes (with a B>A>>D gradient) and chromosome compartments (with a telomere>core>>centromere gradient) exhibited differences in their content of structural variation (Figure S3). In summary, our variant dataset provides a comprehensive overview of wheat genomic diversity at various scales (gene, region, chromosome and genome), and represent a rich source of genetic information for exploitation by both the academic and agricultural research communities (Figure 1, circles #1 to #3).

Phylogenetic and principle component analyses revealed three major factors driving the partitioning of diversity within our panel (Figure 2): vernalization requirement (winter vs spring), historical groups (groups I to IV, oldest to newest: old landraces to modern elite lines) and geographical origin (Europe, Asia, Oceania, Africa and America), Figure 2A and Figure S4. Among the 11 major tree clades chosen on the criteria of size, representativeness and statistical support, permutation tests for the conservation of clade monophyly significantly confirmed a strong grouping for all three dimensions ($p\text{-value} < 10e-6$). However, the deep structure of the phylogeny is centered around continental difference, and subsequently more recent shifts in growth habit traits (such as vernalization requirement) resulting from intense selection for yield in modern wheat breeding practices. Superimposing both country and continent of origin onto the phylogenetic clusters suggests that the observed genetic diversity is mainly structured along an east-west axis consistent with established routes of human migration out of the Fertile Crescent. Two paths to Western Europe follow an inland (*via* Anatolia and the Balkans to Central Europe) and coastal (*via* Egypt to the Maghreb and Iberian Peninsula) route, complemented by two additional paths north-east and along the Inner Asian Mountain Corridor, followed by further colonization events in American, Oceanian, African territories (Figure 2B, Figure S5)⁹.

We next explored selection footprints resulting from domestication (comparing wild and domesticated wheats) and breeding (comparing historical bread wheat groups I to IV) using a sliding-window (as opposed to gene-centric) approach to deciphering local reduction in diversity and taking into account the geographical structuring of the wheat panel (Figure 1 circles #4 and #5). For the detection of domestication signals, we computed the nucleotide diversity per site (Tajima’s π) over non-overlapping 1 Mb sliding windows for wild diploid (*T. urartu*, *A. speltooides*, *A. tauschii*), wild tetraploid (*T. dicoccoides*) and the domesticated hexaploid (*T. aestivum*) wheats from Asia, where the previous diploid and tetraploid progenitors in our panel originated. Contrasts between wild wheat ancestors and hexaploid landraces support considerable heterogeneity in the reduction of diversity (RoD) during the domestication process along the wheat genome (Figure S6). Strongly affected genomic regions (1,221), showing a loss of at least four-fifths of the diversity (RoD > 0.8, red dots in Fig 1 circle #5), cover 9.2% of the wheat genome (1.2 Gb). Known domestication genes conferring brittle rachis (*Brt*), tenacious glume (*Tg*), homoeologous pairing (*Ph*) and non-free-threshing character (*Q*) were identified within or in close (≤ 5 Mb distance) proximity to these regions. Interestingly, known domestication genes only account for a minority of the observed peaks, suggesting that further domestication genes still need to be discovered (Table S3)¹⁰⁻¹¹, as reported for other grass species such as maize¹².

To unravel regions targeted by breeders during the last centuries of wheat improvement, we compared the RoD statistics in the European panel within historical groups II, III and IV (*i.e.* those subject to breeding) to those of Group I (landraces), Figure 3A. Our results are consistent with two main rounds of diversity reduction, an initial wave between Groups I and II (11.7% of RoD), reflecting early breeding improvement, and a second wave between groups III and IV (13.3% of RoD) that followed the green revolution (*i.e.* renovation of agricultural practices starting between 1950 and the late 1960s). Modern wheat varieties showed an average loss of nucleotide diversity of 21.8% compared to those of Group I, with strong variation within and between chromosomes (Figure 3B). This appeared to be more intense on the A (median RoD = 33.2%) and B (median RoD = 28.0%) subgenomes compared

to the D subgenome (median RoD =5.8%), which may reflect their different contributions to wheat improvement (Figure 3A). To identify genetic markers/regions selected by wheat breeders, we performed a genome-wide scan across all samples using the individual-centric method PCAdapt¹³ to take into account the graduated population structure within and between groups, and at a higher granularity among European and Asian samples separately (Figure S7). We identified 5,089 polymorphic sites exhibiting improvement signals (p-values < 0.0001, red dots in Fig 1 circle #4). Known genes including *Ppd* and *VRN* genes for photoperiod sensitivity and vernalization, *Rht* for reduced height, Glutenin and Gliadin genes involved in seed storage protein accumulation, *FZP* for Frizzy panicle, *GNS* for grain number, *Wx* for waxy as well as the *CUL* gene driving plant architecture, were located close (<5 Mb distance) to these improvement signals (Table S3)¹⁴⁻¹⁷. Large genomic regions (>10 Mb) where selection appears to have occurred during the last centuries (between historical groups I and IV) and eventually became fixed, were observed especially on chromosome 1A and the two most structurally re-arranged chromosomes 4A and 7B of the wheat genome (Figure 3B)¹⁸. Extending the 8,308 and 9,948 polymorphic sites associated to improvement footprints observed in the European and Asian genotypes over 2 Mb overlapping windows, defined a cumulative genomic space of 950 Mb (7% of the genome) and 1.3 Gb (10% of the genome) with selection signatures for the two geographical areas respectively. Interestingly, only 168 Mb (13 to 18% of the previous genomic space under selection) of the genomic regions harboring selection signatures are identical between the European and Asian germplasm, suggesting independent improvement targets from the two geographic origins (Figure S7).

We then tested whether the observed allelic variation could be linked to two key life-history traits, heading date (HD) and plant height (PH) by conducting multi-environment genome-wide association studies (GWAS), Figure 1 circles #6 and #7. We grew and evaluated 435 hexaploid bread wheat genotypes for heading date and plant height in four common garden experiments (partially replicated design) in France (INRA, Clermont-Ferrand), Hungary (ATK, Martonvasar), Turkey (University of Çukurova, Adana) and United Kingdom (KWS, Cambridge). A subset of 390,657 SNPs, stringently filtered for call rate (<0.80) and Minor Allele Frequency (MAF, >0.05) was used for GWAS. We identified 48 and 40 genomic sites significantly associated (p-values of 0.01 and 0.05 FDR significance thresholds) with variation in HD (Figure S8, Table S4) and PH (Figure S9, Table S5) respectively, including regions (<15 Mb) containing known (*Ppd*, *VNR*, *FDL*, *WPCL* for HD and *Rht* for PH)¹⁹ and unknown genes. The current data provide the basis for identifying relevant candidate genes in the previous anonymous detected loci for functional validation, as exemplified for the major HD association detected on the chromosome 2A where *Cry* (Cryptochrome) is putative driver (Figure S8). Notably, diversity, selection footprint and GWAS analyses clearly showed that only a small fraction of homoeologous loci harbour coincident signals, supporting the view that modern hexaploid bread wheats behave genetically as diploids, as previously suggested from the convergent pattern of (also referenced as parallel advantageous) selection shown to be rare between homoeologous regions¹⁴.

Finally, we implemented a network-based phylogenetic approach²⁰⁻²¹ involving the inference of 1,000 trees from repeated random haplotype samples (RRHS) with maximum likelihood, subsequent graph reconstruction analysis and community clustering to reconstruct the reticulated evolutionary history of modern hexaploid bread wheats from their di- and tetraploid progenitors. The resulting clustered consensus network (Figure 4A) comprises signals of vertical (species relationships) and horizontal (reticulation) events within the *Triticum-Aegilops* species complex. The intermediate positioning in network of synthetic polyploid wheats (i.e synthetic *T. turgidum* deriving from *T. durum* x *T. dicoccoides* and synthetic *T. aestivum* deriving from *T. durum* x *A. tauschii*) between their direct progenitors validate the robustness of our phylogenetic inference of the entire wheat panel (Figure 4A, Figure S10). An integrative model of wheat evolution (Figure 4B) was derived from the combined conclusions drawn from the in-depth analysis of the networks' edges and edge weights²⁰⁻²¹ (Figure 4A, Figure S10), and supported through the evaluation of alternative consensus tree topologies²² (Figure S11) and gene flow tests using Patterson's D statistic²³ (Figure S12). For example, we were able to reconstruct, at the subgenome level, the introgressions at the basis of modern synthetic *T. turgidum* (F7 RIL offsprings) polyploids mentioned earlier and detected as hybrids (Figures S10-S11-S12) by all methods with dominant *T. dicoccoides* genotypes and multiple independent *T. durum* introgressions²⁴, illustrating the resolution gained for such combination of complementary approaches.

Our proposed model (Figure 4B) largely refines the widely accepted evolutionary path leading to modern bread wheat with the hybridization of wild diploid AA and SS (close to BB) genotypes leading to wild tetraploid AABB progenitors, which subsequently hybridized with a wild diploid DD genotype resulting in the hexaploid *T. aestivum* (AADDDB) lineage²⁴. In our analysis, the wheat B genome is confirmed to be derived from the *Aegilops* section Sitopsis lineage, which gave rise to *A. speltoides* (SS), while the progenitors of *A. tauschii* and *T. urartu* represent the established origins of the D and A genome lineages, respectively²⁵. *T. araraticum* (also referenced as *T. araraticum* Jakubz) represents the closest wild descendant of the AAGG tetraploid genome ancestor. It appears to have been subsequently domesticated to form *T. timopheevii* (Zhuk.) Zhuk while also hybridizing with *T. boeoticum* leading to the hexaploid *T. zhukovshyi* (Menabde & Ericzjan) lineage (AAAAGG)^{26,27}. The model confirms wild emmer (*T. dicoccoides*) as the closest descendant of the progenitor of the modern A and B wheat

subgenomes of all the modern tetraploid AABB and hexaploid AABBDD genotypes. Our data suggest that during the early phase of domestication and cultivation, a pool of wild emmer wheat *T. diccoides* (Körn. ex Asch. & Graebner) Schweinf. gave rise to at least two distinct lineages of domesticated tetraploids, *T. dicoccum* Schrank ex Schübl. (domesticated emmer, also known as *T. dicoccon* Schrank) and *T. durum* Desf. (domesticated durum or hard or pasta wheat)^{28,29}. Finally, the model supports *T. aestivum* as being most likely derived from an ancestral hybridization event between the previous *T. durum*³⁰ lineage and a D lineage close to wild *A. tauschii*³¹ (Figure 4B, Figure S11). Subsequently, *T. spelta* emerged from the hybridization between the hexaploid *T. aestivum* and the tetraploid *T. dicoccum*, and still harbors evidence of *T. dicoccum* introgressions today (Figure S12). Additional putative reticulation events (Figure S12), supported only by either of the three analytical approaches (network, tree, Patterson's D) need further investigation and were not integrated in our evolutionary model (Figure 4B). Such a reticulated evolutionary scenario would first have led to a founder hexaploid bread wheat gene pool (α community, Figure 4A) that was established during and following domestication. This would likely have consisted of primitive wheat landraces originating in the Fertile Crescent, leading to two (β and γ) derived communities of hexaploids (Figure 4A, Figure S13). While the γ cluster is enriched for modern genotypes from Western Europe (*i.e.* lines originating from 1986 or later, mostly comprising wheat cultivars and current varieties), the β cluster is enriched for Eastern Europe countries formerly part of the Warsaw Pact from May 1955, during the Cold War. The clear separation in evolutionary phylogeny between these two modern pools (β and γ) may reflect how human history and resulting socioeconomic consequences have influenced the genetic makeup of modern wheat germplasm, with β genotypes still grown in Hungary and Ukraine today, while γ genotypes still dominate many parts of the European Union.

CONCLUSION - Bread wheat derives from a reticulated evolution from its di- and tetraploid progenitors involving massive and recurrent hybridization and gene flow events with the *T. durum* lineage being the most likely ancestor of today's bread wheat cultivated germplasm. Such a complex history of hybridizations and gene flows explains the observed partitioning of diversity at the genomic scale (impoverished on the D subgenome) and supports the view that modern hexaploid bread wheats behave genetically as diploids with compartmentalized selective footprints, as well as trait loci, with only a small fraction of homoeologous loci harbouring domestication and/or breeding sweeps or influencing defined phenotypic traits showing coincident signals. Modern bread wheat originated in the Fertile Crescent some 10,000 ybp and the variation observed in the gene pool today has been shaped during domestication by human migration, anthropogenic selection and latterly by breeding. Associations identified between diversity and both known and novel genes influencing plant height and flowering time demonstrate the potential value of our panel for both fundamental and applied studies. Importantly, the hallmarks of adaptation to new environments remain highly topical research subjects during a period of accelerated climate change and both our selective sweep analyses and GWAS highlight targets for future gene and/or allele discovery. The combined data and germplasm collection we report here and made available to the broader research community represents a rich source of genetic diversity that should find application in understanding and improving diverse traits, from environmental adaptation to disease resistance and nutrient use efficiency.

METHODS - Methods, including statements of data availability and any associated genotype codes and references, are available in the online version of the paper.

ACKNOWLEDGEMENTS - The authors wish to thank the INRA- Biological Resources Center on small grain cereal (https://www6.ara.inra.fr/umr1095_eng/Teams/Research/Biological-Resources-Centre) for providing seeds and passport data, and for establishing wheat biorepository. The authors thank the Federal ex situ Genbank Gatersleben, Germany (IPK), the N. I. Vavilov All-Russian Research Institute of Plant Industry, Russia (VIR), Centre for Genetic Resources, WUR, Netherlands (CGN), Kyoto University - National Bioresource Project, Japan (NBRP), the Australian Winter Cereal Collection Tamworth, Australia (AWCC), the National Plant Germplasm System, USA (USDA-ARS), the International Center for Agriculture Research in the Dry Areas (ICARDA), the Max Planck Institute for Plant Breeding Research Cologne, Germany (MPIPZ), the John Innes Centre, UK (JIC) and the WHEALBI consortium for providing plant material and passport data.

AUTHOR CONTRIBUTION - Panel constitution and distribution - François Balfourier, Benjamin Kilian, Nils Stein. **Exome sequencing** - Darren Waite, Sarah Dyer, Joanne Russell, Robbie Waugh. **Variant (SNPs, InDels) calling** - Michael Seidel, Manuel Spannagl, Georg Haberer. **Variant (SNPs, InDels) analysis**: Caroline Pont, David Armisen, Nadia Goué, Michael Seidel, Daniel Lang. **Phylogenetic analysis** - Daniel Lang, Wandrille Duchemin, Michael Seidel, Caroline Pont, Nadia Goué, Georg Haberer. **Diversity analysis & selection footprints** - Thibault Leroy, Caroline Pont, David Armisen. **Field experiments and GWAS** - Alessandro Tondelli, Daniela Bustos-Korts, Caroline Pont, Hakan Özkan, Marta Molnar-Lang, Fred van Eeuwijk, Luigi Cattivi. **Conception, supervision and preparation of the article** - Beat Keller, Joanne Russell, Klaus F.X. Mayer, Robbie Waugh, Nils Stein, Luigi Cattivi, Georg Haberer, Gilles Charmet, Jerome Salse.

FUNDING - The research leading to these results has received funding from the European Community's Seventh Framework Programme (FP7/ 2007-2013) under the grant agreement n°FP7- 613556, Whealbi project (<http://www.whealbi.eu/project/>). RW and JR also acknowledge support from the Scottish Government Research Program and RW from the University of Dundee. HÖ acknowledges support from Çukurova University (FUA-2016-6033). KFXM acknowledges support from the German Federal Ministry of Food and Agriculture (2819103915) and the DFG (SFB924).

REFERENCES

- (1) M. Feldman, A. A. Levy, Genome evolution due to allopolyploidization in wheat. *Genetics*. **192**, 763-774 (2012). doi: 10.1534/genetics.112.146316.
- (2) K. Tanno, G. Willcox, How fast was wild wheat domesticated? *Science*. **311**, 1886 (2006). doi: 10.1126/science.1124635
- (3) T. A. Brown, M. K. Jones, W. Powell, R. G. Allaby, The complex origins of domesticated crops in the Fertile Crescent. *Trends Ecol Evol*. **24**, 103-109 (2009). doi: 10.1016/j.tree.2008.09.008.
- (4) J. P. Bocquet-Appel, S. Naji, M. Vander Linden, J. K. Kozłowski, Detection of diffusion and contact zones of early farming in Europe from the space-time distribution of 14C dates. *J. Archaeol. Sci.* **36**, 807–820 (2009). doi: 10.1016/j.jas.2008.11.004.
- (5) A. Szécsényi-Nagy, G. Brandt, V. Keerl, J. Jakucs, W. Haak, Tracing the genetic origin of Europe's first farmers reveals insights into their social organization. *P. Roy. Soc. B. Biol. Sci.* **282**, (2015). doi: 10.1098/rspb.2015.0339.
- (6) A. B. Damania, J. Valkoun, G. Willcox, C. O. Qualset, The origin of agriculture and crop domestication. (Proceedings of the Harlan symposium, 10-14 May 1997), [first edition]. *International Center for Agricultural Research in the Dry Areas, Aleppo, Syria*. 345pp.
- (7) A. Warr, C. Robert, D. Hume, A. Archibald, N. Deeb, M. Watson. Exome Sequencing: Current and Future Perspectives. *G3 (Bethesda)*. **5**(8), 1543-50 (2015). doi: 10.1534/g3.115.018564.
- (8) The International Wheat Genome Sequencing Consortium (IWGSC) Shifting the limits in wheat research and breeding using a fully annotated reference genome. *Science*. (2018). doi: 10.1126/science.aar7191.
- (9) T.A. Brown, M.K. Jones, W. Powell, R.G. Allaby, The complex origins of domesticated crops in the Fertile Crescent. *Trends Ecol Evol*. **24**(2), 103-9 (2009). doi: 10.1016/j.tree.2008.09.008.
- (10) Y. Matsuoka, Evolution of polyploid triticum wheats under cultivation: the role of domestication, natural hybridization and allopolyploid speciation in their diversification. *Plant Cell Physiol*. **52**(5), 750-64 (2011). doi: 10.1093/pcp/pcr018.
- (11) L. Gao, G. Zhao, D. Huang, J. Jia, Candidate loci involved in domestication and improvement detected by a published 90K wheat SNP array. *Sci Rep*. **7**, 44530 (2017). doi: 10.1038/srep44530.
- (12) [S.I. Wright, I.V. Bi, S.G. Schroeder, M. Yamasaki, J.F. Doebley, M.D. McMullen, B.S. Gaut, The effects of artificial selection on the maize genome. *Science*. **308**\(5726\):1310-4 \(2005\). doi: 10.1126/science.1107891.](#)
- (13) K. Luu, E. Bazin, M.G. Blum. pcadapt: an R package to perform genome scans for selection based on principal component analysis. *Mol Ecol Resour*. **17**(1), 67-77 (2017). doi: 10.1111/1755-0998.
- (14) K. W. Jordan, S. Wang, Y. Lun, L. J. Gardiner, R. MacLachlan, A haplotype map of allohexaploid wheat reveals distinct patterns of selection on homoeologous genomes. *Genome Biol.* **16** (2015). doi: 10.1186/s13059-015-0606-4.
- (15) C.R. Cavanagh, S. Chao, S. Wang, B.E. Huang, S. Stephen, S. Kiani, K. Forrest, C. Sainenac, G.L. Brown-Guedira, A. Akhunova, D. See, G. Bai, M. Pumphrey, L. Tomar, D. Wong, S. Kong, M. Reynolds, M.L. da Silva, H. Bockelman, L. Talbert, J.A. Anderson, S. Dreisigacker, S. Baenziger, A. Carter, V. Korzun, P.L. Morrell, J. Dubcovsky, M.K. Morell, M.E. Sorrells, M.J. Hayden, E. Akhunov, Genome-wide comparative diversity uncovers multiple targets of selection for improvement in hexaploid wheat landraces and cultivars. *Proc Natl Acad Sci U S A*. **110**(20), 8057-62 (2013). doi: 10.1073/pnas.1217133110.
- (16) R. Joukhadar, H.D. Daetwyler, U.K. Bansal, A.R. Gendall, M.J. Hayden, Genetic Diversity, Population Structure and Ancestral Origin of Australian Wheat. *Front Plant Sci*. **8**, 2115 (2017). doi: 10.3389/fpls.2017.02115.
- (17) N.H. Nielsen, G. Backes, J. Stougaard, S.U. Andersen, A. Jahoor, Genetic diversity and population structure analysis of European hexaploid bread wheat (*Triticum aestivum* L.) varieties. *PLoS One*. **9**(4), e94000 (2014). doi: 10.1371/journal.pone.0094000.
- (18) K. M. Devos, J. Dubcovsky, J. Dvorak, C. N. Chinoy, M. D. Gale, Structural evolution of wheat chromosomes 4A, 5A, and 7B and its impact on recombination. *Theor. Appl. Genet.* **91**, 282–288 (1995). doi: 10.1007/BF00220890
- (19) A. Nadolska-Orczyk, I.K. Rajchel, W. Orczyk, S. Gasparis, Major genes determining yield-related traits in wheat and barley. *Theor Appl Genet.* **130**(6):1081-1098 (2017). doi: 10.1007/s00122-017-2880-x

- (20) L.J. Gardiner, R. Joynton, J. Omony, R. Rusholme-Pilcher, L. Olohan, D. Lang, C. Bai, M. Hawkesford, D. Salt, M. Spannagl, K.F.X. Mayer, J. Kenny, M. Bevan, N. Hall, A. Hall, Hidden variation in polyploid wheat drives local adaptation. *Genome Res.* **28**(9):1319-1332 (2018). doi: 10.1101/gr.233551
- (21) [H.E. Lischer, L. Excoffier, G. Heckel, Ignoring heterozygous sites biases phylogenomic estimates of divergence times: implications for the evolutionary history of microtus voles. *Mol Biol Evol.* **31**\(4\):817-31 \(2014\). doi: 10.1093/molbev/mst271.](#)
- (22) L.T. Nguyen, H.A. Schmidt, A. von Haeseler, B.Q. Minh, IQ-TREE: A Fast and Effective Stochastic Algorithm for Estimating Maximum-Likelihood Phylogenies. *Mol Biol Evol.* **32**(1), 268-74 (2015). doi: 10.1093/molbev/msu300.
- (23) S.H. Martin, J.W. Davey, C.D. Jiggins, Evaluating the use of ABBA-BABA statistics to locate introgressed loci. *Mol Biol Evol.* **32**(1):244-57. doi: 10.1093/molbev/msu269.
- (24) R. Ben-David, Z. Peleg, W. Xie, A. Dinooor, A.B. Korol, T. Fahima, Dissection of powdery mildew resistance uncovers different resistance types in the *T. turgidum* L. gene pool. 2008, 11 th Int. wheat genetics symposium.
- (25) M. El Baidouri, F. Murat, M. Veysiere, M. Molinier, R. Flores, Reconciling the evolutionary origin of bread wheat (*Triticum aestivum*). *New Phytol.* **213**, 1477-1486 (2017). doi: 10.1111/nph.14113.
- (26) A.F. Balint, G. Kovacs, J. Sutka, Origin and taxonomy of wheat in the light of recent research. *Acta Agronomica Hungarica*, **48**(3), 301–313 (2000).
- (27) M. Nesbitt, D. Samuel, From Staple Crop to Extinction. The Archaeology and History of the Hulled Wheats. *Proceedings of the first international workshop on hulled wheats* **21**, 41-100 (1996).
- (28) P. Civián, Z. Ivaničová, T.A. Brown, Reticulated origin of domesticated emmer wheat supports a dynamic model for the emergence of agriculture in the fertile crescent. *PLoS One.* **8**(11), e81955 (2013). doi: 10.1371/journal.pone.0081955.
- (29) M. C. Luo, Z. L. Yang, F. M. You, T. Kawahara, J. G. Waines, The structure of wild and domesticated emmer wheat populations, gene flow between them, and the site of emmer domestication. *Theor. Appl. Genet.* **114** 947-959 (2007). doi: 10.1007/s00122-006-0474-0.
- (30) Y. Matsuoaka, S. Nasuda, Durum wheat as a candidate for the unknown female progenitor of bread wheat: an empirical study with a highly fertile F1 hybrid with *Aegilops tauschii* Coss. *Theor Appl Genet.* **109**(8), 1710-7 (2004). Epub 2004 Sep 22
- (31) J. Wang, M. C. Luo, Z. Chen, F. M. You, Y. Wei, *Aegilops tauschii* single nucleotide polymorphisms shed light on the origins of wheat D-genome genetic diversity and pinpoint the geographic origin of hexaploid wheat. *New Phytol.* **198**, 925-937 (2013). doi: 10.1111/nph.12164.

Figure 1: Wheat genome diversity map. Genome heat maps illustrating (from outer to inner circles) the density in genes (①), SNPs (②), InDels (③), genome scan for improvement among European genotypes (④), reduction of diversity during the domestication between wild tetraploids vs domesticated hexaploids for subgenomes A and B and between wild diploids vs domesticated hexaploids for subgenome D (⑤), as well as GWAS for heading date (HD, ⑥), plant height (PH, ⑦) on the 21 chromosomes (from 1A to 7D) illustrated in circles, with the three subgenomes (A, B and D). Homoeologous genes are joined with colored lines between chromosomes in the center (⑧). The three outer circles show centromeres (grey blocks) and telomeres (blue blocks).

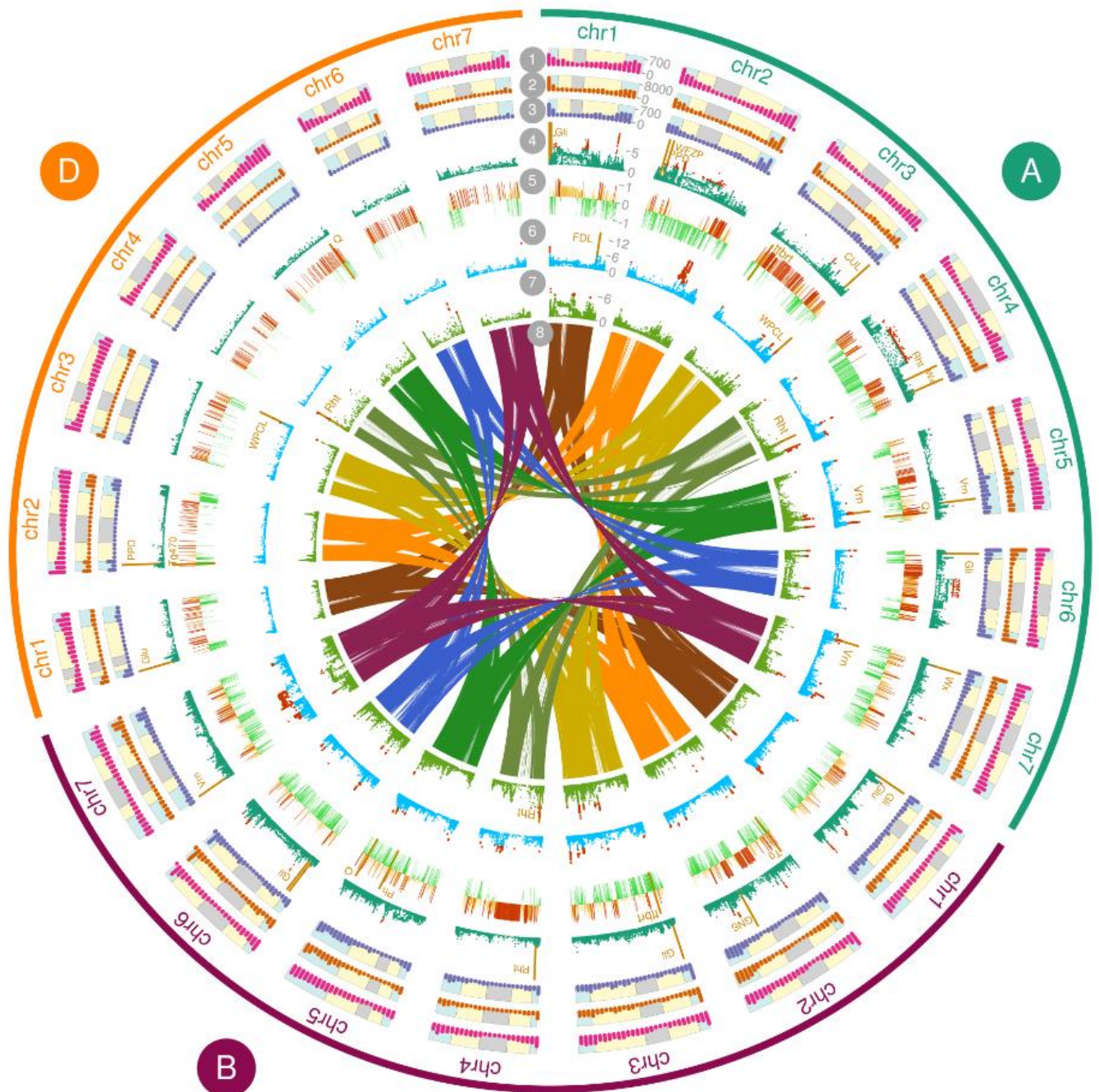
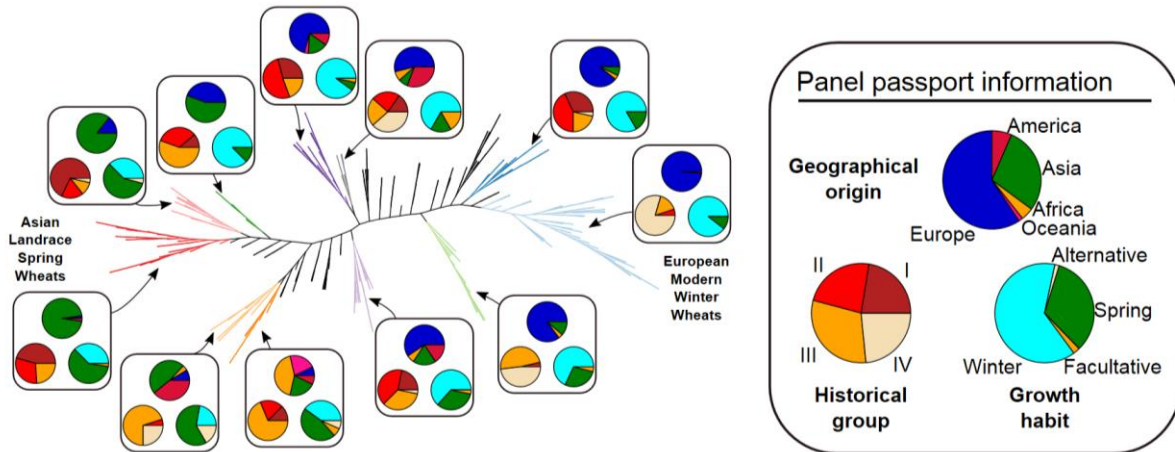


Figure 2: Geographical components of the panel structure. A- Phylogenetic tree of the hexaploid bread wheat genotypes with a color code (right) in pie charts illuminating their geographical origins (see the associated map in panel B), historical groups (I to IV) and growth habit (winter, spring, alternative, and facultative) for each of the 11 major tree clades. B- Phylogenetic relationships between geographical origins (see color legend in panel A) are shown with colored connecting lines illustrating tree edges corresponding to a mean of at least 1 transition per simulation and illuminating the known historical routes of wheat migration, out of the Fertile Crescent (green connecting lines), west through inland (1) and coastal (2) paths, and north-east (3) and along the Inner Asian Mountain Corridor (4) followed by further colonization (black connecting lines) of American (5), African (6), Oceanian (7) territories.

A



B

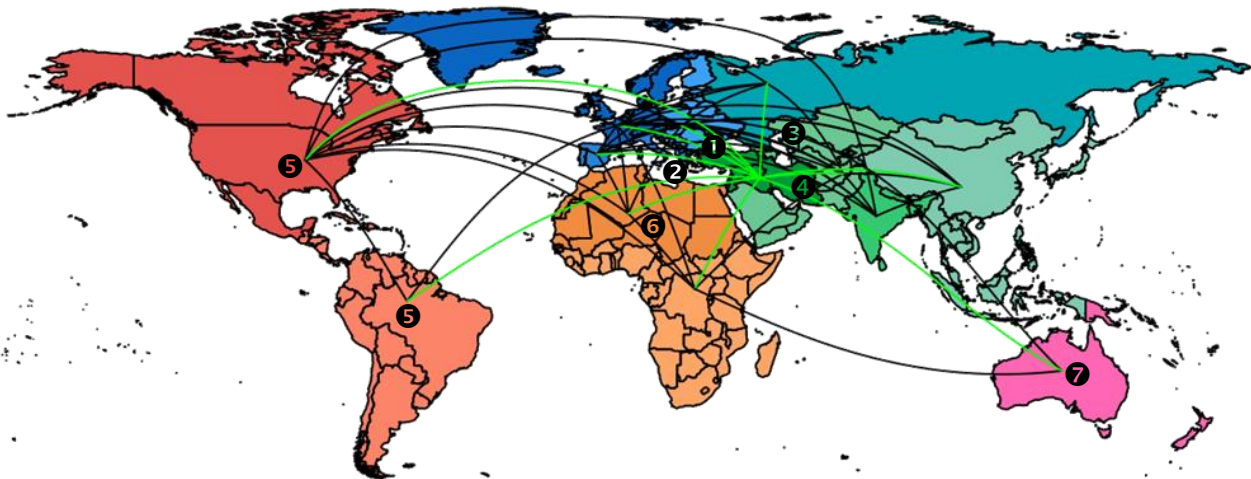
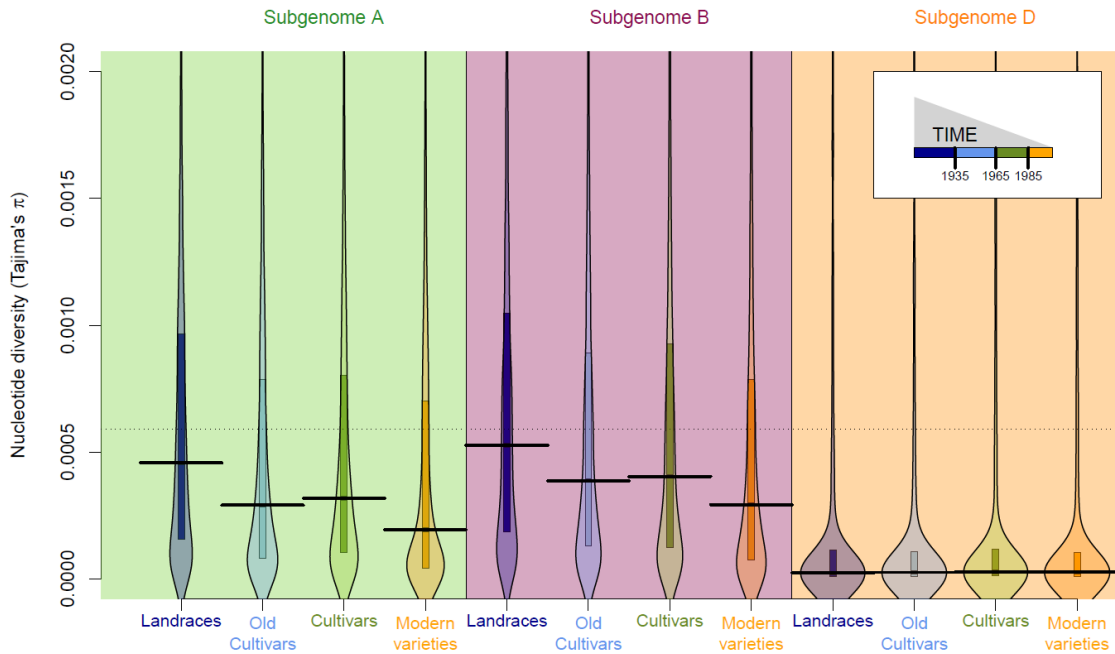


Figure 3: Temporal evolution of wheat diversity. **A-** Nucleotide diversity (y-axis) from the hexaploid wheat genotypes (x-axis) between subgenomes (A, B and D) and historical groups (landraces, old cultivars, cultivars and modern varieties) covering the last centuries of breeding (*cf* timescale legend in the white box). **B-** Chromosomal distribution of nucleotide diversity between landraces (group I) and modern wheats (group IV, dots) with bars illustrating the range of variation in diversity between these two groups (colored in red for ROD \geq 80%). Large regions of reduced diversity are shown in grey boxes.

A



B

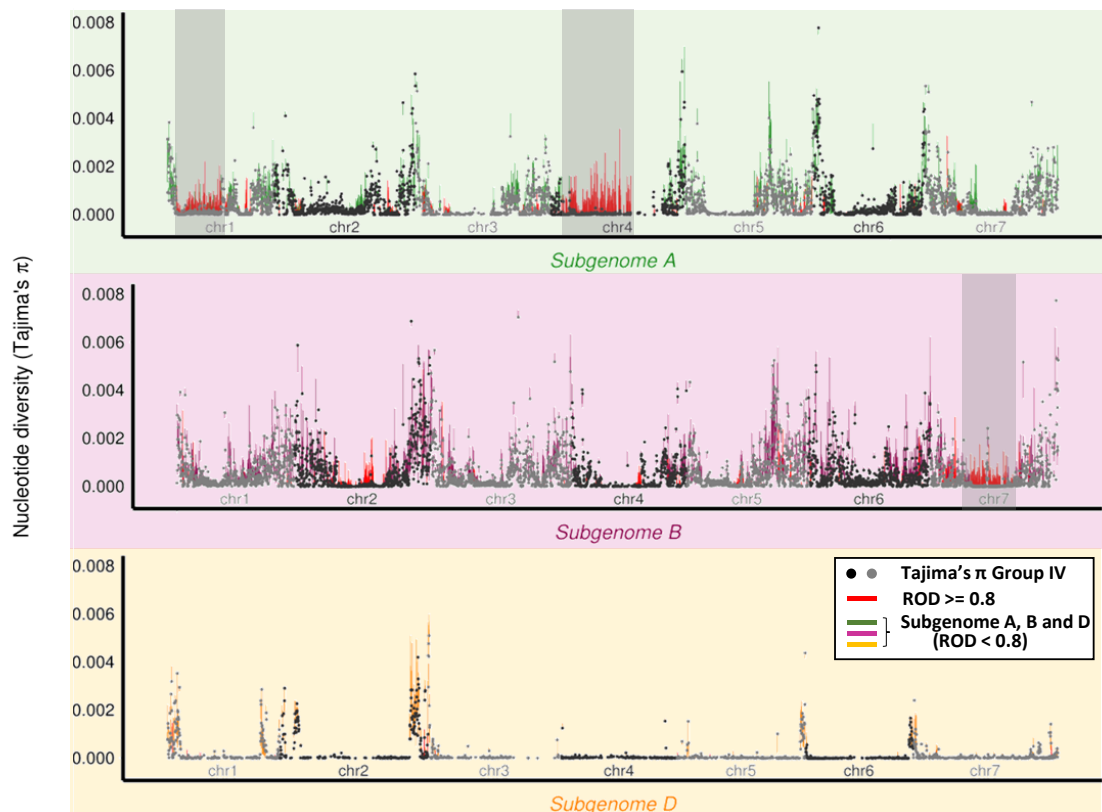
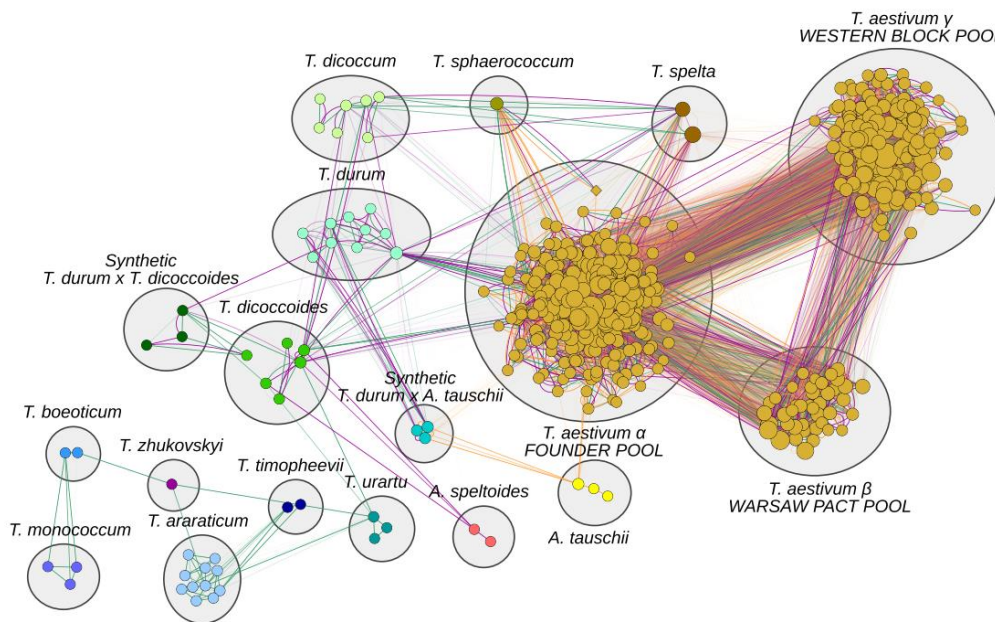
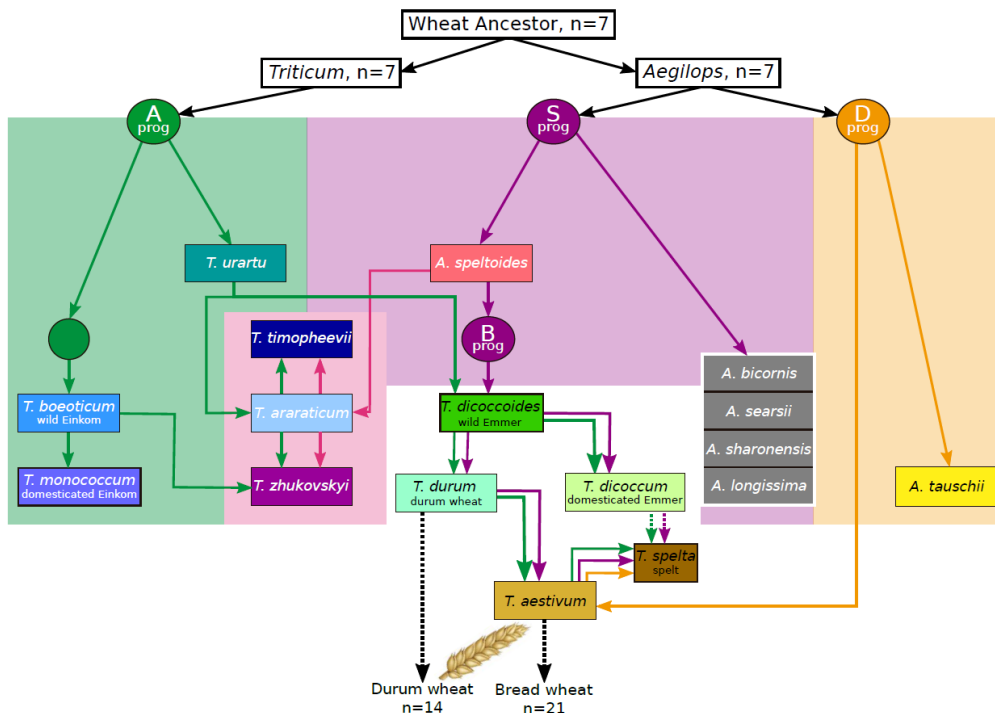


Figure 4: Model of reticulated evolution. **A-** Clustered phylogenetic consensus genotype network of 1000 maximum likelihood tree topologies inferred from repeated random haplotype samples (RRHS). Nodes represent individual genotypes and are color-coded by taxon. Node size is proportional to the number of connections (*i.e.* node degree). Edges represent minimal evolutionary distances in the RRHS trees deduced by the minimal spanning tree (MST) algorithm and are color-coded by the respective subgenome (green: A; purple: B; orange: D). Edge transparency is proportional to the relative number of RRHS trees where the edge was an MST edge (*i.e.* edge weight). **B-** Hexaploid bread wheat evolutionary scenario based on the stronger edges of the subgenomes phylogenetic networks (extracted using a minimum spanning tree available in Figure S11) with green, purple and yellow brown columns illustrating respectively the path from the A, B and D subgenomes with the species-centered color-code used in panel A. Arrow colors illustrate the phylogenetic relatedness between subgenomes (plain arrows are indicative of the main, vertical signal; and dashed arrows show alternative path well supported by the inferred topologies and indicative of introgression or gene flow). Circles illuminate putative extinct ancestor intermediates. Additional *Sitopsis* species (white framed grey boxes) were not part of this study, but are included for completeness.

A



B



ONLINE METHODS

Plant material - The wheat panel consists of 487 genotypes comprising 13 diploid, 38 (including 25 AABB) tetraploid and 436 (including 435 AABBDD) hexaploid genotypes including landraces, cultivars and currently grown varieties from 68 countries. For a detailed description of all lines/varieties used in this study see Table S1 and passport information available at https://urgi.versailles.inra.fr/download/iwgs/IWGSC_RefSeq_Annotations/v1.0/iwgs_refseqv1.0_Wheatbi_GWAS.zip. The genotypes were structured into four historical groups: landraces (group I, <1935), old cultivars (group II from 1936 to 1965), cultivars (group III, from 1966 to 1985) and modern varieties (group IV, >1986). The genotypes have been grouped according to their country of origins with Tk: Turkmenia; Af: Afghanistan; Ar: Armenia; Az: Azerbaijan; Ch: China; Ko: Korea; In: India; Ir: Iran; Is: Israel; Ja: Japan; Le: Lebanon; Ne: Nepal; Pa: Pakistan; Sy: Syria; Ta: Tajikistan; Tu: Turkey; Ru: Russia; Au: Australia; Nz: New Zealand; Al: Albania; As: Austria; Be: Belgium; Bu: Bulgaria; Cr: Croatia; Cz: Czech republic; Dn: Denmark; Fi: Finland; Fr: France; Go: Georgia; Ge: Germany; Gr: Greece; Hu: Hungary; It: Italy; La: Latvia; Po: Poland; Pr: Portugal; Ro: Romania; Sp: Spain; Sw: Sweden; Sz: Switzerland; Nt: Netherlands; Ur: Ukraine; Uk: United Kingdom; Fyrm: Former Yugoslav Republic of Macedonia; Al: Algeria; Eg: Egypt; Et: Ethiopia; Ke: Kenya; Mo: Morocco; Ni: Niger; Sa: South Africa; Tn: Tunisia; Zi: Zimbabwe; Ag: Argentina; Br: Brazil; Ca: Canada; Co: Colombia; Me: Mexico; Ur: Uruguay; Usa: United States of America. The genotypes have been finally grouped according to their region/continent of origins with Fertile Crescent (Ir, Is, Le, Sy, Tu), Central Asia (Af, Ar, Az, Go, Pa, Ta, Tk), Eastern Asia (Ch, Ja, Ko), Northern Asia (Ru), Central Europe (Al, Bu, Cr, Cz, Fi, Hu, La, Po, Ro, Ur, Fyrm), Southern Europe (Gr, It, Pr, Sp), Western Europe (As, Be, Dn, Fr, Ge, Sw, Sz, Nt, Uk), Indian Peninsula (In, Ne), Northern Africa (Al, Eg, Mo, Tn), Sub-Saharan Africa (Et, Ke, Ni, Sa, Zi), South America (Ag, Br, Co, Ur), North America (Ca, Me, Usa), Oceania (Au, Nz).

Exome sequencing - As the large wheat genome consists of >80% mobile and repeated elements, whole-genome resequencing is a cost-intensive and likely highly error-prone approach to comprehensively catalogue genetic diversity. To circumvent this limitation, we used a wheat exome-based target enrichment sequencing assay to capture variation in and around the gene-containing regions of 487 wheat genotypes. We selected Roche's Nimblegen SeqCap EZ wheat exome design (120426_Wheat_WEC_D02), <https://sequencing.roche.com/en/products-solutions/by-category/target-enrichment/shareddesigns.html>. This is a design comprising 106.9Mb of low copy regions of the wheat genome developed by the Wheat Exome consortium^{7,14}. To optimize the cost, we used a multiplex of six individually barcoded accession DNAs, combined prior to capture. Captured DNA were sequenced as paired ends (2x125bp) on Illumina HiSeq instruments using HiSeq2500 high output mode. Genomic DNA (gDNA) samples were checked using the PerkinElmer DropSense in order to verify gDNA integrity. Samples were quantified by Picogreen assay and normalized to 20 ng/ul in 10 nM Tris-HCl (pH 8.0) as suggested in the NimbleGen SeqCap EZ Library SR protocol. The gDNA was fragmented at the mean fragment size of 350 bp and whole genome libraries were prepared according to the Kapa Library Preparation protocol and quantified by Nanodrop. Six libraries were pooled and used for the hybridization with the SeqCap Ez oligo pool (Design Name: 120426_Wheat_WEC_D02) in a thermocycler at 47°C for 72 h. Capture beads were used to pull down the complex of capture oligos and genomic DNA fragments and unbound fragments were removed by washing. Enriched fragments were amplified by PCR and the final library was quantified by qPCR and visualized by Agilent Bioanalyser. Sequencing libraries were normalized to 2nM, NaOH denatured and used for cluster amplification on the cBot. The clustered flow cells were sequenced on Illumina HiSeq2500 high output mode with a 6-plex strategy (*i.e.* 6 samples per HiSeq lane) with a 125 bp paired-end run module. Exome capture (Nimblegen) and next generation sequencing (Illumina) delivered on average 34 million read pairs per genotype.

Variant (SNPs, InDels) calling – Raw reads were mapped to the hexaploid Chinese Spring reference sequence v1.0 using the 'mem' subcommand of BWA (version 0.7.12, <http://bio-bwa.sourceforge.net/>). Samtools (version 1.3, <http://samtools.sourceforge.net/>; <http://www.htslib.org/>) was used to mark duplicate reads. Variants were called using samtools/bcftools (version 1.3) and filtered for overlap to exonic regions (+/- 1 Kbp) based on the current IWGSC genome annotation v1.0. Genotypes were subsequently filtered for a minimum sequencing depth (DP) of 3 and a genotype quality (GQ) of at least 10. Two sets of genotype calls from experiments with Axion 35k and iSelect 80k SNP arrays (details from CerealsDB, <http://www.cerealsdb.uk.net/>) with a total of 38 genotypes in common between either of those sets and the exome capture were used to approximate optimal filter criteria leading to the lowest false discovery rate (FDR). Variant positions were removed if the total count of samples with defined genotype (*e.g.* not missing) was below 10 or the minor allele frequency was below 1% to derive the initial set of variants. This set was further subjected to imputation using beagle (default parameters) and the output was again analyzed for false discovery rate by comparison to iSelect genotype information. Based on this evaluation, the optimal trade-off between FDR, number of variants and missing values was considered to be 0.6 for genotype probability (GP, estimated by beagle) and 4% minor allele frequency (MAF, after imputation) and the final imputed variant dataset was generated applying these criteria. We detected 620,158 small-scale

variant positions on to the IWGSC Refseqv1.0 wheat genome assembly (targeting 41,032 of the 110,790 high confidence HC genes). The variants comprised 56,163 Indels (9%) and 563,995 SNPs (91%). 595,939 of the variants (96%) were found in the 435 AABBDD hexaploid genotypes (Table S2).

Phylogenetic analysis - Hexaploids phylogeny- The analysis of phylogeny for the 435 hexaploid bread wheat was inferred on an alignment of 91,554 SNPs (for a total of 65,467 distinct alignment patterns) found on triplets (2,855) of orthologous genes conserved in all three subgenomes A, B and D. The data was analyzed with iqtrees²⁰ (GTR+GAMMA(4) model), with 1,000 ultrafast bootstraps³². Geographical regions for ancestral nodes were reconstructed using the following protocol: 10,000 simulations were performed using the stochastic mapping algorithm of the R phytools package³³ (using the equal rates model), the region of a node was then chosen as the one with maximum sampled frequency. Eleven major tree clades were identified based on criterion of size, representativeness and statistical support to offer a good coverage of the tree, while taking into account sampling bias for European individuals. **Di-Tetra-Hexaploids phylogeny-** To account for ambiguities and possible biases in phylogenetic inference from SNP data arising from varying levels of heterozygosity, linkage disequilibrium (LD), incomplete lineage sorting and reticulate evolution, we implemented a network-based approach to reconstruct the species history and community structure in the sampled *Triticeae* genotypes. To this end, we stringently filtered biallelic, polymorphic SNPs present in >90% of the genotypes from non-imputed data accounting for LD (delivering 15,490 filtered SNPs) and implemented a repeated random haplotype sampling procedure including heterozygous sites (RRHS²¹) to infer 1,000 maximum likelihood tree topologies with the ASC_GTRGAMMA model and JC69 distances in RAxML (asc-corr=felsenstein). While these RRHS trees were analyzed also in the form of conventional consensus topologies and densitree visualizations, to infer taxonomic clades, we analyzed the evolutionary distances among the tips of the 1,000 trees using the minimum spanning tree (MST) algorithm in Python. The MST graphs were subsequently combined into a weighted, phylogenetic consensus network whose nodes were clustered into clades using the Newman-Girvan Edge-Betweenness algorithm in Cytoscape 3.6³⁴. The clustered network topology was plotted considering edge-betweenness in Cytoscape and taxonomic clades were inferred by intersection of community clusters with taxon information which was annotated using the AutoAnnotate plugin³⁴. The relative number of RRHS trees where a respective edge was selected by the MST algorithm were used as edge weights and were interpreted similar to bootstrap support values in the consensus tree topologies. The composition, geographical and historical origins of the identified wheat communities were analyzed using χ^2 tests and barplots in R. Gene flow in subgenomes A and B was investigated with the Patterson's D statistic (or ABBA-BABA statistic) using ANGSD³⁵ with a threshold of Z statistic > 4 ³⁶. An integrative model (Figure 4B) of wheat evolution was built by manual consolidation of the support values of the edges in the phylogenetic consensus network (Figure S10 and table S7), the various consensus and IUPAC tree topologies (Figure S11), the ABBA-BABBA results (Figure S12) as well as the literature. Where species relationships remained ambiguous on the sole basis of the network approach, i.e. when similar phylogenetic relatedness between groups of genotypes defines several possible evolutionary paths between putative progenitors and descendants, we then considered the results of the ABBA-BABA statistical test (Figure S12 as well as Table S6), and the existing literature when available. The Figure 4B only reports the reticulation events identified on the basis of phylogenetic consensus networks supported by the ABBA-BABA analysis in both the A and B subgenomes.

Diversity analysis & selection footprints – Improvement- Genome scans for selection among the hexaploid samples were performed under PCAdapt¹³, an individual-based method of genome scan able to handle massive NGS data. Given that PCAdapt is based on principal components, this method does not require any partitioning of the dataset in different groups and can therefore be applied on continuous pattern of population structure. This method is therefore conceptually robust to any source of errors associated with the boundaries of these groups and can take into account the gradual variation among all individuals of the improvement continuum (i.e. time series-like data). For each dataset, selection of the best number of principal components (K) was performed after a first assessment of the percentage of variance explained by 20 principal components. Analyses were performed assuming K=4 for the whole dataset and K=3 for both European and Asian datasets. Computations were run under R version 3.4.3. Candidate genes for improvement are either associated with highly significant p-values or considered in close vicinity (0 to 5 Mb) to loci with domestication signatures (Table S3). Tajima's π and D was computed over 1 Mb non-overlapping sliding windows using seq-stat on European genotypes to take into account the strong signal of intercontinental genetic signatures. To perform this analysis, we took into account the number of sites covered by reads aligned to the reference. All sites with a total depth of coverage greater than 1,461 (i.e. at least 3 reads per individual on average) were considered as covered. A ROD (reduction of diversity) index was then estimated for each 1 Mb window by comparing diversity of each group (II, III or IV) to "Landraces" (Group I) as following: $1 - (\pi_{\text{Group}} / \pi_{\text{Landraces}})$. To further explore population structure, principal Component Analysis (PCA) was performed with the R package FactoMineR³⁷. Signatures of improvement were detected for loci associated with a pvalue < 0.0001 , i.e. a $-\log_{10}$ -transformed p-value > 4 . **Domestication-** Similarly, domestication signatures were identified using differences in Tajima's π between diploid, tetraploid and hexaploid genotypes by computing the ROD index over 1Mb windows. Signatures of domestication were detected for regions associated with ROD > 0.8 . Candidate genes for domestication were considered in close vicinity (0 to 5 Mb) to loci with

domestication signature (Table S3). Visualization were performed with R³⁸ packages such as graphics, stats, circlize and edextend³⁹⁻⁴². To further explore population structure, principal Component Analysis (PCA) was performed with the R package FactoMineR⁴³.

Field experiments and GWAS - These analyses focused on 435 hexaploid wheat genotypes evaluated for heading date and plant height in four common garden experiments in France (INRA, Clermont-Ferrand), Hungary (ATK, Martonvasar), Turkey (University of Çukurova, Adana) and United Kingdom (KWS, Cambridge). Trials were grown under an augmented partially-replicated design with 20% of the genotypes replicated twice and two check cultivars assigned uniformly to eight plots. Raw data were corrected for spatial heterogeneity using replicated controls and the SpATS package in R⁴⁴. After filtering out SNPs with Call Rate <0.80 and Minor Allele Frequency (MAF) <0.05, a final set of 390,657 SNPs were used for subsequent analysis. Finally, circular genome maps were drawn under the R package circlize⁴⁵. A chromosome-specific kinship matrix was calculated using 1,000 SNPs sampled at random from each chromosome. In this chromosome-specific kinship, A^{AB} , is the realized additive genetic relationship matrix calculated from all molecular markers along the whole genome, except those in the chromosome being tested⁴⁶. For example, to test SNPs in chromosome 1A, A^{AB} was calculated with SNPs sampled from all chromosomes, except those from 1A. A^{AB} was calculated following the equation proposed by Astle and Balding⁴⁷, with as typical entry for the relationship between genotypes i and j :

$$A_{ij}^{AB} = \frac{1}{K} \sum_{k=1}^K \frac{(x_{ik} - 2p_k)(x_{jk} - 2p_k)}{2p_k(1-p_k)} \quad (1)$$

where x_{ik} is a marker score indicating the allele count for the minor frequency allele (2, 1, 0) for genotype i at marker k , and p_k is the corresponding allele frequency. The matrix above was calculated using the “realizedAB” option in the “kin” function of the Synbreed package⁴⁸.

A multi-environment mixed model GWAS analysis was performed analogous to the method described by Millet et al.⁴⁹ and Thoen et al.⁵⁰. Correction for population structure and kinship was done on the basis of eigen vectors (“principal components”) extracted from the chromosome specific Astle and Balding kinship matrices, A^{AB} . The number of significant principal components was calculated following Patterson⁵¹. We scanned the genome with the following single locus model:

$$y_{ij} = \mu + E_j + \sum_{p=1}^P (x_{ip}^{PC} \beta_p^G) + G_i + \sum_{p=1}^P (x_{ip}^{PC} \beta_{jp}^{GE}) + x_i^{SNP} \beta_j^{SNP} + GE_{ij} + \varepsilon_{ij} \quad (2)$$

In Equation (2), μ is an intercept term, E_j the fixed environmental main effect x_{ip}^{PC} stands for the genotype specific scores on the p -th kinship principal component, with $p=1\dots P$, and β_p^G and β_{jp}^{GE} are the corresponding fixed regression coefficients for these principal components correcting for population structure with respect to the genotype main effect and the GxE interaction, respectively. β_j^{SNP} is a term for the fixed SNP effect, while x_i^{SNP} contains the marker information. This means that fitted QTLs are allowed to have an environment specific effect, or, that at each marker position, QTLs model main effect and a QTLxE term simultaneously. The test for β_j^{SNP} being zero in all environments or being non zero in at least one environment was a Wald test^{52,53}. G_i is a random genotypic main effect, GE_{ij} is a random genotype by environment interaction. The random terms for G_i and GE_{ij} have variances V_G and V_{GE} , that were restricted to be positive. The error term ε_{ij} is environment-specific and was confounded with the GE_{ij} term. The model was fitted in ASREML-R (VSN-International, 2016). Genomic control was applied a posteriori to correct for inflation⁵⁴.

The genome-wide significance threshold with multiple testing correction was calculated following the method proposed⁵⁵. For each chromosome, the correlation matrix for the SNPs was calculated. Then, the effective number of independent tests per chromosome was estimated from the eigenvalues of the correlation matrix. The effective number of independent tests was summed across chromosomes (M_{eff}) and the significance threshold for individual markers was calculated as $\alpha_p = 1 - (1 - \alpha_e)^{1/M_{eff}}$, where the genome wide test level was $\alpha_e = 0.05$.

Data availability. All data analyzed and generated during this study are included in this published article and its supplementary information files (6 tables and 13 figures) and are available online at https://urgi.versailles.inra.fr/download/iwgs/IWGSC_RefSeq_Annotations/v1.0/iwgs_refseqv1.0_Whealbi_GWAS.zip (Catalog of imputed and non-imputed variants as vcf file and passport information for the 487 genotypes as .xls file). The Whealbi SNPs data can be displayed in open access on the IWGSC reference genome browser⁵⁶ at https://urgi.versailles.inra.fr/jbrowseiwgsc/gmod_jbrowse/?data=myData%2FIWGSC_RefSeq_v1.0.

Software. Relevant source codes, workflow and analysis scripts used to conduct the results presented in the different section of the MS (structural variant detection, phylogenetic analysis, selective sweeps characterization, GWAS investigation), were deposited in a public github repository and are made available at <https://github.com/dandaman/whealbiCode>:

- Code and data to simulate hexaploid wheat ancestral region of origin (used for Figure2B)

- Code and data for the permutation tests to test the grouping of three character: continent of origin, growth habit, and historical group (Figure S4).

-Seqstat code source used for selection footprint analysis are available at <https://figshare.com/s/122efbec2e3632188674#/articles/7484705> (Figure 3, Figures S6-S7).

- Source code, documentation and results in form of Python and R Jupyter Notebooks and Snakemake workflows to perform RRHS, phylogenetic inference using the RRHS and IUPAC alignments as well as calculation and analysis of the MST-weighted phylogenetic consensus network (Figure 4A, Figure S10-S13).

(32) B.Q. Minh, M.A. Nguyen, A. von Haeseler, Ultrafast Approximation for Phylogenetic Bootstrap. *Mol Biol Evol.* **30**(5):1188-95 (2013). doi: 10.1093/molbev/mst024.

(33) L.J. Revell, phytools: an R package for phylogenetic comparative biology (and other things). *Methods Ecol. Evol.*, **3**, 217-223 (2012). doi.org/10.1111/j.2041-210X.2011.00169.x

(34) M. Kucera, R. Isserlin, A. Arkhangorodsky, G.D. Bader, AutoAnnotate: A Cytoscape app for summarizing networks with semantic annotations. *FI000Res.* **5**, 1717 (2016). eCollection 2016.

(35) Thorfinn Sand Korneliussen, Anders Albrechtsen and Rasmus Nielsen. ANGSD: Analysis of Next Generation Sequencing Data. *BMC Bioinformatics* **15**:356 (2014) doi.org/10.1186/s12859-014-0356-4

(36) E.Y. Durand, N. Patterson, D. Reich, M. Slatkin, Testing for ancient admixture between closely related populations. *Mol Biol Evol.* **28**(8):2239-52 (2011). doi: 10.1093/molbev/msr048.

(37) S. Lê, J. Josse, F. Husson, FactoMineR: An R Package for Multivariate Analysis. *Journal of Statistical Software*, **25**(1):1-18 (2008). 10.18637/jss.v025.i01

(38) R Core Team (2014) R: A language and environment for statistical computing. R Foundation for Statistical Computing, Vienna, Austria URL <http://www.R-project.org>

(39) H. Chipman, R. Tibshirani, Hybrid hierarchical clustering with applications to microarray data. *Biostatistics.* **7**, 286–301 (2006). doi: 10.1093/biostatistics/kxj007

(40) S. Schmidtlein, L. Tichy, F. Hannes, F. Ulrike, A brute-force approach to vegetation classification. *J. Veg. Sci.* **21**, 1162–1171 (2010). doi: 10.1111/j.1654-1103.2010.01221.x

(41) D.M. Witten, R. Tibshirani, A framework for feature selection in clustering. *J. Am. Stat. Assoc.* **105**, 713–726 (2010). doi: 10.1198/jasa.2010.tm09415

(42) T. Galili, dendextend: an R package for visualizing, adjusting and comparing trees of hierarchical clustering. *Bioinformatics.* **31**(22), 3718-20 (2015). doi: 10.1093/bioinformatics/btv428

(43) S. Lê, J. Josse, F. Husson, FactoMineR: an R package for multivariate analysis. *Journal of Statistical Software.* **25**, 1–18 (2008). doi: 10.18637/jss.v025.i01.

(44) M.X. Rodríguez-Álvarez, M.P. Boer, F.A. van Eeuwijk, P.H. Eilers, Correcting for spatial heterogeneity in plant breeding experiments with P-splines. *Spatial Statistics.* **23**, 52-71 (2017). doi: 10.1016/j.spasta.2017.10.003

(45) Z. Gu, L. Gu, R. Eils, M. Schlesner, B. Brors, circlize Implements and enhances circular visualization in R. *Bioinformatics.* **30**(19), 2811-2 (2014). doi: 10.1093/bioinformatics/btu393.

(46) R. Rincet, L. Moreau, H. Monod, E. Kuhn, A.E. Melchinger, R.A. Malvar, J. Moreno-Gonzalez, S. Nicolas, D. Madur, V. Combes, F. Dumas, T. Altmann, D. Brunel, M. Ouzunova, P. Flament, P. Dubreuil, A. Charcosset, T. Mary-Huard, Recovering power in association mapping panels with variable levels of linkage disequilibrium. *Genetics.* **197**(1), 375-87 (2014). doi: 10.1534/genetics.113.159731.

(47) W. Astle, D.J. Balding, Population structure and cryptic relatedness in genetic association studies. *Stat Sci.* **24**, 451–471 (2009). doi: 10.1214/09-STS307.

(48) V. Wimmer, T. Albrecht, H.J. Auinger, C.C. Schön, synbreed: a framework for the analysis of genomic prediction data using R. *Bioinformatics.* **28**(15), 2086–2087 (2012). doi: 10.1093/bioinformatics/bts335.

(49) E.J. Millet, C. Welcker, W. Kruijer, S. Negro, A. Coupel-Ledru, S.D. Nicolas, J. Laborde, C. Bauland, S. Praud, N. Ranc, T. Presterl T, Genome-wide analysis of yield in Europe: allelic effects vary with drought and heat scenarios. *Plant physiology.* **172**(2), 749-64 (2016). doi: 10.1104/pp.16.00621.

(50) M.P. Thoen, N.H. Davila Olivas, K.J. Kloth, S. Coolen, P.P. Huang, M.G. Aarts, J.A. Bac-Molenaar, J. Bakker, H.J. Bouwmeester, C. Broekgaarden, J. Bucher, Genetic architecture of plant stress resistance: multi-trait genome-wide association mapping. *New Phytologist.* **213**(3), 1346-62 (2017). doi: 10.1111/nph.14220.

(51) N. Patterson, A.L. Price, D. Reich D, Population Structure and Eigenanalysis. *PLoS Genet.* **2**(12), e190 (2006). doi: 10.1371/journal.pgen.0020190.

(52) S.J. Welham, R. Thompson, Likelihood Ratio Tests for Fixed Model Terms using Residual Maximum Likelihood. *J. R. Statist. Soc.* **59**(3), 701-714 (1997). doi: 10.1111/1467-9868.00092.

(53) M.P. Boer, D. Wright, L. Feng, D.W. Podlich, L. Luo, M. Cooper, F.A. van Eeuwijk, A mixed-model quantitative trait loci (QTL) analysis for multiple-environment trial data using environmental covariables for QTL-by-environment interactions, with an example in maize. *Genetics.* **177**(3), 1801-13 (2007). Doi: 10.1534/genetics.107.071068.

(54) B. Devlin, K. Roeder K, Genomic control for association studies. *Biometrics* **55**, 997–1004 (1999). Doi: 10.1111/j.0006-341X.1999.00997.x

- (55) J. Li, L. Ji, Adjusting multiple testing in multilocus analyses using the eigenvalues of a correlation matrix. *Heredity (Edinb)*. **95**(3), 221–227 (2005). doi:10.1038/sj.hdy.6800717.
- (56) [M. Alaux, J. Rogers, T. Letellier, R. Flores, F. Alfama, C. Pommier, N. Mohellibi, S. Durand, E. Kimmel, C. Michotey, C. Guerche, M. Loaec, M. Lainé, D. Steinbach, F. Choulet, H. Rimbart, P. Leroy, N. Guilhot, J. Salse, C. Feuillet; International Wheat Genome Sequencing Consortium, E. Paux, K. Eversole, A.F. Adam-Blondon, H. Quesneville, Linking the International Wheat Genome Sequencing Consortium bread wheat reference genome sequence to wheat genetic and phenomic data. *Genome Biol.* **19**\(1\):111 \(2018\). doi: 10.1186/s13059-018-1491-4.](#)

SUPPLEMENTARY ONLINE MATERIAL

TABLE OF CONTENT

<u>SECTIONS</u>	<u>PAGES</u>
<u>Table S1:</u> <i>Wheat genotype panel.</i>	2
<u>Table S2:</u> <i>Wheat structural variants.</i>	3
<u>Table S3:</u> <i>Genes/loci with selection signatures.</i>	4
<u>Table S4:</u> <i>Genes/loci of GWAS for heading date (HD).</i>	5
<u>Table S5:</u> <i>Genes/loci of GWAS for plant height (PH).</i>	7
<u>Table S6:</u> <i>Inference of gene flow using Patterson's D.</i>	9
<u>Table S7:</u> <i>Edge support of the minimum spanning trees of the phylogenetic network.</i>	11
<u>Figure S1:</u> <i>Sequence coverage at the genome scale.</i>	13
<u>Figure S2:</u> <i>Chromosomal distribution of structural variants.</i>	15
<u>Figure S3:</u> <i>Distribution of structural (SNPs, InDels) variants.</i>	16
<u>Figure S4:</u> <i>Wheat genotypes relatedness and components of the panel structuration.</i>	17
<u>Figure S5:</u> <i>Geographical component of the panel structuration.</i>	21
<u>Figure S6:</u> <i>Selection (domestication) signatures.</i>	22
<u>Figure S7:</u> <i>Selection (breeding) signatures.</i>	23
<u>Figure S8:</u> <i>GWAS for heading date (HD).</i>	34
<u>Figure S9:</u> <i>GWAS for plant height (PH).</i>	35
<u>Figure S10:</u> <i>Inference of reticulated evolutionary scenario with phylogenetic networks.</i>	36
<u>Figure S11:</u> <i>Wheat phylogenetic relationships.</i>	37
<u>Figure S12:</u> <i>Inference of reticulated evolutionary scenario with ABBA-BABA test.</i>	39
<u>Figure S13:</u> <i>Network analysis of bread wheat community structure.</i>	40

Table S1: Wheat genotype panel. The wheat diversity panel consisting of 487 genotypes is detailed in the current table with the number of genotypes separated by ploidy level (di-, tetra- and hexaploid), the historical categories (landraces, old cultivars, cultivars and modern varieties for the 435 hexaploid genotypes) as well as the continents of origin (Africa, America, Asia, Europe and Oceania).

		Africa	America	Asia	Europe	Oceania	NA	TOTAL
Ploidy levels	Diploid	0	0	12	1	0	0	13
	Tetraploid AB	1	1	18	5	0	0	25
	Tetraploid AG	0	0	13	0	0	0	13
	Hexaploid ABD	18	28	123	255	6	5	435
	Hexaploid GAA	0	0	0	1	0	0	1
	TOTAL	19	29	166	262	6	5	487
Hexaploids ABD	Group I (Landraces)	5	5	52	31	2	0	95
	Group II (Old cultivars)	5	12	24	56	2	0	99
	Group III (Cultivars)	8	11	34	70	2	5	130
	Group IV (Current varieties)	0	0	7	92	0	0	99
	NA	0	0	6	6	0	0	12
	TOTAL	18	28	123	255	6	5	435

Note: Detailed passport information for the 487 genotypes are made available at https://urgi.versailles.inra.fr/download/iwgc/IWGC_RefSeq_Annotations/v1.0/iwgc_refseqv1.0_Wheatbi_GWAS.zip

Table S2: Wheat structural variants. Exome sequencing of the 435 AABBDD hexaploid genotypes delivered 595,939 variants detailed in the current table with the number of variants (SNPs and InDels), the number of genic and non-genic variants and associated ratio (genic/non-genic) with the number of targeted genes per chromosomes.

Chr	SNPs	InDels	Variants	Genic variants	Non-genic variants	Ratio genic/non-genic	Genes
1A	29526	3213	32739	17855	14884	1,20	2334
1B	37125	3719	40844	23640	17204	1,37	2476
1D	11451	1158	12609	8019	4590	1,75	984
2A	36398	3792	40190	23415	16775	1,40	2923
2B	52083	4959	57042	35326	21716	1,63	3184
2D	20377	1695	22072	15956	6116	2,61	1344
3A	27116	2964	30080	17350	12730	1,36	2280
3B	40405	4223	44628	25419	19209	1,32	2874
3D	10732	805	11537	7921	3616	2,19	867
4A	25807	2707	28514	16683	11831	1,41	2268
4B	18760	2063	20823	12141	8682	1,40	1840
4D	2133	208	2341	1407	934	1,51	408
5A	28917	3197	32114	17763	14351	1,24	2461
5B	37473	3875	41348	24626	16722	1,47	2716
5D	6557	668	7225	4866	2359	2,06	759
6A	29338	2914	32252	19854	12398	1,60	1991
6B	39341	3744	43085	24441	18644	1,31	2412
6D	8760	718	9478	6486	2992	2,17	757
7A	36616	3748	40364	22729	17635	1,29	2815
7B	33348	3296	36644	20792	15852	1,31	2331
7D	9203	807	10010	6603	3407	1,94	1008
Total	541466	54473	595939	353292	242647	1,46	41032

Chr = Chromosomes

SNPs = Single Nucleotide Polymorphism

InDels = Insertions / Deletions

Note: Detailed information for the 595939 variants are made available at https://urgi.versailles.inra.fr/download/iwgs/IWGS_RefSeq_Annotations/v1.0/iwgs_refseqv1.0_Wheatbi_GWAS.zip. 'SNPs/InDels/Variants' columns count include those associated with 'NA' high confidence annotation (ANNHC==NA), 'Genes' column does not count genes with only 'Upstream' and 'Downstream' variants despite they might have an associated ANNHC. 'Non-genic' variants include both 'Upstream' and 'Downstream' variants as well as variants without associated ANNHC. In any case, a variant is only considered if we have at least a non-imputed REF and an ALT variant amongst the 435 genotypes.

Table S3: Genes/loci with selection signatures. A- DOMESTICATION -The table shows the list of genes (lines) within genomic windows (1 Mb) showing the signatures of domestication based on ROD values with the chromosome, the position, the ROD value (between diploid vs tetraploids, diploids vs hexaploids and between tetraploids vs hexaploids) as well as the closest (distance in bp) regions of domestication signature (referred to as ‘closest’ for diploid vs tetraploids, diploids vs hexaploids and between tetraploids vs hexaploids), cf details in Supplementary Figure S6. In dark and light red are respectively highlighted candidate genes associated with a ROD > 0.8 or in close vicinity (0 to 5 Mb) to a regions of domestication signature. **B- IMPROVEMENT**- The table illustrates the list of genes (lines) with a Fst log10 p-value with the chromosome, the position, the log p-value of Fst value (for European genotypes, Asian genotypes and the total panel) as well as the closest (distance in kb) loci of improvement signature (referred to as ‘closest’ for European genotypes, Asian genotypes and the total panel), cf details in Supplementary Figure S7. Candidate genes in close vicinity (0 to 5 Mb, light red) to a regions of improvement signature (-log₁₀ p-value > 4, dark red).

A

Ch	Candidate gene	Start	End	ROD			CLOSEST	CLOSEST	CLOSEST
				Diplo/Tetra	Diplo/Hexa	Tetra/Hexa	Diplo/Tetra (bp)	Diplo/Hexa (bp)	Tetra/Hexa (bp)
2B	Tg1-D1-2B_TraesCS2B01G069900	37014771	37016949	NA	NA	0.51661305	2014771	14771	1983051
2B	Tg1-D1-2B_TraesCS2B01G070100	37215637	37217426	NA	NA	0.51661305	2215637	215637	1782574
2B	Tg1-D1-2B_TraesCS2B01G070200	37232704	37234837	NA	NA	0.51661305	2232704	232704	1765163
2B	Tg1-D1-2B_TraesCS2B01G070300	37249866	37252001	NA	NA	0.51661305	2249866	249866	1747999
2B	Tg1-D1-2B_TraesCS2B01G070600	37357849	37359766	NA	NA	0.51661305	2357849	357849	1640234
2D	Tg1-D1-2D_TraesCS2D01G058000	23025170	23026950	NA	1	NA	NA	22525171	NA
2D	Tg1-D1-2D_TraesCS2D01G058100	23044249	23046449	NA	1	NA	NA	22544250	NA
2D	Tg1-D1-2D_TraesCS2D01G058200	23052167	23054186	NA	1	NA	NA	22552168	NA
3A	ttbrt2-3A_TraesCS3A01G101100	65701162	65701940	NA	NA	1	18298060	20701162	65201163
3A	ttbrt2-3A_TraesCS3A01G101200	65764573	65765252	NA	NA	1	18234748	20764573	65264574
3B	ttbrt1-3B_TraesCS3B01G118900	88966485	88967048	NA	NA	NA	32952	32952	28966485
5A	Q / WAP2-5A_TraesCS5A01G473800	650127258	650130900	NA	NA	0.869697263	338127258	3127258	649627259
5B	Ph1-5B_TraesCS5B01G256100	439001606	439002484	-1.345118483	-2.865789242	-0.648440908	4001606	4001606	9001606
5B	Q / WAP2-5B_TraesCS5B01G486900	658092415	658095219	0.3590729	0.474488772	0.180076442	92415	16904781	7092415
5D	Q / WAP2-5D_TraesCS5D01G486600	521712820	521716475	NA	NA	NA	NA	283525	NA

B

Ch	Candidate gene	Start	End	EUROPE		ASIA		TOTAL	
				CLOSEST (bp)	Log10 p-value	CLOSEST (bp)	Log10 p-value	CLOSEST (bp)	Log10 p-value
2A	PPD-2A_TraesCS2A01G081900	36933684	36938202	1014296	6.222608561	34558461	7.653283701	NA	NA
2D	PPD-2D_TraesCS2D01G079600	33952048	33956269	3622559	4.969301935	14331120	4.217516053	NA	NA
2A	WFZP-2A_TraesCS2A01G116900	66848645	66849948	NA	NA	13422647	7.569832191	1404207	4.18149316
2B	taGNS4-DWARF11-2B_TraesCS2B01G350400	49779514	497799657	1411567	4.112672964	34516519	4.412915567	80805948	5.716901037
3A	taCUL4-3A_TraesCS3A01G489000	716756231	716759651	NA	NA	3463121	4.127070788	NA	NA
4A	Rht-A1_TraesCS4A01G271000	582477351	582479578	5427350	5.067481185	2457065	7.096465632	115554948	4.074652166
4B	Rht1-4B_TraesCS4B01G043100	30861268	30863723	163355874	4.364068417	2702645	4.926662236	NA	NA
5A	Vrn1-5A_TraesCS5A01G391700	587411454	587423416	1982007	4.085109533	6043921	4.540690006	35027756	4.513724705
7B	Vrn3-7B_TraesCS7B01G013100	9702354	9704354	62597913	4.680303618	4185401	4.18632876	NA	NA
7A	Wx-7A_TraesCS7A01G070100	35765406	35769104	3713171	4.109418316	11859876	4.569052393	NA	NA
4A	Wx-4A_TraesCS4A01G418200	688097145	688100962	3506602	4.250229066	38111058	6.440864543	NA	NA
1A	Ta_Omegagli_1_1AS_TraesCS1A01G008200LC	3019865	3021011	NA	NA	1807980	5.027761558	NA	NA
1A	Ta_Omegagli_5_1AS_TraesCS1A01G040200LC	16373919	16375293	25732139	4.099262322	2227548	4.534072986	21126300	4.274351555
1B	Ta_Gammagli_2_1BS_TraesCS1B01G010400	4965590	4966767	NA	NA	654	13.20496222	NA	NA
1B	Ta_LMWglu_m_4_1BS_TraesCS1B01G013500	6436429	6437481	NA	NA	1812540	5.376062278	NA	NA
1D	Ta_LMWglu_m_3_IDS_TraesCS1D01G007400	3709269	3710801	NA	NA	1212352	9.498772259	NA	NA
3B	Ta_Alphagli_1_6AS_TraesCS6A01G048900	24921651	24922607	94197322	4.055958953	1231267	11.276844	NA	NA
6A	Ta_Alphagli_9_6AS_TraesCS6A01G049800	25581107	25582249	NA	NA	1349900	4.673679708	NA	NA
6B	Ta_Alphagli_6_6B_TraesCS6B01G086000LC	43384370	43385438	NA	NA	843720	4.393608745	1410315	4.246574756
6B	Ta_Alphagli_18_6B_TraesCS6B01G086500	62653690	62655549	NA	NA	4940623	4.316523025	NA	NA

Table S4: Genes/loci of GWAS for heading date (HD). List of 48 significant loci with information on chromosome, position, $-\log_{10}(p)$, reference allele frequency (Freq_ref), mean heading date value for genotypes carrying the reference allele (MeanHD_ref), alternative allele frequency (Freq_alt), mean heading value for genotypes carrying the alternative allele (MeanHD_alt). Candidate genes known to control wheat flowering time are also indicated, along with their distance relative to the peak marker: *Ppd*, *VNr*, *FDL* (Flowering Locus D like), *WPCL* (Phytoclock).

GWAS INFORMATION								GENE INFORMATION		
SNP	Chr	Position (Bp)	$-\log_{10}p$	Freq_alt	Freq_ref	MeanHD_alt	MeanHD_ref	Locus	Distance (bp)	Gene
WTa_0004c0	1A	3 925 345	7.05	0.33	0.67	193.26	197.98			
WTa_005e27	1A	493 919 389	5.14	0.11	0.89	194.49	197.73	<i>FDL2-1A</i>	4 613 242	TraesCS1A01G306300
WTa_098362	1A	532 090 225	5.15	0.06	0.94	194.50	200.48			
WTa_098ae0	1B	3 145 926	5.39	0.07	0.93	194.38	200.73			
WTa_01164e	1B	642 195 298	8.62	0.32	0.68	196.47	190.77			
WTa_01b54a	2A	576 658 412	21.00	0.28	0.72	193.46	198.31			
WTa_01aedf	2A	542 651 377	21.88	0.30	0.70	193.79	197.24			
WTa_0222b2	2B	65 103 645	6.76	0.33	0.67	196.31	191.82	<i>Ppd-B1</i>	Not anchored	TraesCSU01G196100
WTa_027762	2B	612 677 432	5.91	0.15	0.85	194.24	198.29			
WTa_0a0f7b	2B	704 722 984	6.72	0.20	0.80	194.27	197.16			
WTa_02cb56	2B	793 150 109	6.06	0.37	0.63	194.89	194.73			
WTa_0338c6	3A	20 790 590	5.26	0.47	0.53	192.16	197.83			
WTa_0371de	3A	541 219 918	7.09	0.22	0.78	194.11	197.46			
WTa_038ba0	3A	658 890 298	7.46	0.23	0.77	193.97	197.75			
WTa_0a62fb	3A	739 398 905	6.42	0.34	0.66	194.67	195.14	<i>WPCL-A1</i>	713 783	TraesCS3A01G526600
WTa_03ca44	3B	26 587 395	5.86	0.25	0.75	193.46	198.90			
WTa_03fd37	3B	412 247 309	7.04	0.12	0.88	194.15	199.72			
WTa_1009876	3B	661 828 498	6.96	0.34	0.66	194.83	194.84			
WTa_04321e	3B	721 054 655	8.21	0.11	0.89	194.70	195.88			
WTa_0a8b72	3B	801 310 052	10.55	0.09	0.91	194.40	199.32			
WTa_048148	3D	604 700 005	8.57	0.11	0.89	194.44	198.12	<i>WPCL-D1</i>	3 222 796	TraesCS3D01G531900
WTa_049455	4A	69 323 150	6.01	0.40	0.60	194.24	195.74			
WTa_04c457	4A	597 715 179	10.56	0.32	0.68	193.12	198.48			
WTa_0ab5ee	4A	698 017 543	5.48	0.12	0.88	194.65	196.14			
WTa_04e890	4A	719 060 514	5.71	0.18	0.82	194.76	195.16			
WTa_04f5b3	4A	735 168 126	6.00	0.05	0.95	194.60	199.03			
WTa_051528	4B	28 943 424	5.76	0.10	0.90	194.17	200.55			
WTa_0acb27	4B	428 008 325	7.46	0.46	0.54	192.29	197.87			
WTa_054aa7	4B	617 324 528	6.99	0.05	0.95	194.73	196.76			
WTa_0571ab	5A	18 673 706	5.55	0.05	0.95	194.80	195.39			
WTa_05a506	5A	470 932 716	5.54	0.06	0.94	194.76	195.96			
WTa_05cd79	5A	582 940 178	7.63	0.31	0.69	192.84	199.21	<i>Vrn- A1</i>	4 471 276	TraesCS5A01G391700
WTa_05e925	5A	676 593 045	9.76	0.13	0.87	194.19	199.10			
WTa_0604fe	5B	36 187 575	8.18	0.25	0.75	193.53	198.72			
WTa_0651f8	5B	550 849 380	5.91	0.34	0.66	194.68	195.12			
WTa_066c0b	5B	636 914 997	7.29	0.50	0.50	193.25	196.44			

WTa_0b1881	5B	668 826 335	7.49	0.44	0.56	194.60	195.12			
WTa_06b2c4	6A	768 807	7.77	0.18	0.82	194.03	198.52			
WTa_0b47c0	6A	600 404 207	5.90	0.09	0.91	194.42	198.79			
WTa_07680b	6B	145 889 587	9.03	0.37	0.63	193.88	196.49			
WTa_0b6a61	6B	657 090 484	6.74	0.46	0.54	194.98	194.66			
WTa_07c1aa	6B	696 302 933	5.85	0.43	0.57	196.89	192.08			
WTa_0832a6	7A	61 817 674	7.32	0.35	0.65	192.88	198.40	Vrn-A3	9 852 180	TraesCS7A01G115400
WTa_0876d1	7A	545 066 157	5.91	0.20	0.80	193.94	198.39			
WTa_0890f3	7A	657 090 590	9.34	0.09	0.91	194.42	199.24			
WTa_08ccad	7B	109 934 421	10.50	0.11	0.89	194.06	200.94			
WTa_08de86	7B	245 621 526	10.37	0.09	0.91	194.71	196.17			
WTa_091d76	7B	702 323 253	5.99	0.23	0.77	193.69	198.63			

Table S5: Genes/loci of GWAS for plant height (PH). List of 40 significant loci with information on chromosome, position, $-\log_{10}(p)$, reference allele frequency (Freq_ref), mean plant height value for genotypes carrying the reference allele (MeanPH_ref), alternative allele frequency (Freq_alt), mean plant height value for genotypes carrying the alternative allele (MeanPH_alt). Candidate genes known to control plant height are also indicated, along with their distance relative to the peak marker; *Rht* B1 and additional determinants of the trait that still remain to be identified.

GWAS INFORMATION								GENE INFORMATION		
SNP	Chr	Position (Bp)	$\log_{10}p$	Freq_alt	Freq_ref	MeanPH_alt	MeanPH_ref	Locus	Distance (bp)	Gene
WTa_0012b7	1A	14 139 090	6.9	0.18	0.82	94.55	106.42			
WTa_003a69	1A	297 874 484	5.81	0.08	0.92	95.76	107.13			
WTa_005e2b	1A	493 919 653	5.56	0.11	0.89	94.76	112.26			
WTa_00a323	1B	24 351 197	4.78	0.1	0.9	95.41	107.98			
WTa_00f99e	1B	555 050 237	6.59	0.07	0.93	95.50	112.25			
WTa_011425	1B	639 071 657	6.61	0.13	0.87	99.12	73.09			
WTa_01aecd	2A	542 651 377	4.84	0.3	0.7	95.21	99.97			
WTa_022e13	2B	105 693 461	5.7	0.43	0.57	101.78	89.86			
WTa_024fa1	2B	249 518 161	7.28	0.06	0.94	95.39	114.96			
WTa_02e4c1	2D	26 435 328	4.13	0.12	0.88	99.63	75.16			
WTa_038b2e	3A	657 927 878	5.7	0.17	0.83	93.22	113.95			
WTa_03ff18	3B	418 890 134	7.06	0.17	0.83	94.80	106.01			
WTa_04249e	3B	655 492 298	8.47	0.12	0.88	93.99	116.69			
WTa_044fa5	3B	801 126 924	5.33	0.13	0.87	94.34	89.70			
WTa_047de8	3D	598 012 984	6.09	0.16	0.84	93.66	112.79			
WTa_049455	4A	69 323 150	6.95	0.4	0.6	90.17	106.56			
WTa_04c473	4A	597 847 219	5.31	0.4	0.6	101.59	89.18	<i>Rht-A1</i>	15 369 868	TraesCS4A01G271000
WTa_0ab80a	4A	715 811 193	9.15	0.11	0.89	98.19	84.80			
WTa_04fc6b	4A	739 524 085	8.05	0.41	0.59	101.99	89.02			
WTa_0517e6	4B	43 751 460	7.47	0.11	0.89	99.12	76.76	<i>Rht-B1</i>	12 890 192	TraesCS4B01G043100
WTa_056214	4D	16 156 318	8.74	0.12	0.88	99.58	70.93	<i>Rht-D1</i>	2 624 744	TraesCS4D01G040400
WTa_0ada7c	5A	1 201 636	5.65	0.11	0.89	94.29	96.77			
WTa_05cd79	5A	582 940 178	7.51	0.31	0.69	92.17	106.50			
WTa_05e925	5A	676 593 045	7.54	0.13	0.87	95.16	106.52			
WTa_0b1b09	5B	689 225 862	6.52	0.42	0.58	89.19	107.02			
WTa_0b2a77	5D	550 418 603	5.13	0.33	0.67	102.17	85.51			
WTa_100f74e	6A	635 418	5.92	0.42	0.58	110.27	93.97			
WTa_06e09a	6A	68 132 978	5.58	0.37	0.63	102.83	86.35			
WTa_070d20	6A	555 230 205	5.57	0.07	0.93	95.10	118.41			
WTa_10101a5	6A	447 628 696	6.73	0.42	0.58	107.29	94.55			
WTa_0763d0	6B	132 345 397	6.52	0.21	0.79	93.80	107.16			
WTa_077796	6B	208 178 702	6.31	0.11	0.89	98.14	84.66			
WTa_0b6a61	6B	657 090 484	5.08	0.46	0.54	88.44	106.48			
WTa_07d83d	6B	715 887 242	5.24	0.17	0.83	98.45	87.61			
WTa_07f3af	6D	402 836 584	8.44	0.23	0.77	102.06	78.07			
WTa_083823	7A	77 494 119	4.8	0.11	0.89	95.95	102.16			
WTa_0890f3	7A	657 090 590	7.67	0.09	0.91	94.44	120.49			

WTa_0897c3	7A	677 848 259	5.76	0.36	0.64	93.48	102.33
WTa_08cbd8	7B	105 886 261	6.11	0.27	0.73	93.25	105.90
WTa_08e7fc	7B	380 855 540	6.16	0.17	0.83	94.67	106.03

Table S6: Inference of gene flow using Patterson's D. Patterson's D and Z values were inferred using ANGSD³⁰ and *T. dicoccoides* as outgroup population. Tests relevant to the chosen consensus topology are highlighted in red (right). Z-values retained for figure S12 are highlighted in the colour relevant to their subgenome (green for subgenome A and purple for subgenome B).

D	Z	H1	H2	H3	H4	subgenome
-0,496	-37,955	T_durum	T_spelta	T_durum_x_T_dicoccoides	T_dicoccoides	A
-0,363	-27,399	T_durum	T_aestivum	T_durum_x_T_dicoccoides	T_dicoccoides	A
0,493	37,767	T_dicocum	T_durum	T_durum_x_T_dicoccoides	T_dicoccoides	A
0,017	1,341	T_dicocum	T_spelta	T_durum_x_T_dicoccoides	T_dicoccoides	A
-0,227	-14,171	T_aestivum	T_spelta	T_durum_x_T_dicoccoides	T_dicoccoides	A
0,228	14,506	T_dicocum	T_aestivum	T_durum_x_T_dicoccoides	T_dicoccoides	A
-0,131	-8,697	T_durum	T_aestivum	T_dicocum	T_dicoccoides	A
0,199	14,140	T_aestivum	T_spelta	T_dicocum	T_dicoccoides	A
0,074	4,314	T_durum	T_spelta	T_dicocum	T_dicoccoides	A
-0,195	-9,444	T_aestivum	T_spelta	T_durum	T_dicoccoides	A
-0,516	-45,331	T_durum	T_aestivum	T_durum_x_T_dicoccoides	T_dicoccoides	B
-0,500	-40,551	T_durum	T_spelta	T_durum_x_T_dicoccoides	T_dicoccoides	B
0,533	47,446	T_dicocum	T_durum	T_durum_x_T_dicoccoides	T_dicoccoides	B
0,060	4,646	T_dicocum	T_aestivum	T_durum_x_T_dicoccoides	T_dicoccoides	B
0,071	5,144	T_dicocum	T_spelta	T_durum_x_T_dicoccoides	T_dicoccoides	B
0,015	1,123	T_aestivum	T_spelta	T_durum_x_T_dicoccoides	T_dicoccoides	B
0,217	18,826	T_aestivum	T_spelta	T_dicocum	T_dicoccoides	B
0,034	2,295	T_durum	T_aestivum	T_dicocum	T_dicoccoides	B
0,218	16,102	T_durum	T_spelta	T_dicocum	T_dicoccoides	B
0,091	5,549	T_aestivum	T_spelta	T_durum	T_dicoccoides	B
-0,475	-35,937	T_durum	T_durum_x_T_dicoccoides	T_spelta	T_dicoccoides	A
-0,464	-32,289	T_durum	T_durum_x_T_dicoccoides	T_aestivum	T_dicoccoides	A
-0,417	-30,561	T_durum	T_durum_x_T_dicoccoides	T_dicocum	T_dicoccoides	A
-0,360	-25,778	T_dicocum	T_durum_x_T_dicoccoides	T_spelta	T_dicoccoides	A
0,447	34,538	T_durum_x_T_dicoccoides	T_aestivum	T_spelta	T_dicoccoides	A
0,375	28,985	T_durum_x_T_dicoccoides	T_spelta	T_dicocum	T_dicoccoides	A
0,274	19,308	T_durum_x_T_dicoccoides	T_aestivum	T_dicocum	T_dicoccoides	A
0,245	13,332	T_durum_x_T_dicoccoides	T_spelta	T_aestivum	T_dicoccoides	A
-0,049	-2,716	T_dicocum	T_durum_x_T_dicoccoides	T_aestivum	T_dicoccoides	A
-0,027	-1,347	T_durum_x_T_dicoccoides	T_spelta	T_durum	T_dicoccoides	A
0,095	4,905	T_dicocum	T_durum_x_T_dicoccoides	T_durum	T_dicoccoides	A
0,121	7,560	T_durum_x_T_dicoccoides	T_aestivum	T_durum	T_dicoccoides	A
0,364	22,524	T_dicocum	T_durum	T_aestivum	T_dicoccoides	A
0,266	19,698	T_dicocum	T_spelta	T_aestivum	T_dicoccoides	A
0,244	13,007	T_dicocum	T_aestivum	T_durum	T_dicoccoides	A
-0,135	-7,350	T_durum	T_spelta	T_aestivum	T_dicoccoides	A
0,024	1,281	T_dicocum	T_durum	T_spelta	T_dicoccoides	A
0,062	3,555	T_durum	T_aestivum	T_spelta	T_dicoccoides	A
0,071	4,130	T_dicocum	T_aestivum	T_spelta	T_dicoccoides	A
0,097	5,666	T_dicocum	T_spelta	T_durum	T_dicoccoides	A
0,128	7,087	T_durum	T_aestivum	T_spelta	T_dicoccoides	B
0,179	11,724	T_dicocum	T_spelta	T_durum	T_dicoccoides	B
0,085	5,470	T_dicocum	T_aestivum	T_durum	T_dicoccoides	B
0,088	6,187	T_dicocum	T_aestivum	T_spelta	T_dicoccoides	B
0,051	3,042	T_dicocum	T_durum	T_aestivum	T_dicoccoides	B
-0,430	-32,924	T_durum	T_durum_x_T_dicoccoides	T_spelta	T_dicoccoides	B
-0,399	-32,780	T_durum	T_durum_x_T_dicoccoides	T_aestivum	T_dicoccoides	B

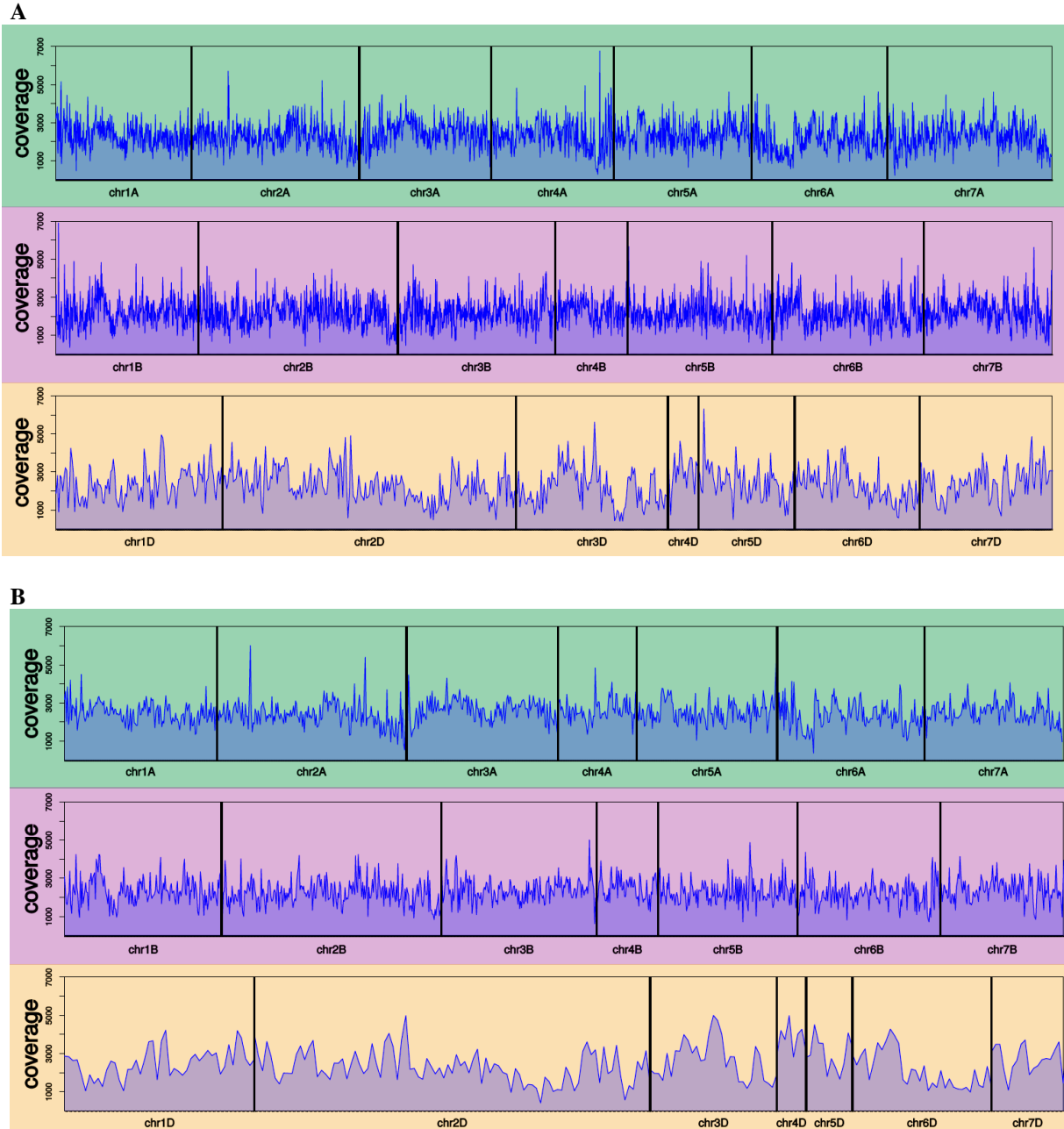
-0,366	-33,666	T_durum	T_durum_x_T_diccooides	T_dicoccum	T_diccooides	B
-0,335	-24,297	T_dicoccum	T_durum_x_T_diccooides	T_spelta	T_diccooides	B
-0,234	-16,020	T_dicoccum	T_durum_x_T_diccooides	T_aestivum	T_diccooides	B
0,427	33,251	T_durum_x_T_diccooides	T_spelta	T_aestivum	T_diccooides	B
0,415	28,803	T_durum_x_T_diccooides	T_aestivum	T_spelta	T_diccooides	B
0,396	33,753	T_durum_x_T_diccooides	T_spelta	T_dicoccum	T_diccooides	B
0,299	24,092	T_dicoccum	T_spelta	T_aestivum	T_diccooides	B
0,290	23,243	T_durum_x_T_diccooides	T_aestivum	T_dicoccum	T_diccooides	B
0,217	14,702	T_durum	T_spelta	T_aestivum	T_diccooides	B
0,208	12,220	T_dicoccum	T_durum_x_T_diccooides	T_durum	T_diccooides	B
-0,148	-8,147	T_durum_x_T_diccooides	T_aestivum	T_durum	T_diccooides	B
-0,088	-4,545	T_durum_x_T_diccooides	T_spelta	T_durum	T_diccooides	B
-0,040	-2,342	T_dicoccum	T_durum	T_spelta	T_diccooides	B

Table S7: Edge support of the minimum spanning trees of the phylogenetic network. The table delivers the subgenome specific inter-species edges of the minimum spanning trees of the phylogenetic network, maximizing the weight of the kept edges (plotted in Figure S10). Edges are linking a pair of accessions ('Id 1' and 'Id 2' columns) corresponding to a specific couple of species ('Species 1' and 'Species 2' columns) in phylogenetic network for the subgenome A, B or D ('Genome' column). The 'Support' column corresponds to the fraction of minimal spanning trees which support the corresponding edge.

Id_1	Id_2	Support	Genome	Species_1	Species_2
WW-241	WW-476	1	A	Triticum_sphaerococcum	Triticum_aestivum
WW-263	WW-242	1	A	Triticum_boeoticum	Triticum_zhukovskyi
WW-181	WW-179	1	A	Triticum_turgidum	Triticum_dicoccoides
WW-182	WW-179	1	A	Triticum_turgidum	Triticum_dicoccoides
WW-257	WW-249	0,867	A	Triticum_dicoccoides	Triticum_urartu
WW-249	WW-235	0,859	A	Triticum_urartu	Triticum_araraticum
WW-180	WW-257	0,819	A	Triticum_turgidum	Triticum_dicoccoides
WW-241	WW-083	0,798	A	Triticum_sphaerococcum	Triticum_aestivum
WW-260	WW-243	0,791	A	Triticum_dicoccoides	Triticum_dicoccum
WW-249	WW-242	0,78	A	Triticum_urartu	Triticum_zhukovskyi
WW-486	WW-245	0,707	A	Triticum_durum_x_Aegilops_tauschii	Triticum_durum
WW-234	WW-269	0,573	A	Triticum_araraticum	Triticum_timopheevii
WW-262	WW-384	0,516	A	Triticum_durum	Triticum_aestivum
WW-240	WW-264	0,503	A	Triticum_spelta	Triticum_dicoccum
WW-252	WW-253	0,497	A	Triticum_boeoticum	Triticum_monococcum
WW-241	WW-358	0,488	A	Triticum_sphaerococcum	Triticum_aestivum
WW-222	WW-262	0,451	A	Triticum_aestivum	Triticum_durum
WW-262	WW-368	0,436	A	Triticum_durum	Triticum_aestivum
WW-240	WW-265	0,411	A	Triticum_spelta	Triticum_dicoccum
WW-262	WW-455	0,362	A	Triticum_durum	Triticum_aestivum
WW-262	WW-260	0,334	A	Triticum_durum	Triticum_dicoccoides
WW-240	WW-394	0,305	A	Triticum_spelta	Triticum_aestivum
WW-179	WW-182	1	B	Triticum_turgidum	Triticum_dicoccoides
WW-476	WW-241	1	B	Triticum_aestivum	Triticum_sphaerococcum
WW-265	WW-240	0,946	B	Triticum_dicoccum	Triticum_spelta
WW-300	WW-241	0,934	B	Triticum_aestivum	Triticum_sphaerococcum
WW-180	WW-178	0,866	B	Triticum_turgidum	Triticum_durum
WW-243	WW-257	0,673	B	Triticum_dicoccum	Triticum_dicoccoides
WW-257	WW-264	0,606	B	Triticum_dicoccoides	Triticum_dicoccum
WW-486	WW-204	0,544	B	Triticum_durum_x_Aegilops_tauschii	Triticum_durum
WW-259	WW-274	0,505	B	Triticum_dicoccoides	Aegilops_speltoides
WW-486	WW-245	0,423	B	Triticum_durum_x_Aegilops_tauschii	Triticum_durum
WW-257	WW-262	0,418	B	Triticum_dicoccoides	Triticum_durum
WW-262	WW-299	0,404	B	Triticum_durum	Triticum_aestivum
WW-500	WW-262	0,36	B	Triticum_aestivum	Triticum_durum
WW-262	WW-240	0,343	B	Triticum_durum	Triticum_spelta
WW-455	WW-271	0,304	B	Triticum_aestivum	Triticum_spelta
WW-271	WW-299	0,291	B	Triticum_spelta	Triticum_aestivum
WW-300	WW-241	0,817	D	Triticum_aestivum	Triticum_sphaerococcum
WW-241	WW-476	0,797	D	Triticum_sphaerococcum	Triticum_aestivum
WW-066	WW-248	0,645	D	Triticum_durum_x_Aegilops_tauschii	Aegilops_tauschii
WW-490	WW-241	0,392	D	Triticum_aestivum	Triticum_sphaerococcum
WW-358	WW-241	0,316	D	Triticum_aestivum	Triticum_sphaerococcum
WW-490	WW-248	0,223	D	Triticum_aestivum	Aegilops_tauschii
WW-114	WW-240	0,162	D	Triticum_aestivum	Triticum_spelta

WW-487	WW-240	0,144	D	Triticum_aestivum	Triticum_spelta
WW-394	WW-240	0,135	D	Triticum_aestivum	Triticum_spelta
WW-222	WW-271	0,098	D	Triticum_aestivum	Triticum_spelta
WW-290	WW-271	0,081	D	Triticum_aestivum	Triticum_spelta

Figure S1: Sequence coverage at the genome scale. The figure illustrates the sequence coverage for each captured gene (A) and homoeolog triplet (B) for the 21 chromosomes (with genes in order) for the 435 hexaploid bread wheat genotypes. C- Boxplot of the normalized coverage (mean: 569.9341, standard deviation: 201.7955) between chromosomes (1 to 7) and subgenomes (A, B and D). The plain and dashed horizontal red lines respectively show the 1 and 1.96 standard deviation variation levels (corresponding to coverage intervals of respectively [366.1386,771.7296] and [174.4149,965.4532]). Medians all stays within the 1 standard deviation limit, as well as all 1st and 3rd quartiles.



c

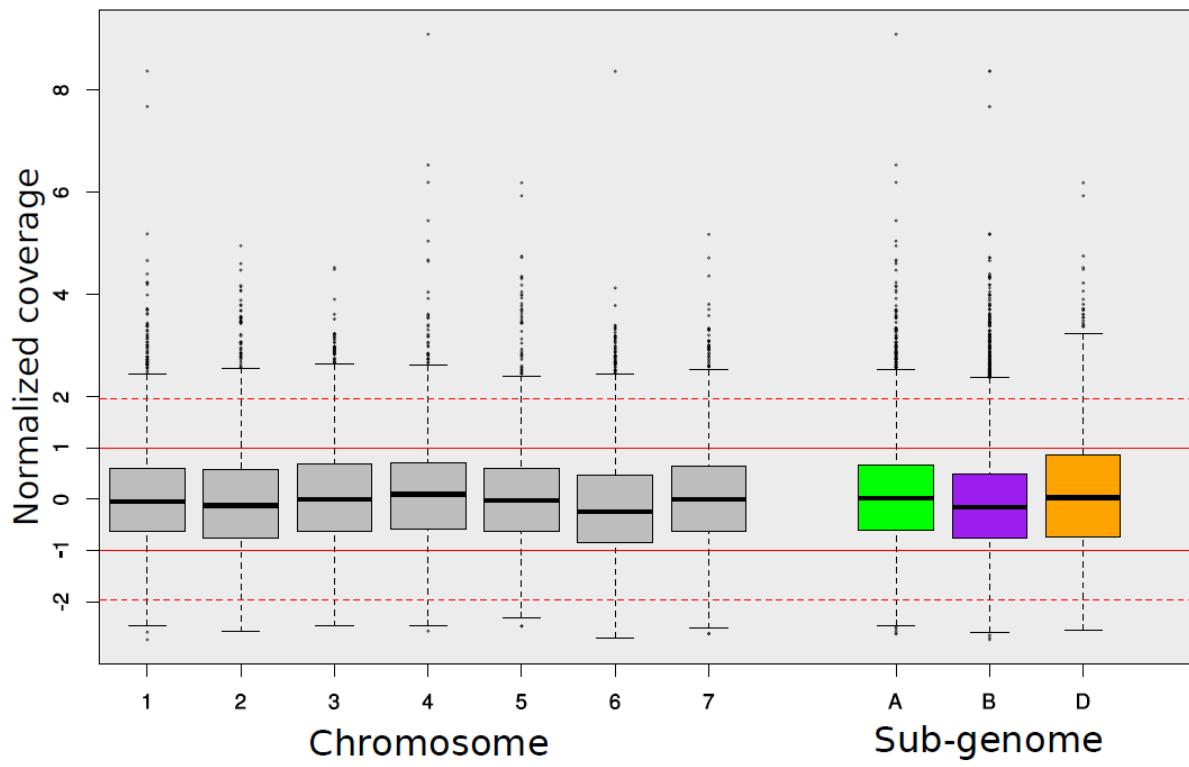
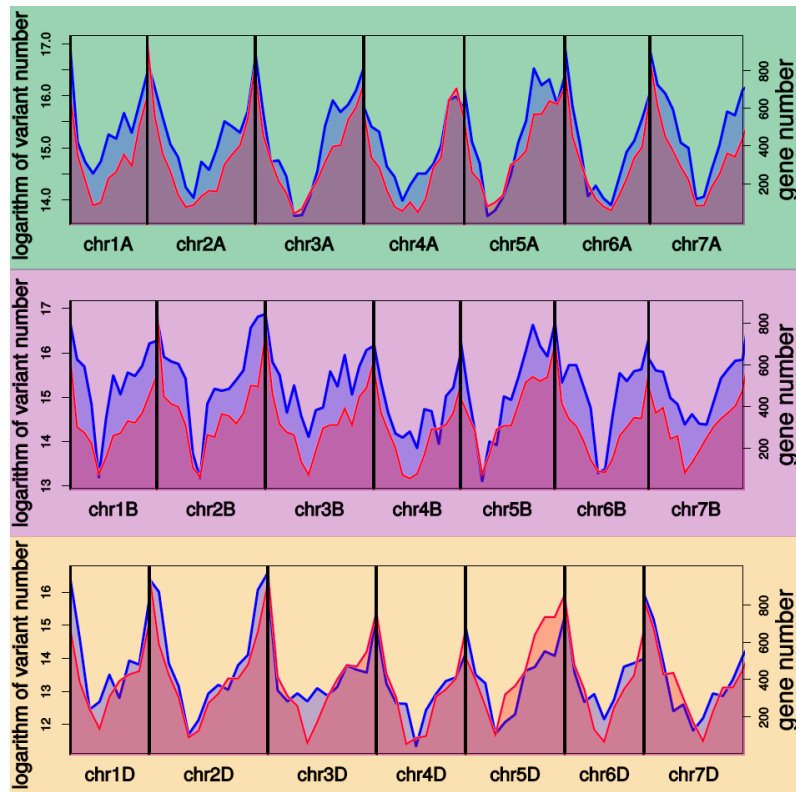


Figure S2: Chromosomal distribution of structural variants. **A-** Chromosome-wide distribution of genes (purple) as well as structural variants (blue) within 50 Mb sliding windows for the A (top), B (center) and D (bottom) subgenomes. **B-** Correlation between gene and structural variant distributions for subgenome A (left), B (center) and D (right) over 25 Mb sliding windows.

A



B

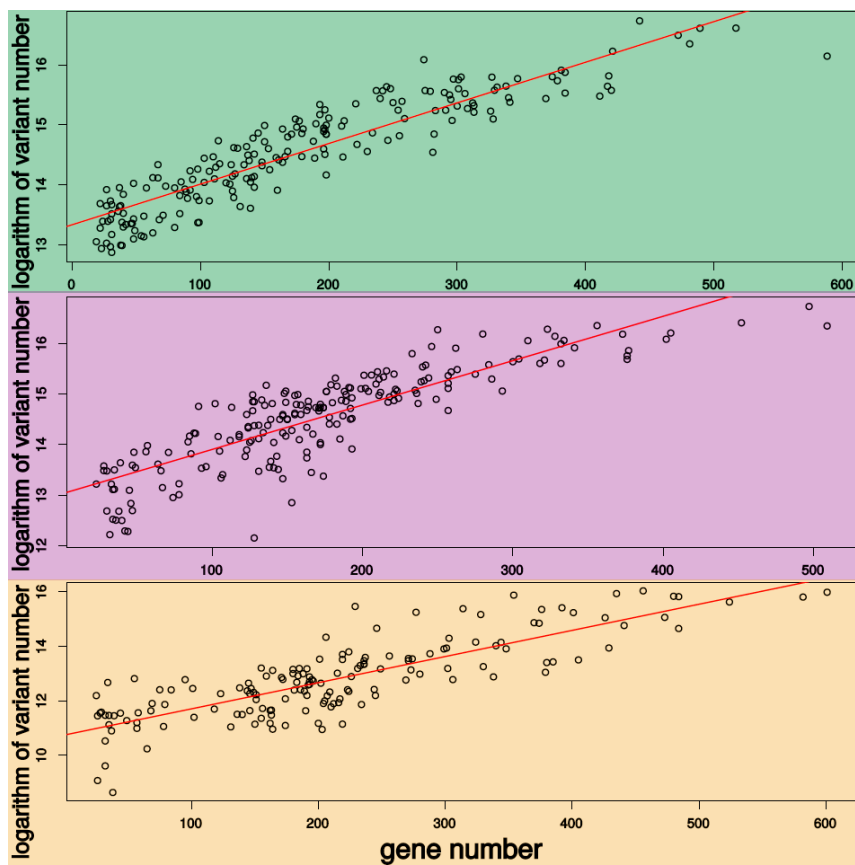
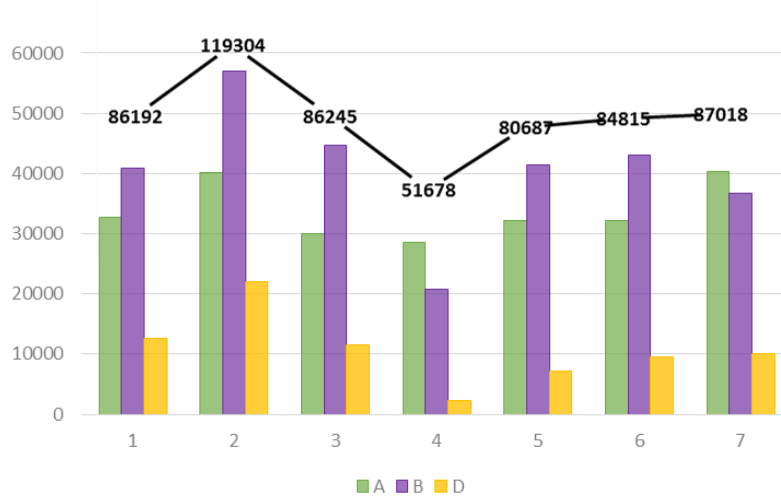
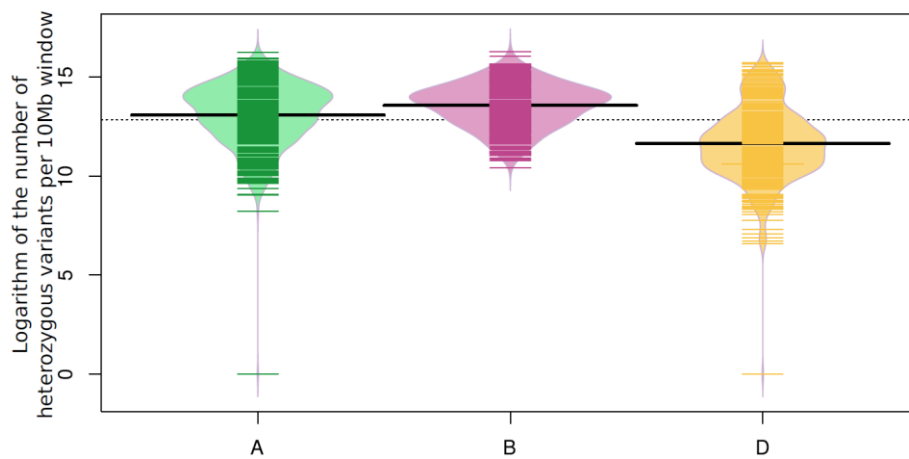


Figure S3: Distribution of structural (SNPs, InDels) variants. A- Number of structural variants (SNPs, InDels and total variants, y-axis) for each subgenome (A in green, B in purple and D in yellow) of the seven chromosomal groups (x-axis). Total number of variants per subgenomes are shown as black curve. Heterozygous variants' density per ten megabase windows in subgenomes (A, B and D; cf panel B) and genomic compartments (telomeric, core and centromeric; cf panel C). Values illustrated as bean plots with average and overall average values represented as solid and dotted black bar respectively.

A



B



C

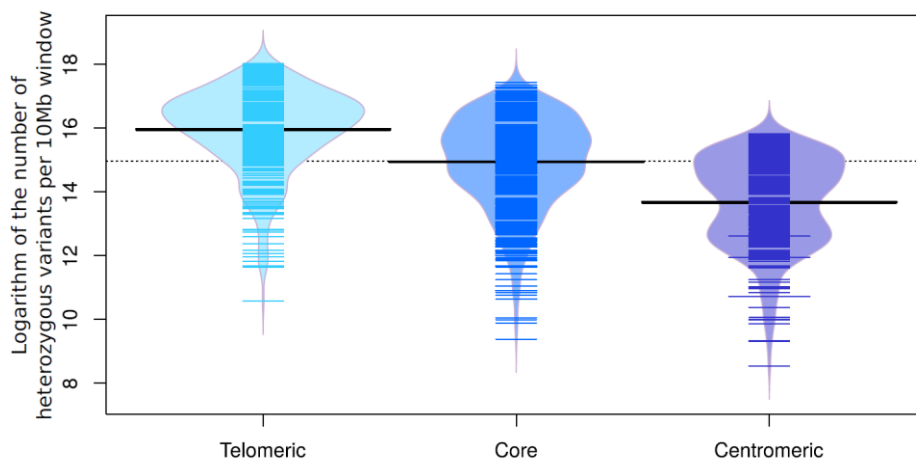
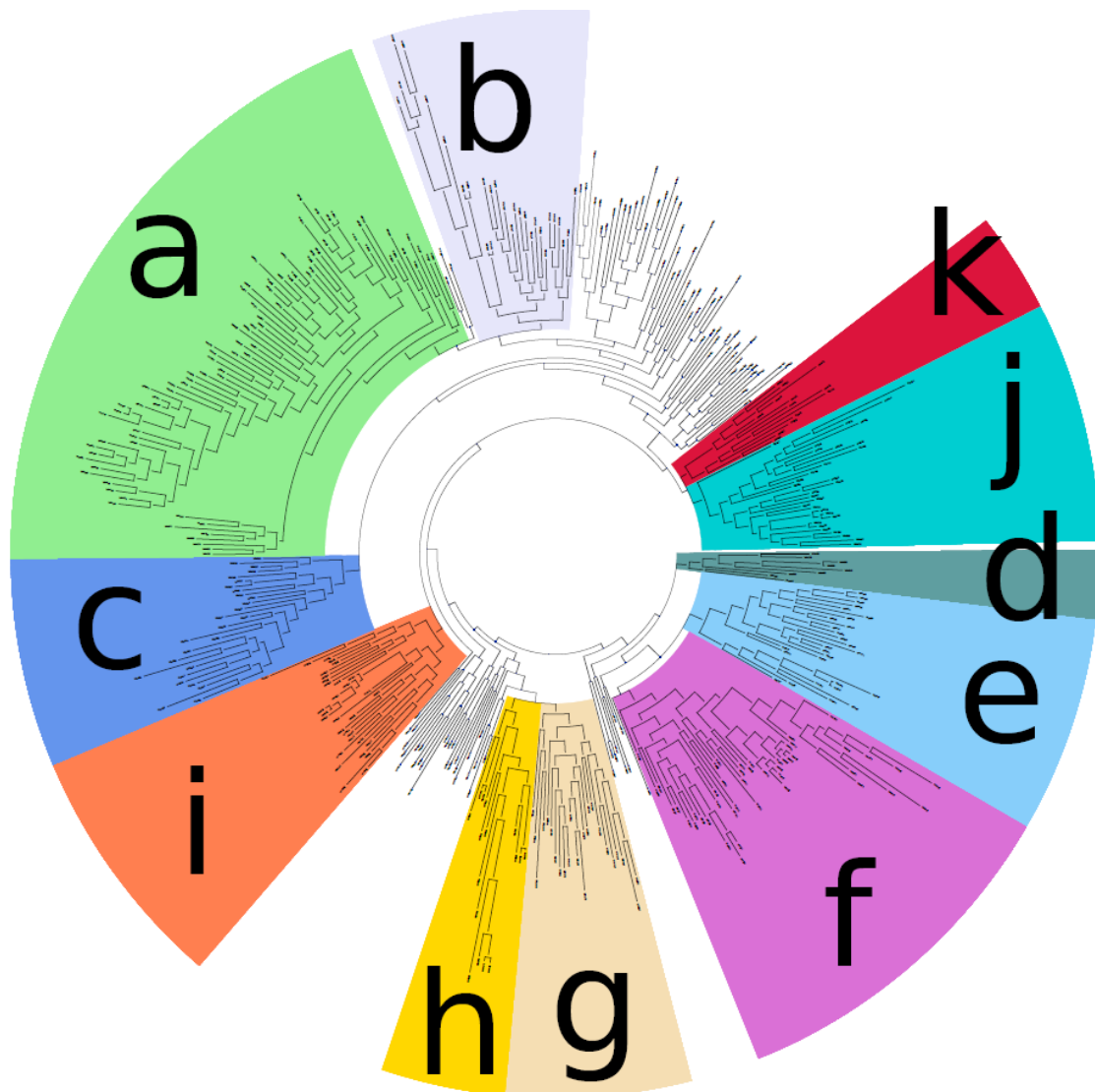
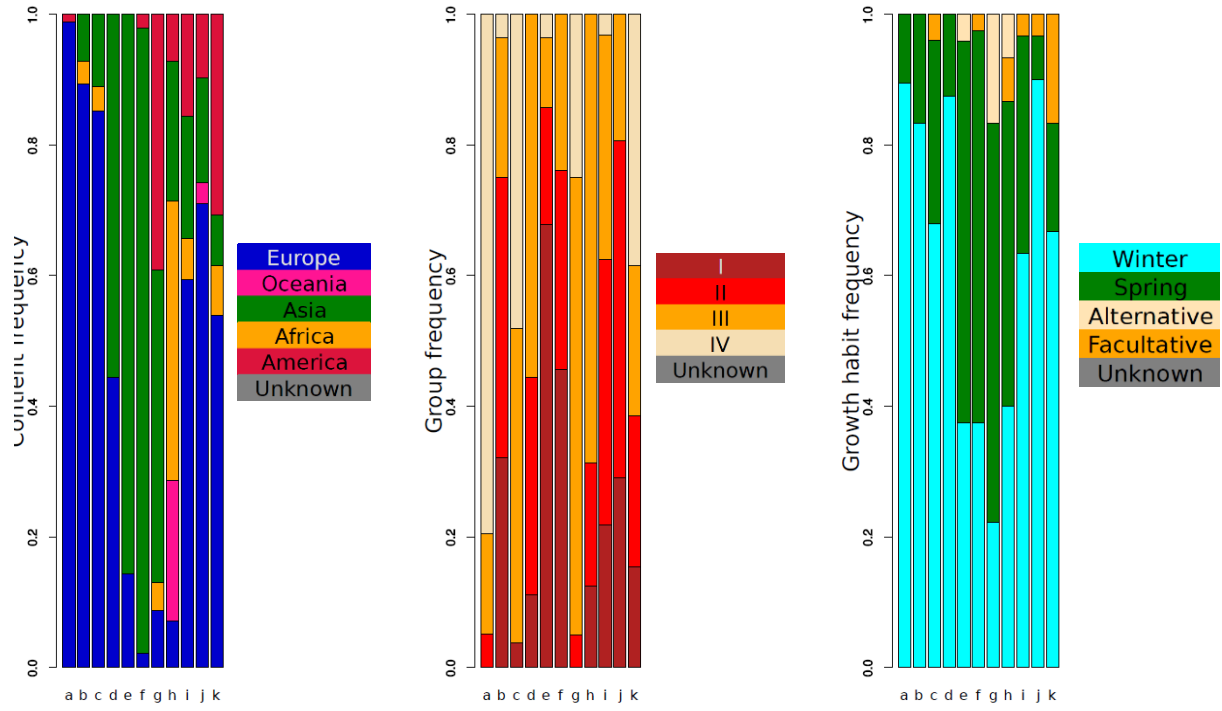
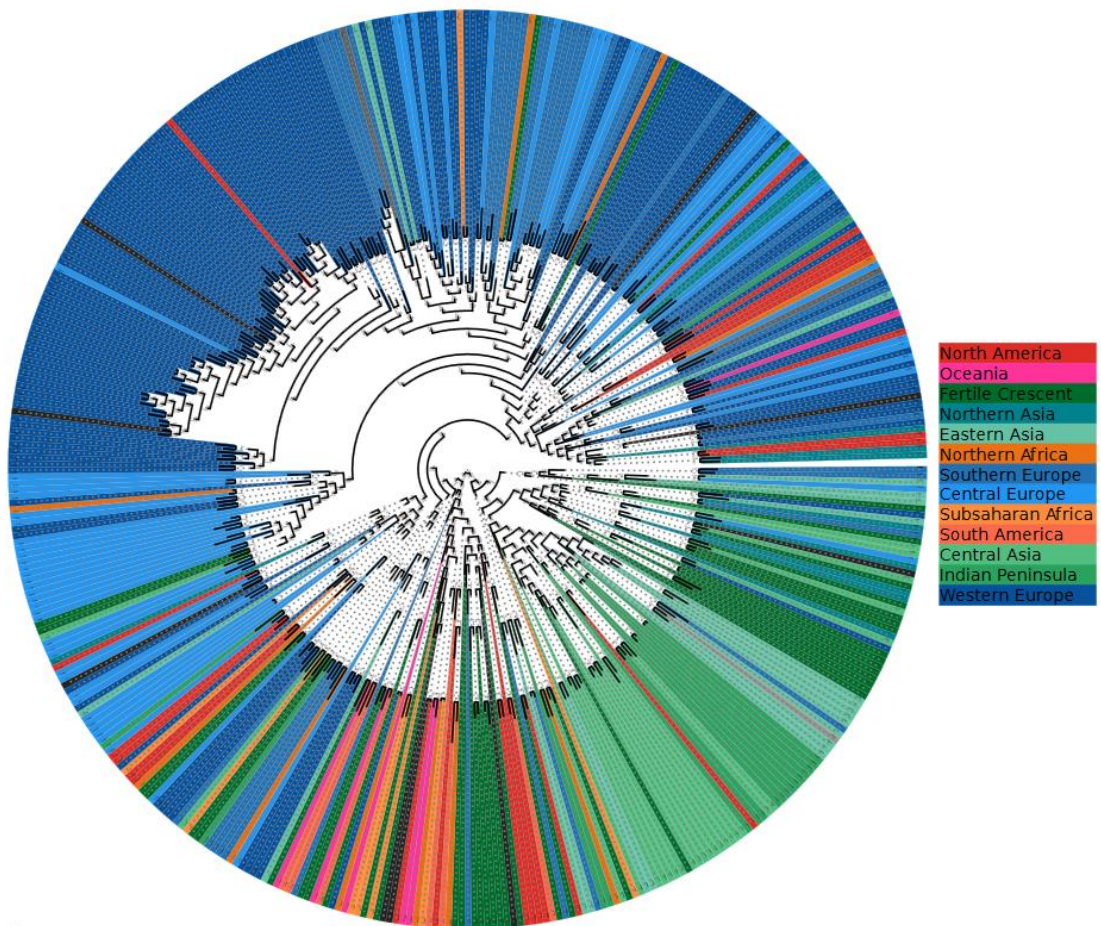


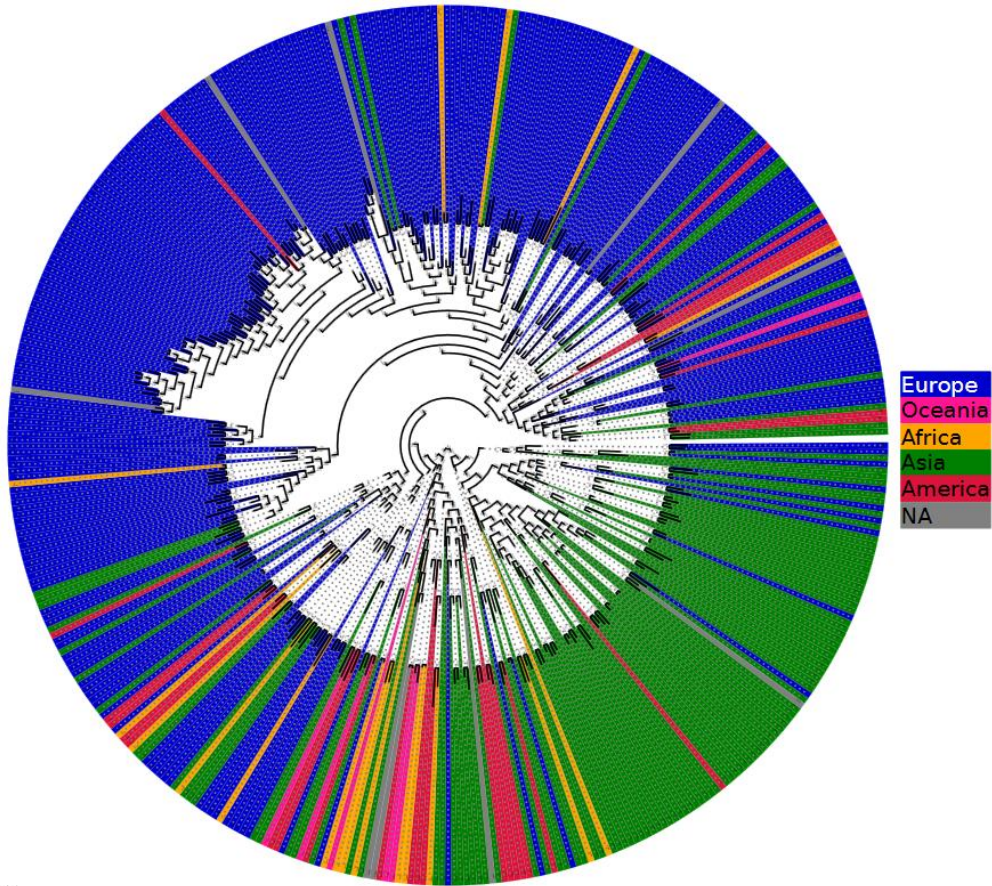
Figure S4: Wheat genotypes relatedness and components of the panel structuration. **A-** Phylogeny of the 435 hexaploid bread wheat genotypes with phylogenetic clades (a to k) shown in colors. The presented clades were chosen on criterion of size, representativeness and statistical support to offer a good coverage of the tree, while taking into account sampling bias for European individuals. **B-** Geographical origin, historical groups (I to IV) and growth habit characters composition of chosen representative clades (a to k) on the *T. aestivum* phylogeny. To compare the level of structuration of the data according to the origins, groups and growth habit traits, we performed mean comparison t-tests for the distribution of mode frequency for of all clades in the (unrooted) tree (excluding leaf clades, and individual with an unknown trait). Results indicate that the group trait has a significantly lower mean modal frequency than the origins or growth habit traits (p -value $< 2.2e-16$ for both). No significant difference was detected between the geographical origins and growth habit traits (p -value=0.09349). Additionally, we computed the minimal number of character transitions needed along the phylogeny to explain the extant data (with the rationale that a variable which strongly structures the phylogeny will require less transitions than a variable which does not). The results show that geographical origin requires less transitions (73 transitions) than either historical group (141 transitions) and growth habit (89 transitions) traits. Taken together, these results suggest that geographical origin most strongly structures the phylogeny of modern hexaploid wheats. Illustration of the phylogeny according to the geographical origins (either at the region (C) or continent (D) scales), historical groups (E) and growth habit (F) levels. Unknown categories are depicted in grey in panels B-C-D-E-F.

A

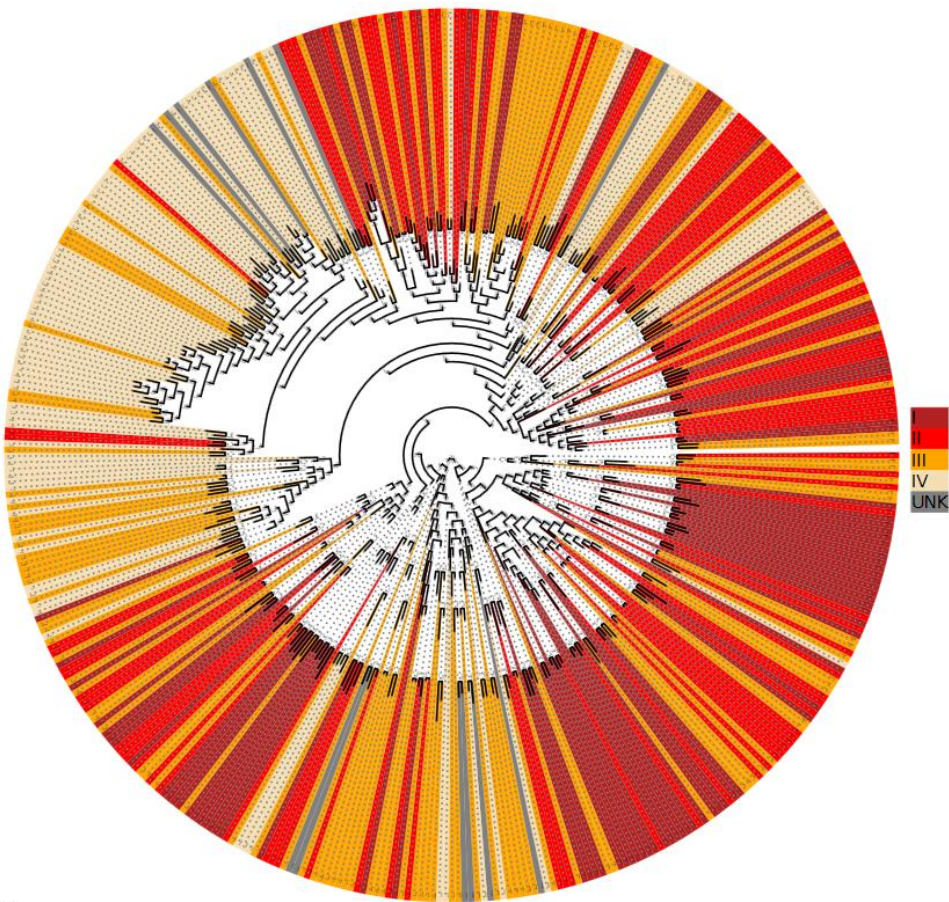


B**C**

D



E



F

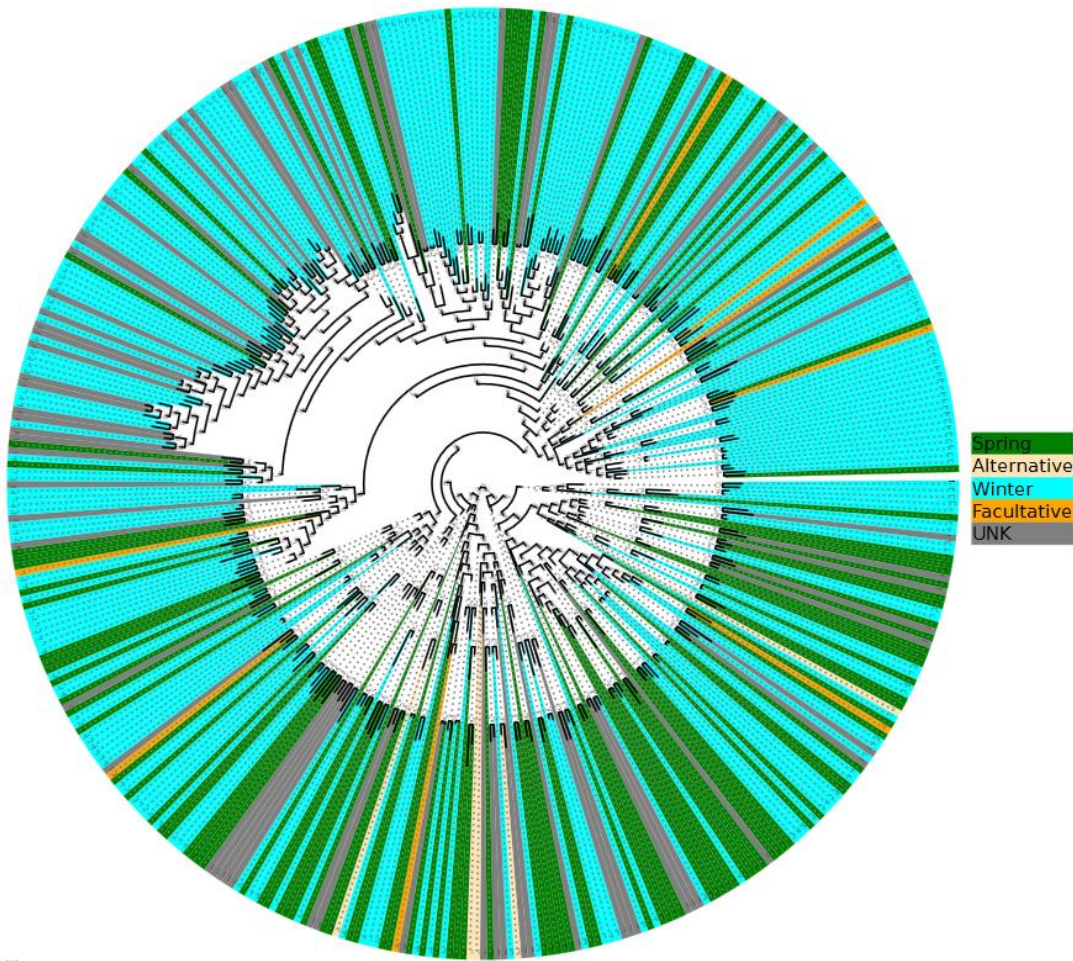


Figure S5: Geographical component of the panel structuration. **TOP**- Principal Component Analysis (PCA) of diversity among the 487 genotypes grouped into distinct polyploidy levels (di-, tetra- and hexaploid) and historical groups (I to IV) according to the colored code legend (top right). The diversity within the diversity panel differentiate the polyploidy levels. **CENTER** - Principal Component Analysis (PCA) of diversity among the 435 hexaploid genotypes grouped into geographical origins according to the colored code legend (top right). **BOTTOM** – World map showing different colors for continents (America, Oceania, Asia, West-East Europe and the Fertile Crescent). The known historical routes of wheat migration (green arrows), west through inland (❶) and coastal (❷) paths, and north-east (❸) and along the Inner Asian Mountain Corridor (❹) followed by further colonization (black connecting lines) of American (❺), African (❻), Oceanian (❼) territories, support the genotypes panel structure.

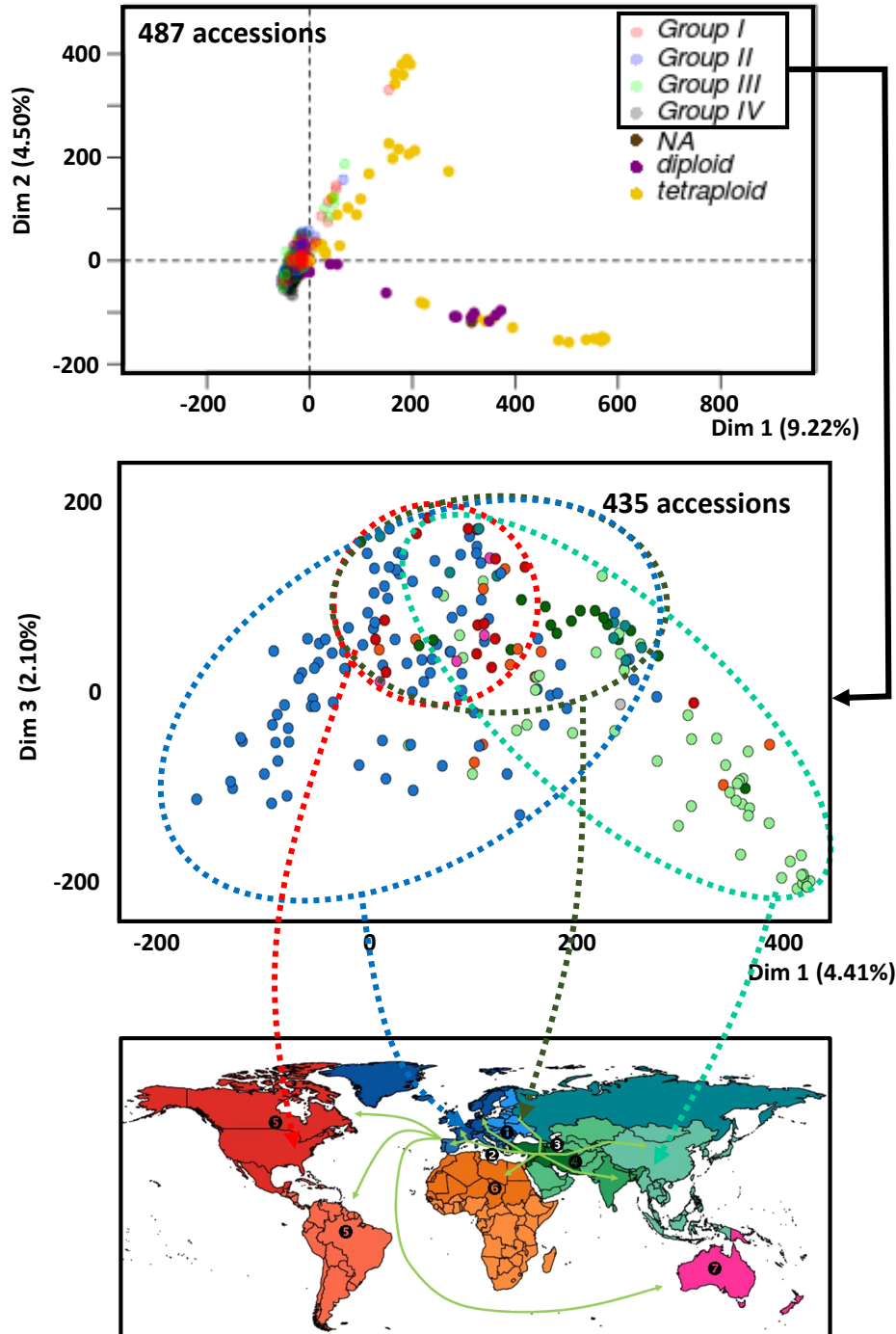


Figure S6: Selection (domestication) signatures. ROD values (>0.8 in red) at the subgenome (A, B and D) and chromosome (1 to 7 level) between (from the outer to the inner circle) between diploids vs tetraploids, between diploids vs hexaploids and between tetraploids vs hexaploids. 427, 877 and 1,221 regions with domestication signature are identified respectively (from outer to inner circles) between diploids vs tetraploids, between diploids vs hexaploids and between tetraploids vs hexaploids.

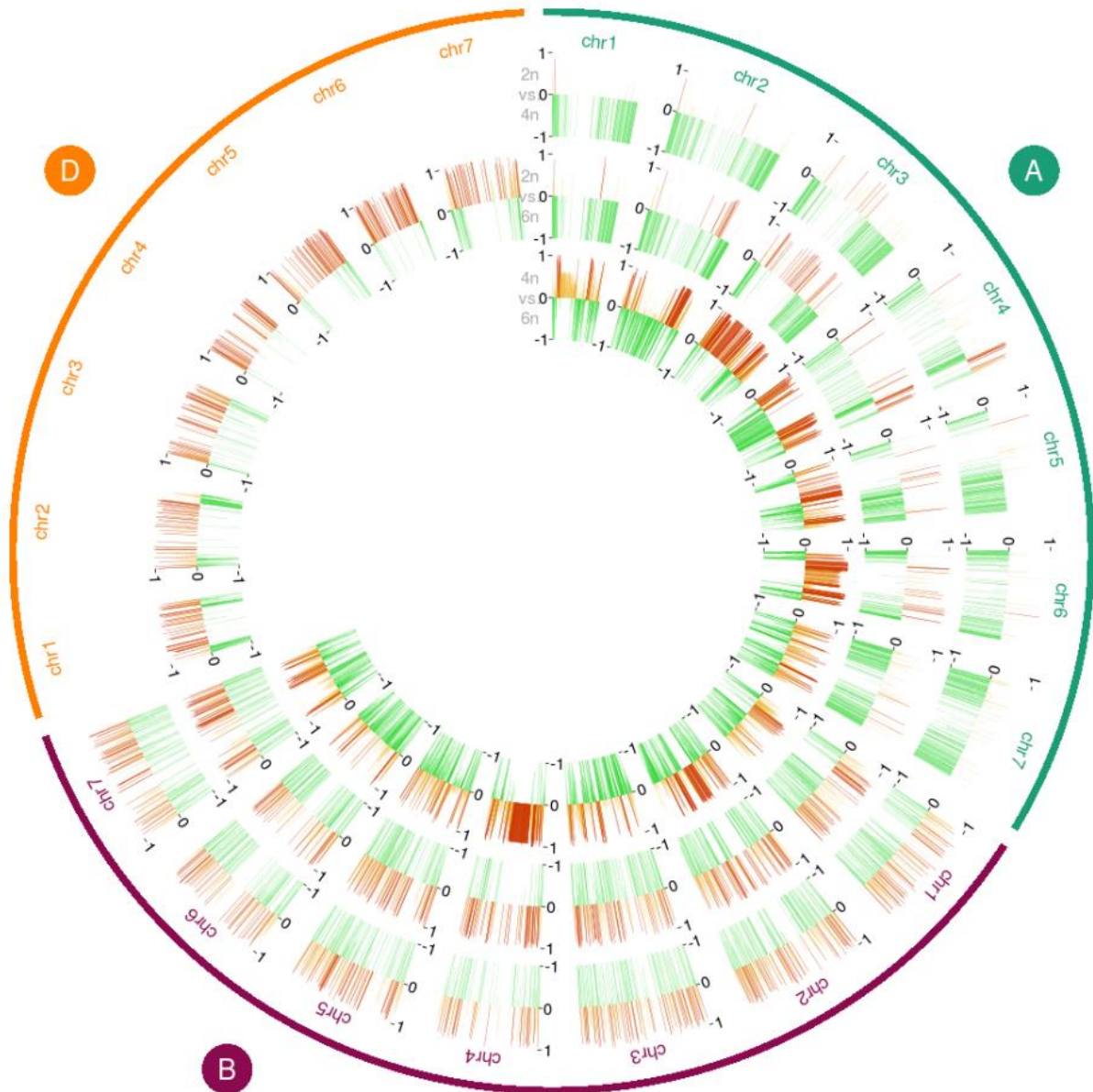
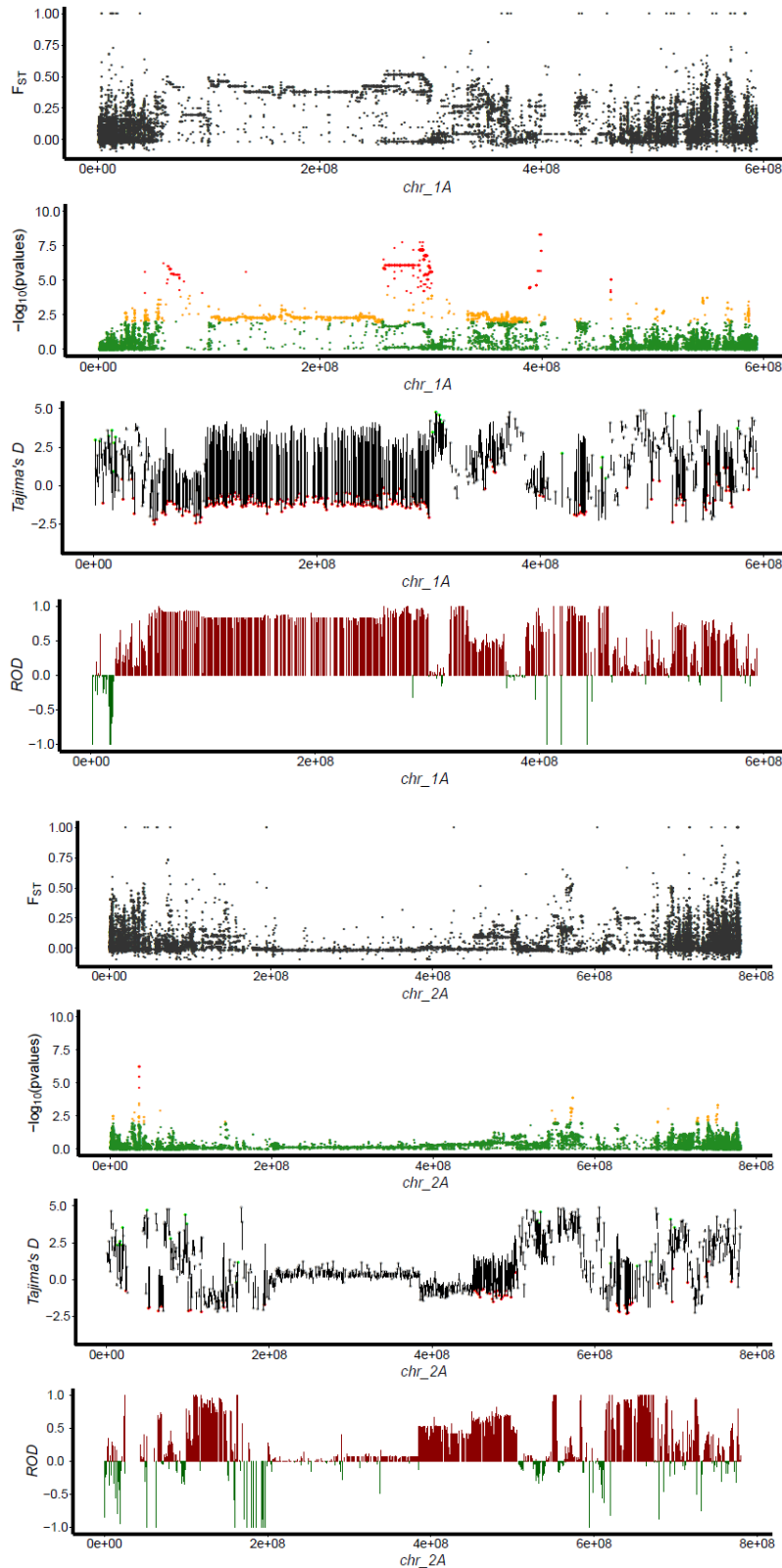
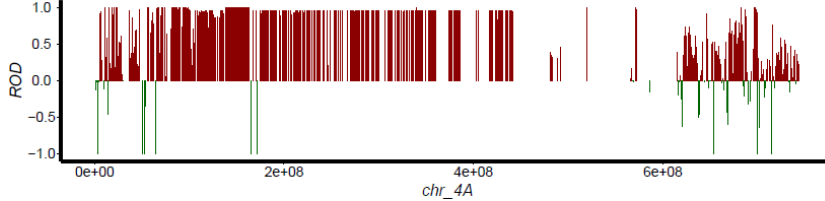
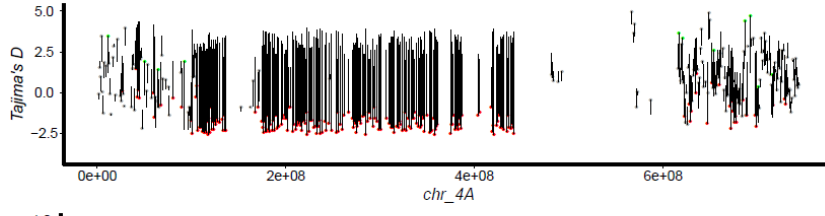
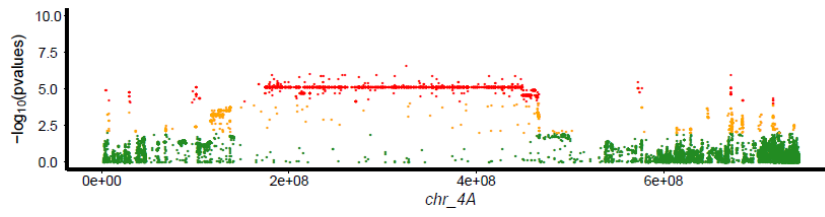
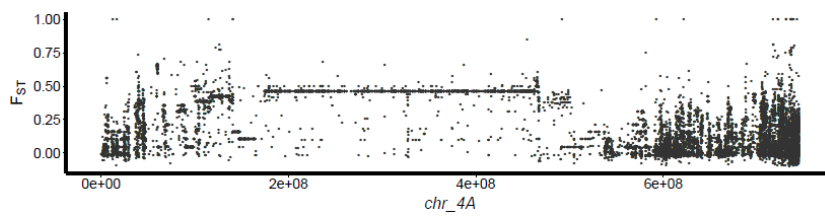
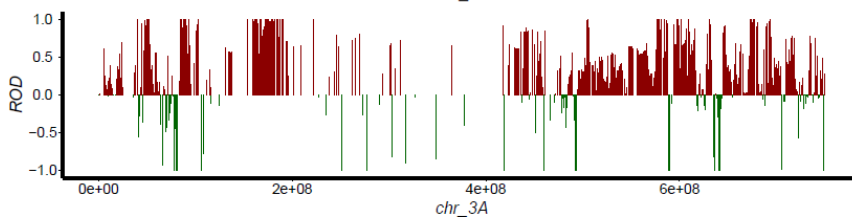
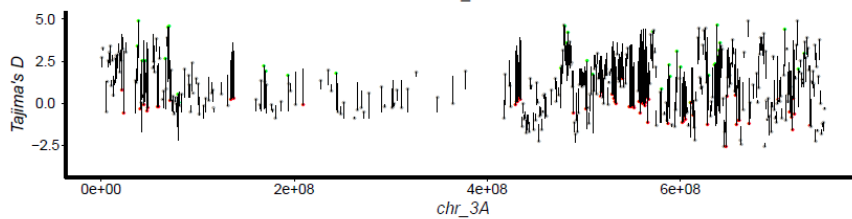
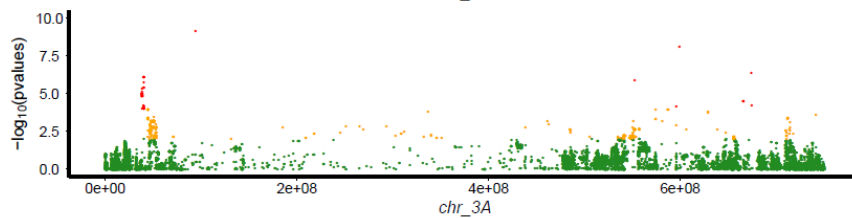
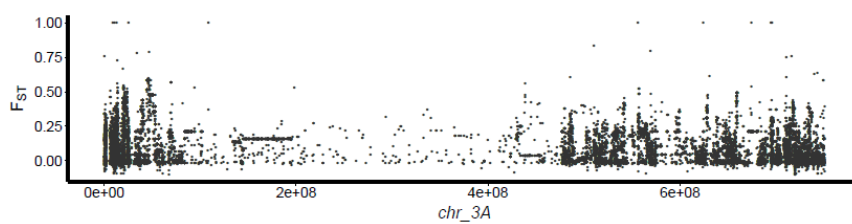
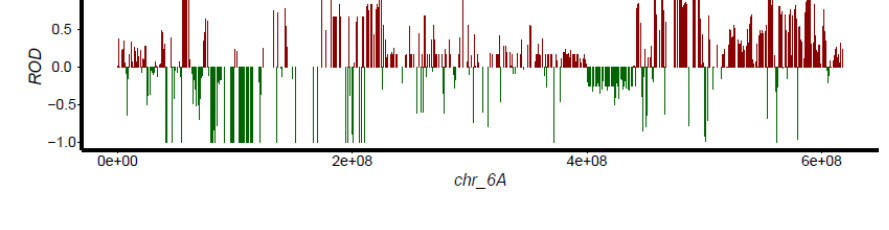
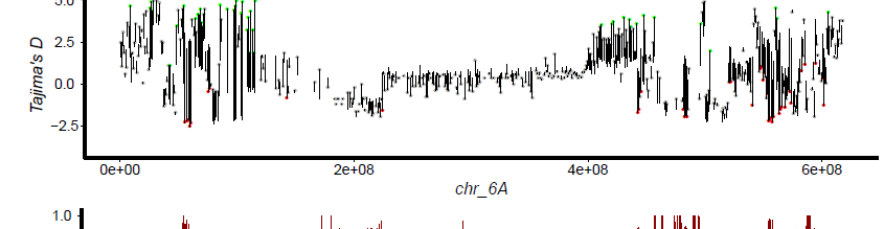
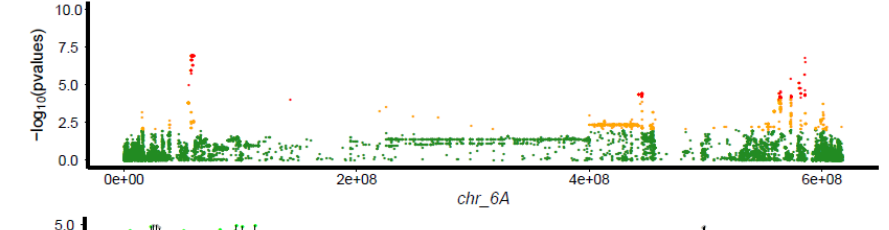
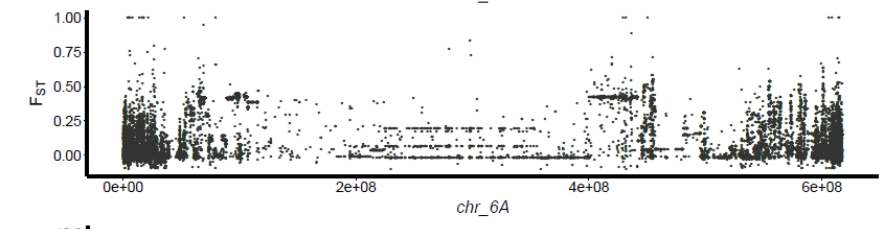
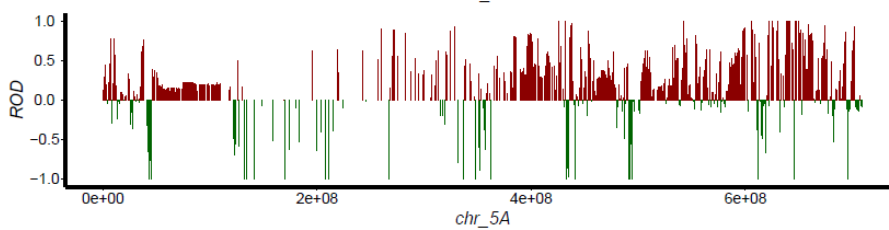
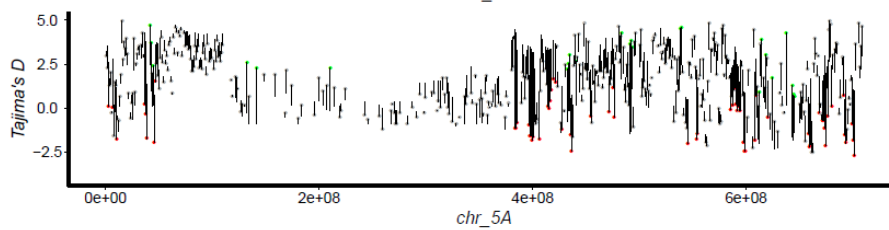
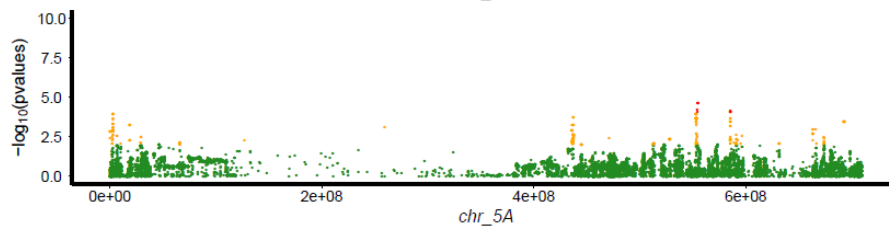
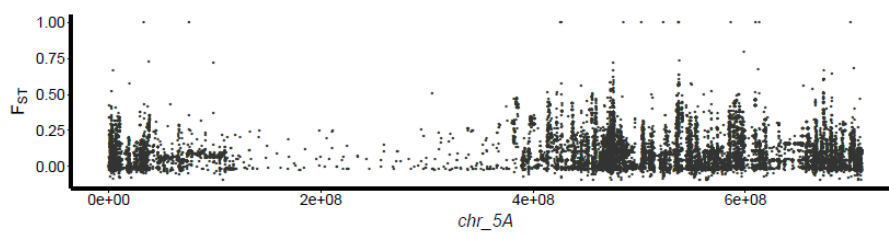


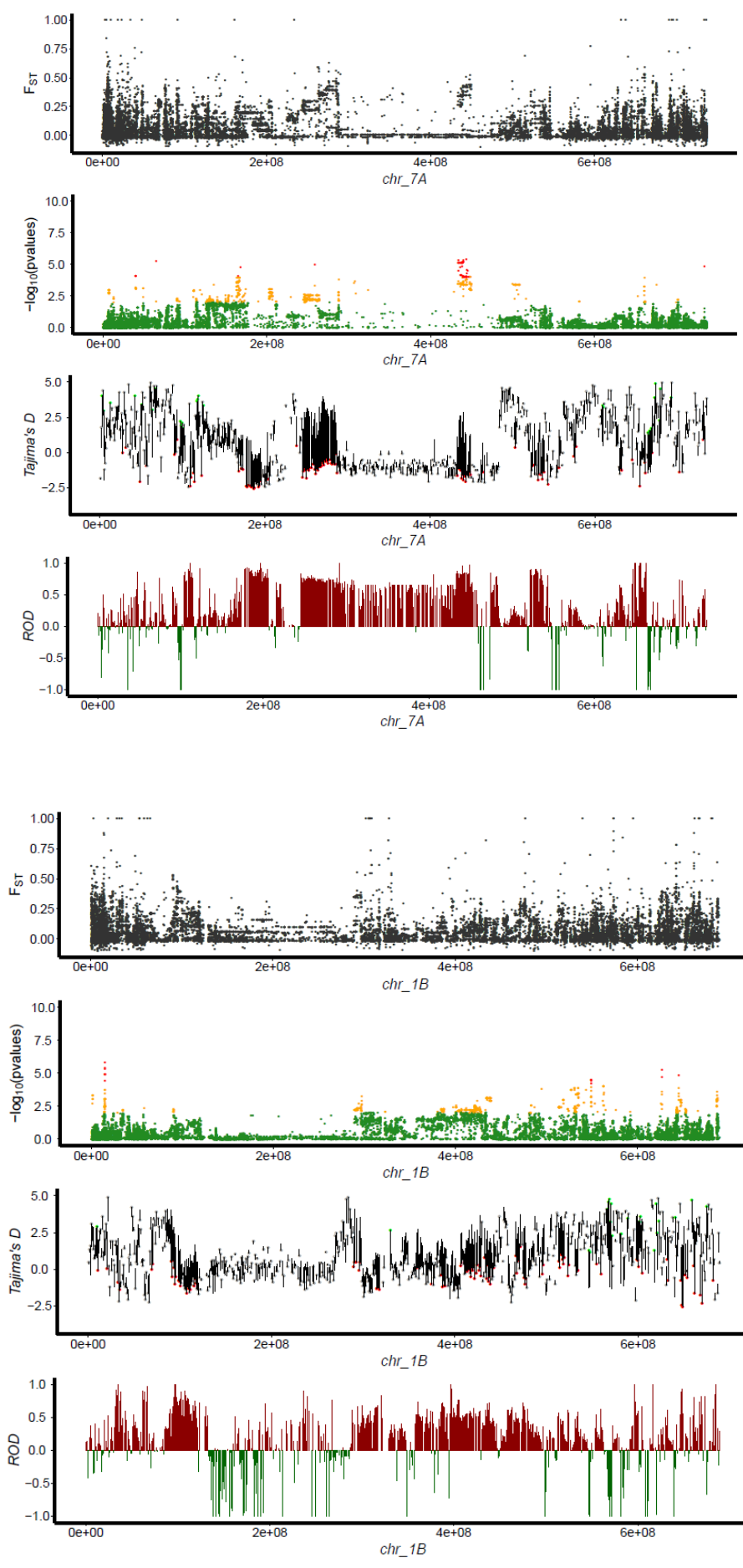
Figure S7: Selection (breeding) signatures. A- Chromosome by chromosome Manhattan plots of fixation index (F_{ST}) between groups I and IV, \log_{10} -transformed p-values of PCAdapt (>4 in red), Tajima's D and ROD, y-axis) in the European hexaploid bread wheat. **B-** \log_{10} -transformed p-values (>4 in red) at the subgenome (A, B and D) and chromosome (1 to 7 level) for (from the outer to the inner circles) the 435 hexaploid bread wheat genotypes, the European genotypes and the Asian genotypes. 8,308, 9,948 and 5,089 loci with improvement signature were identified respectively for the European genotypes, for the Asian genotypes and for the total panel. Large regions (previous loci extended over 2 Mb overlapping windows) of improvement signatures are shown in yellow boxes.

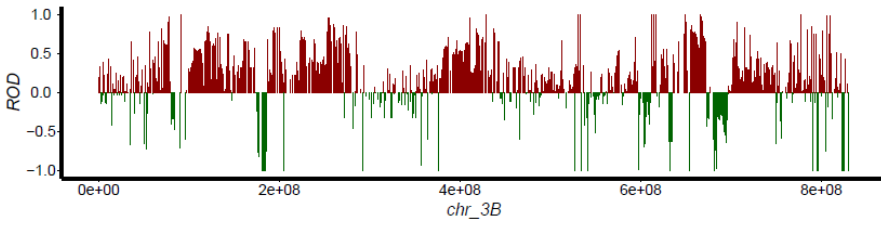
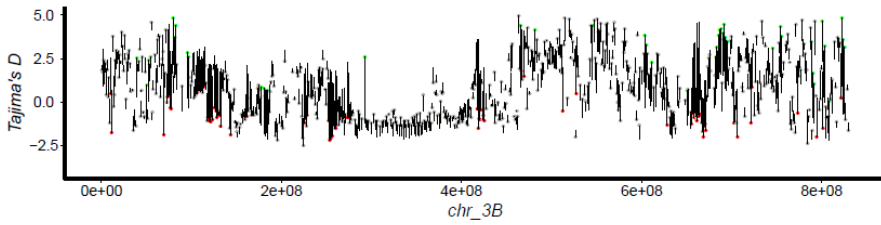
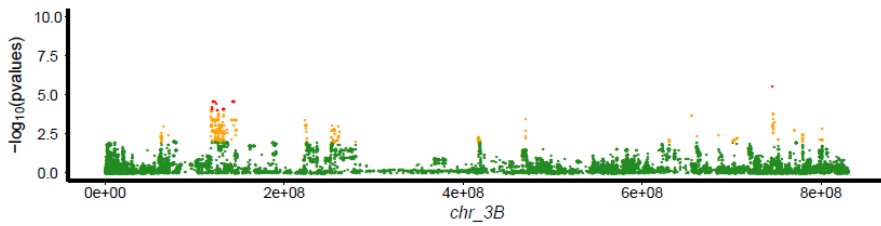
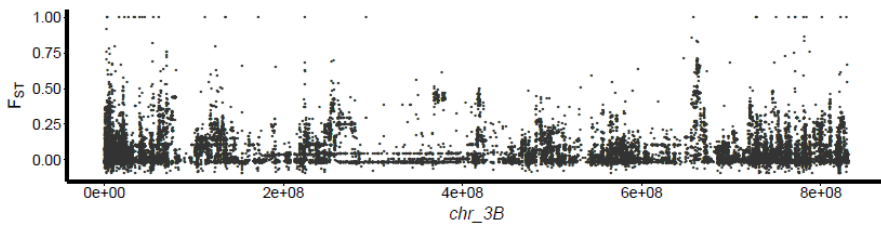
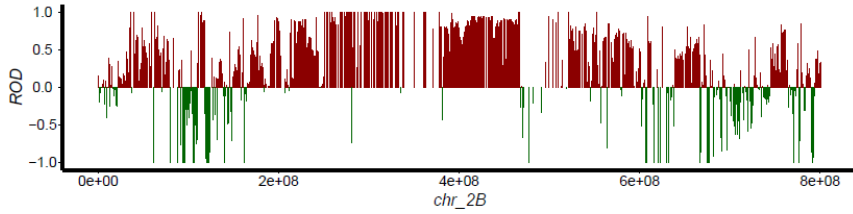
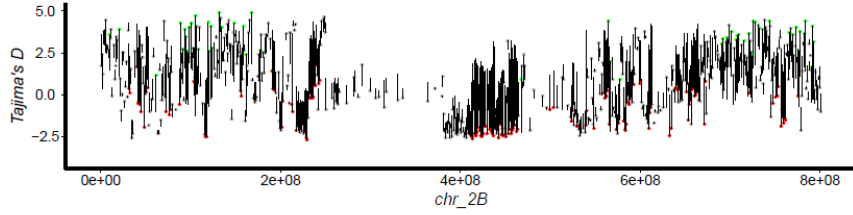
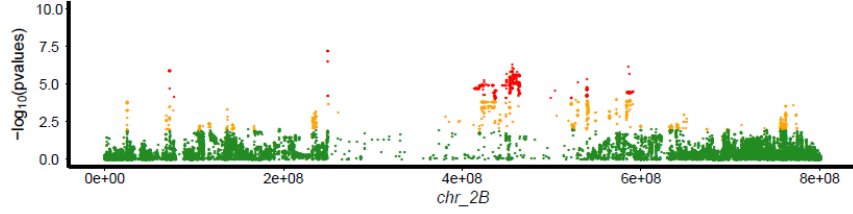
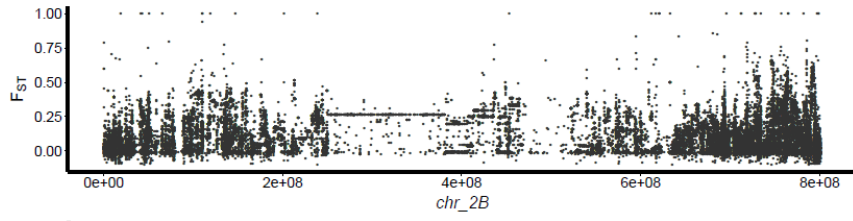
A

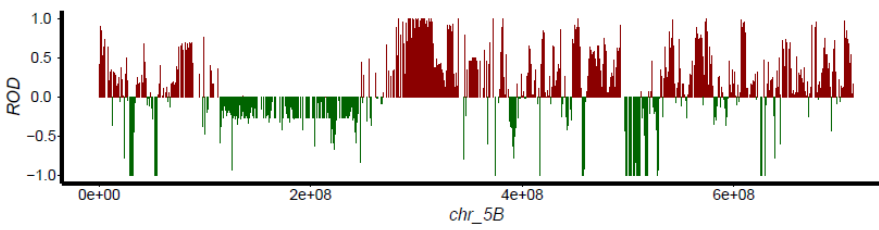
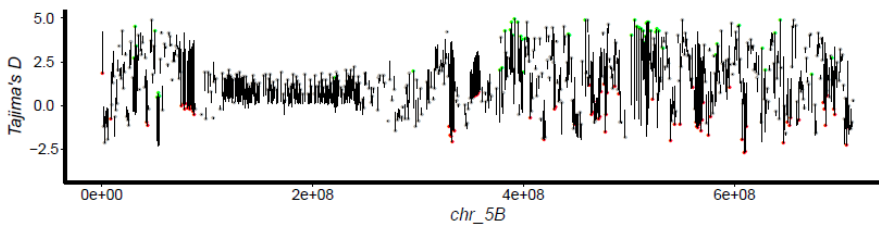
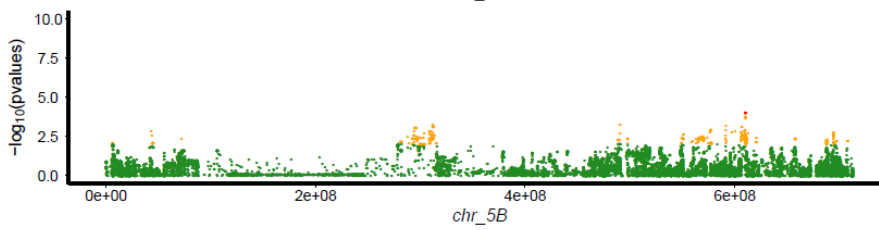
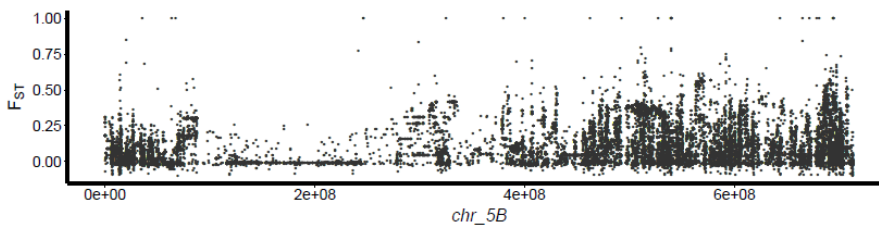
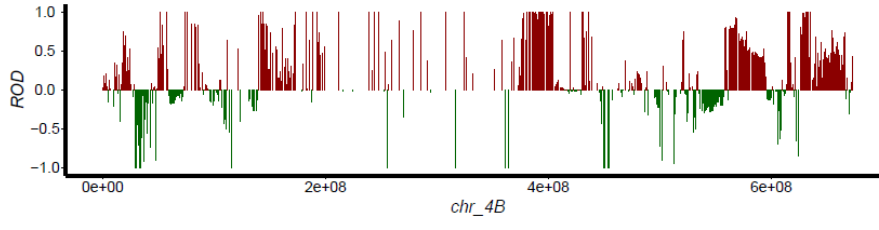
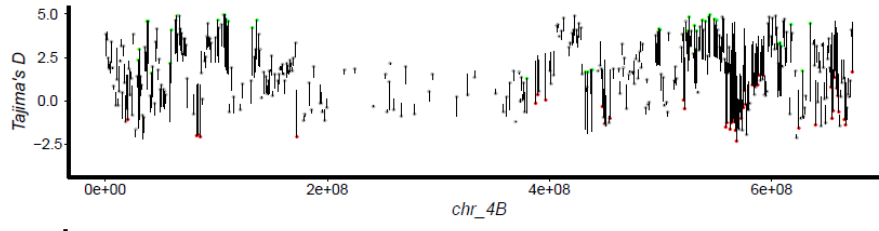
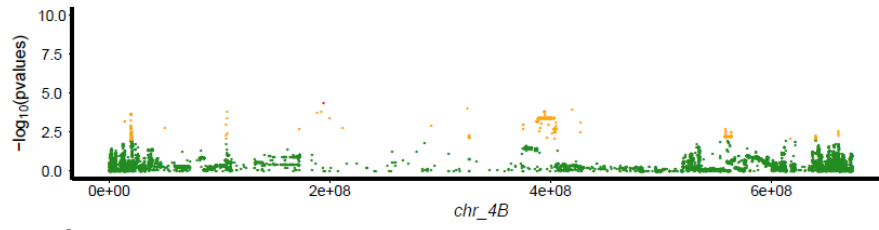
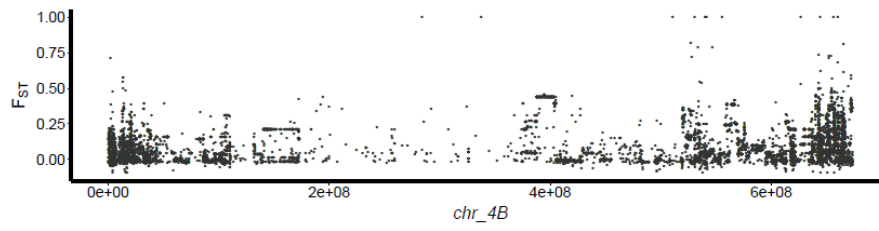


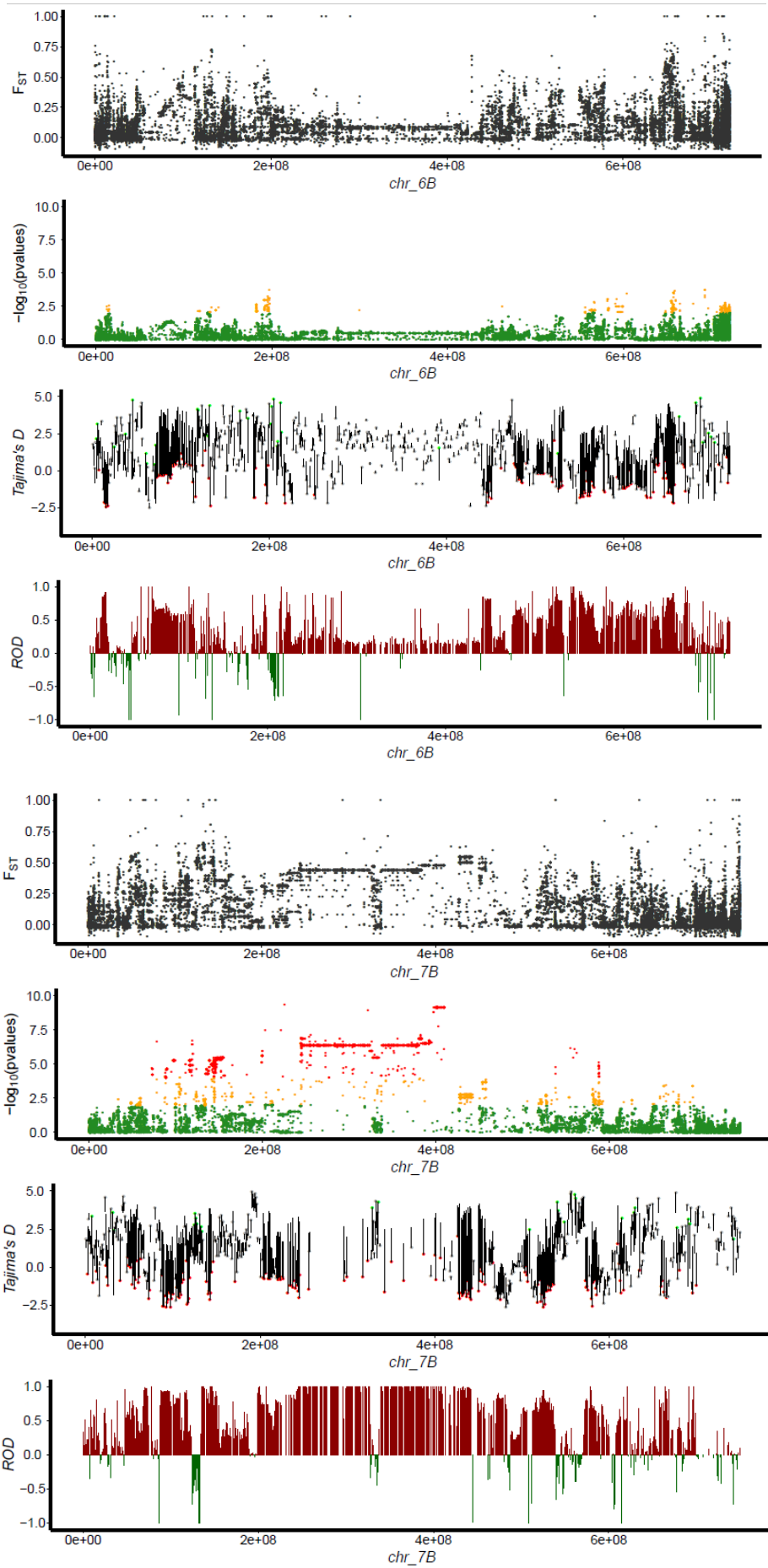


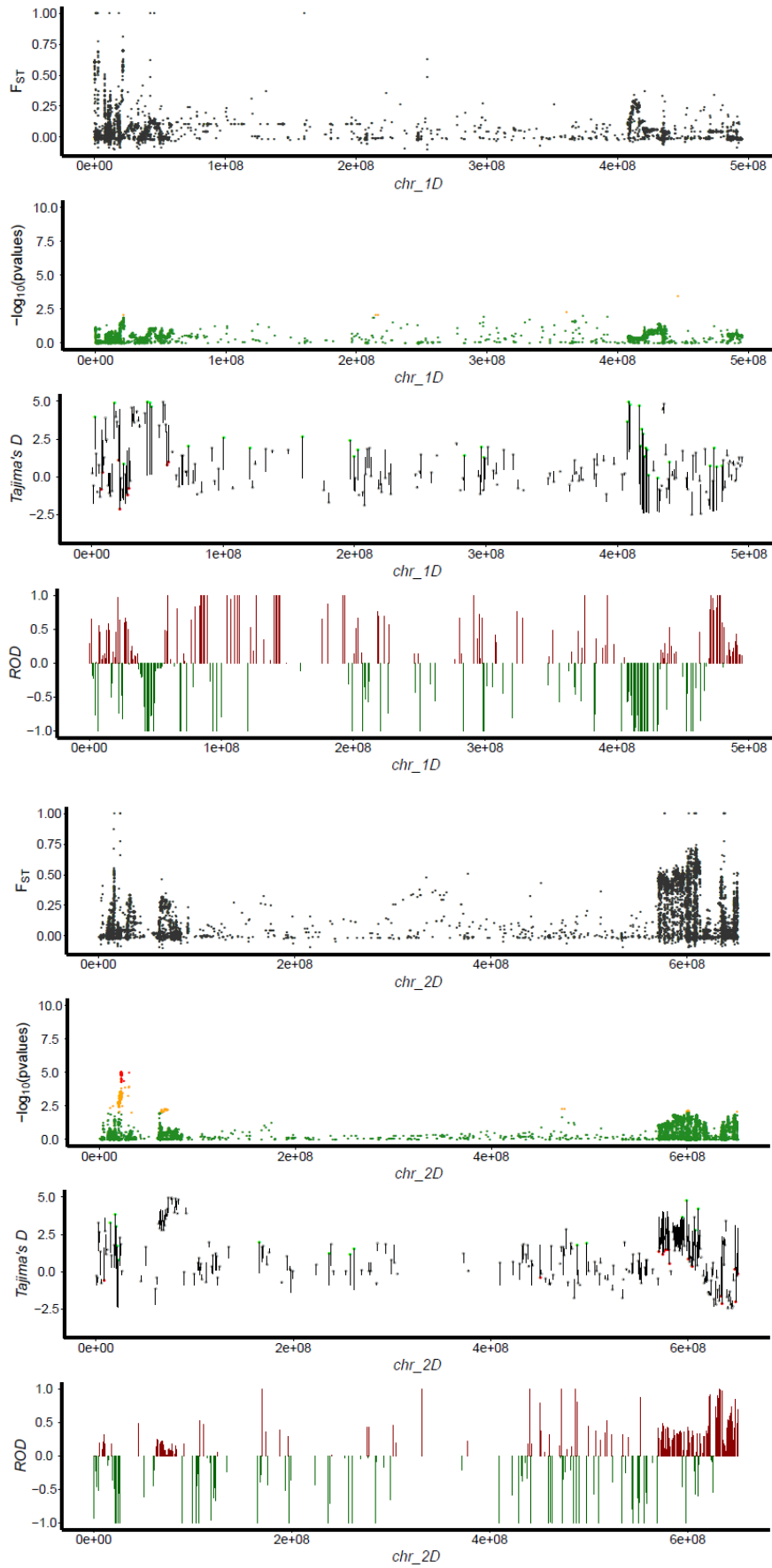


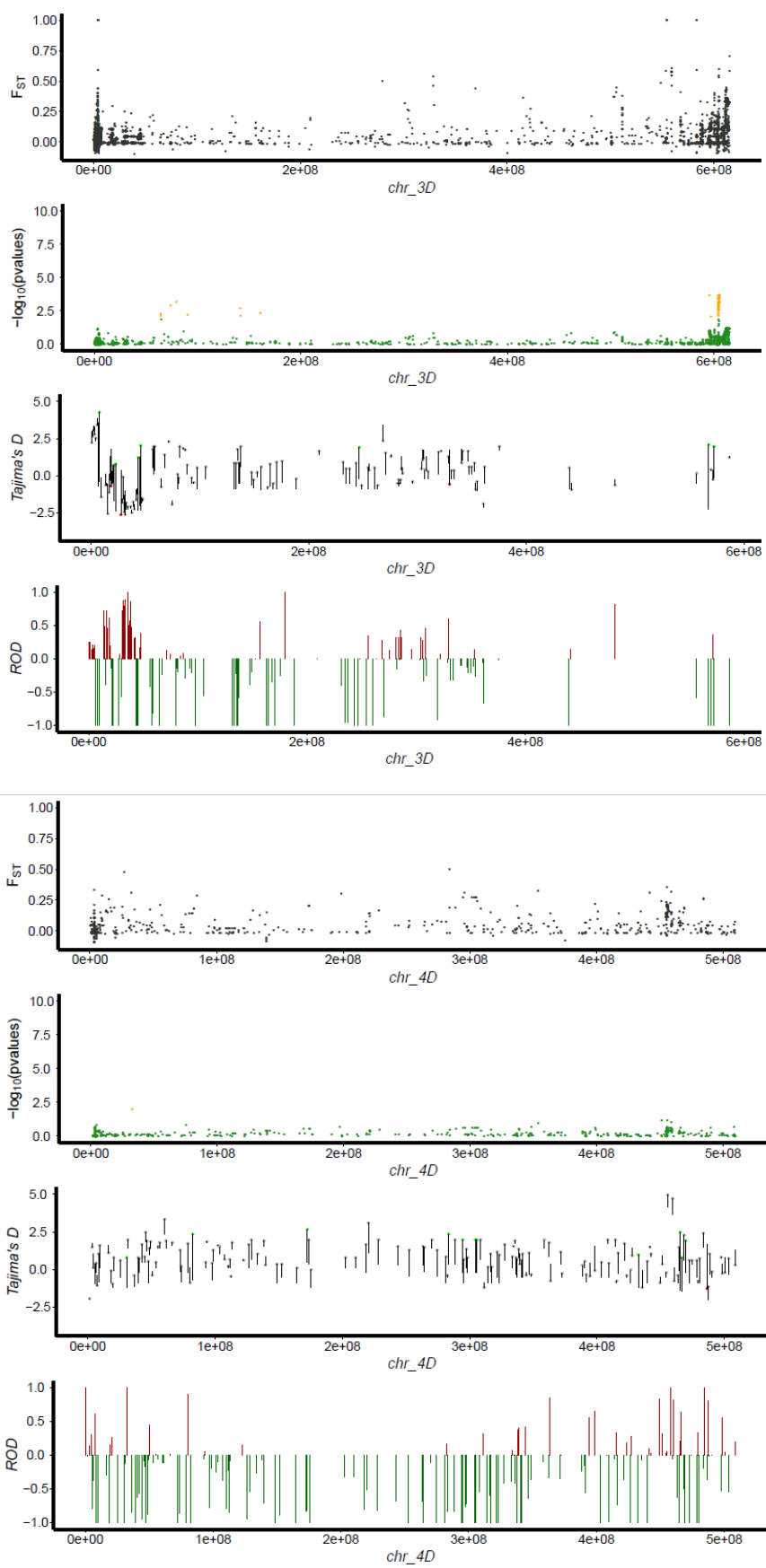


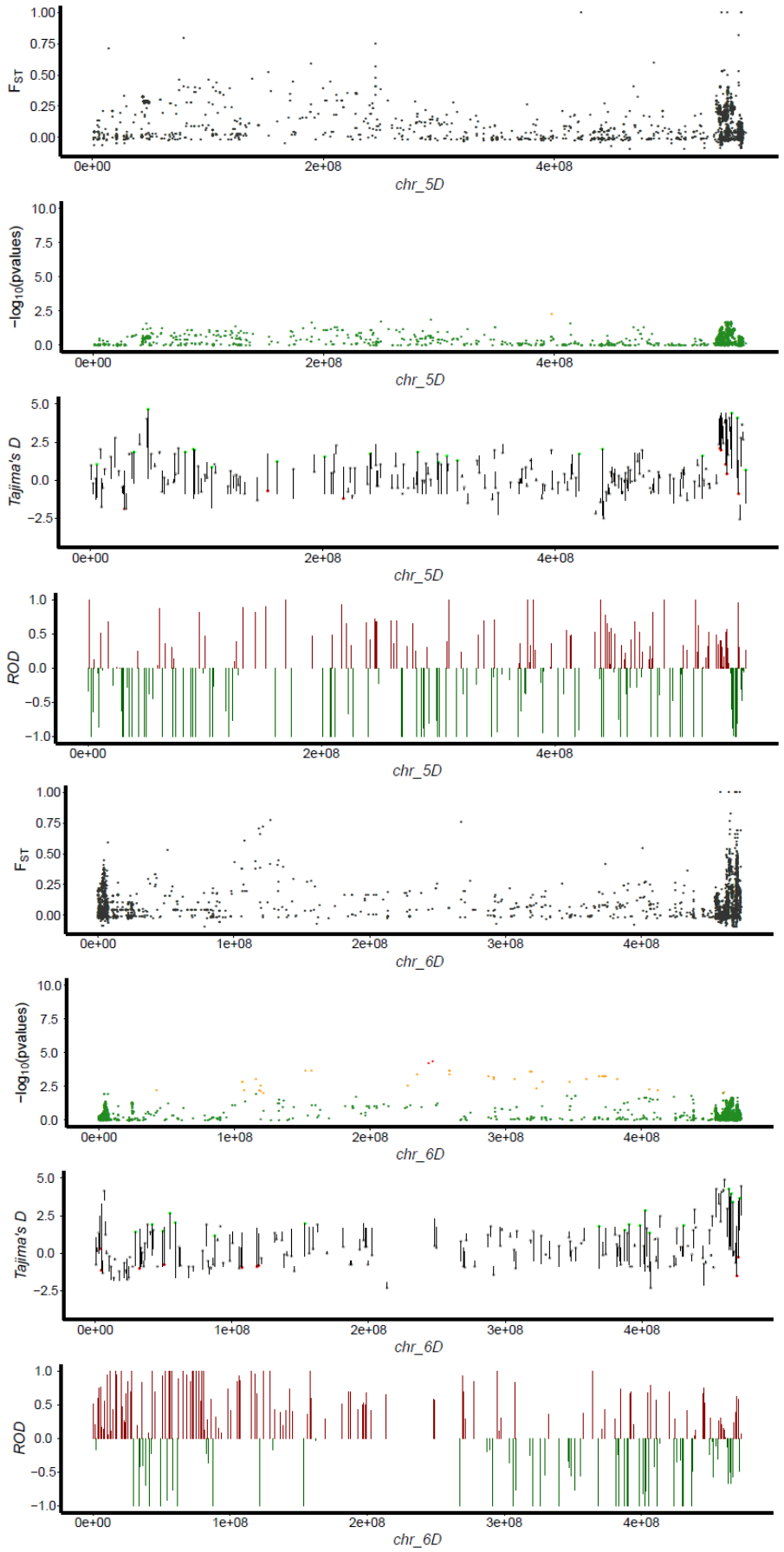


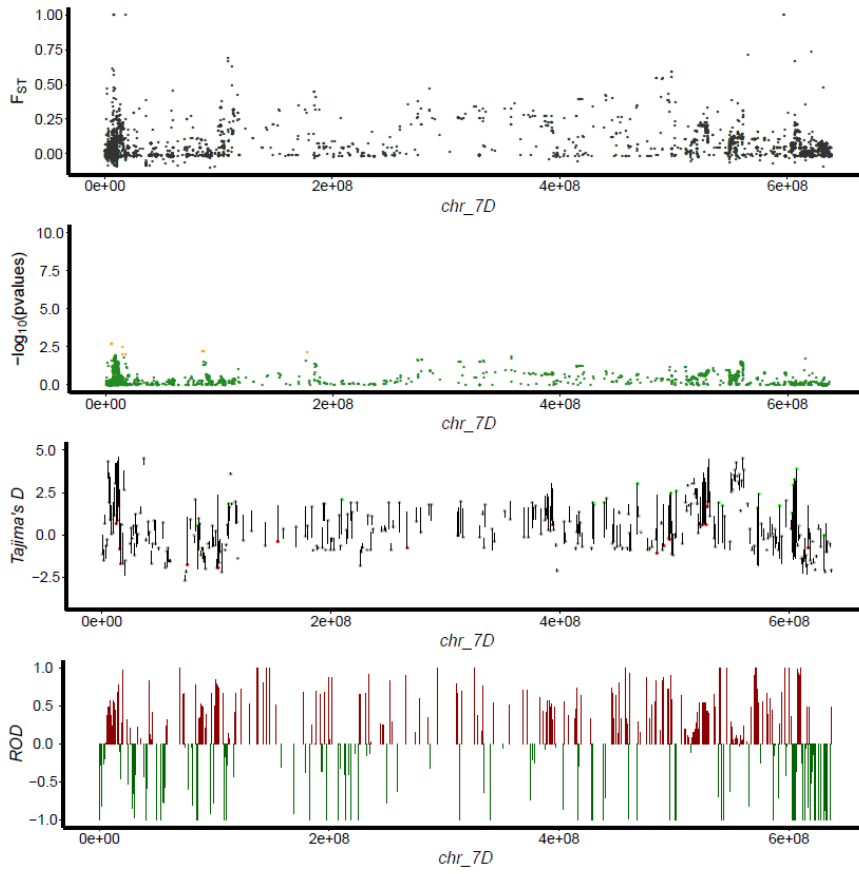












B

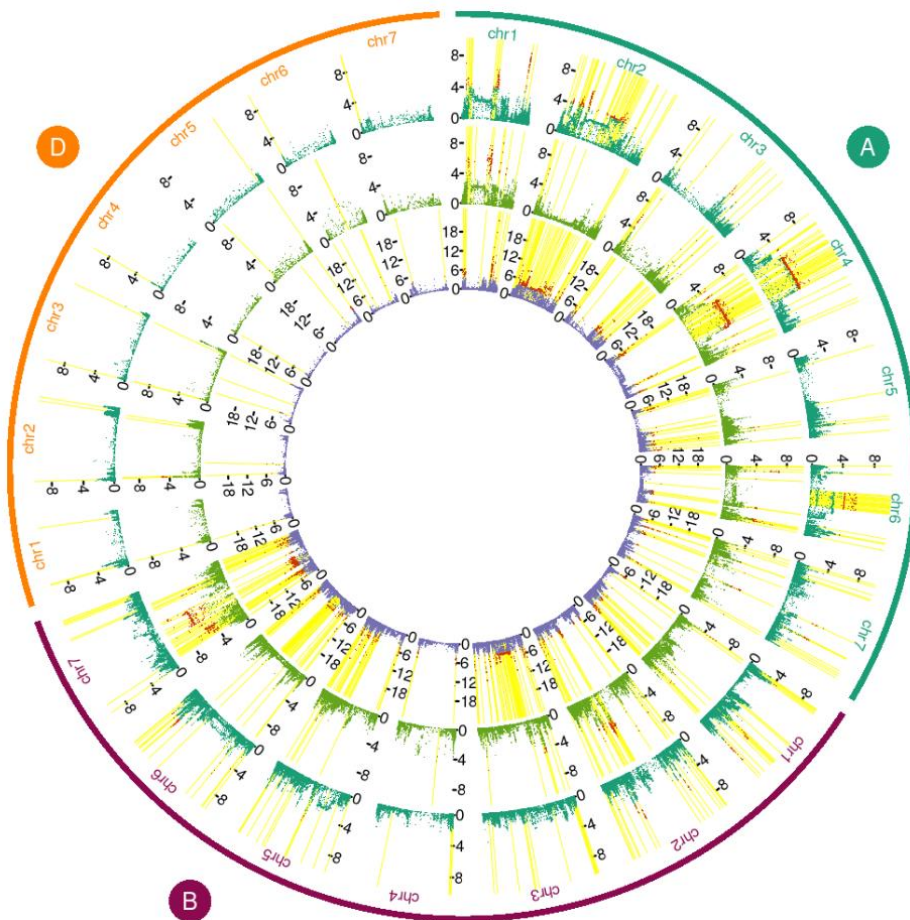
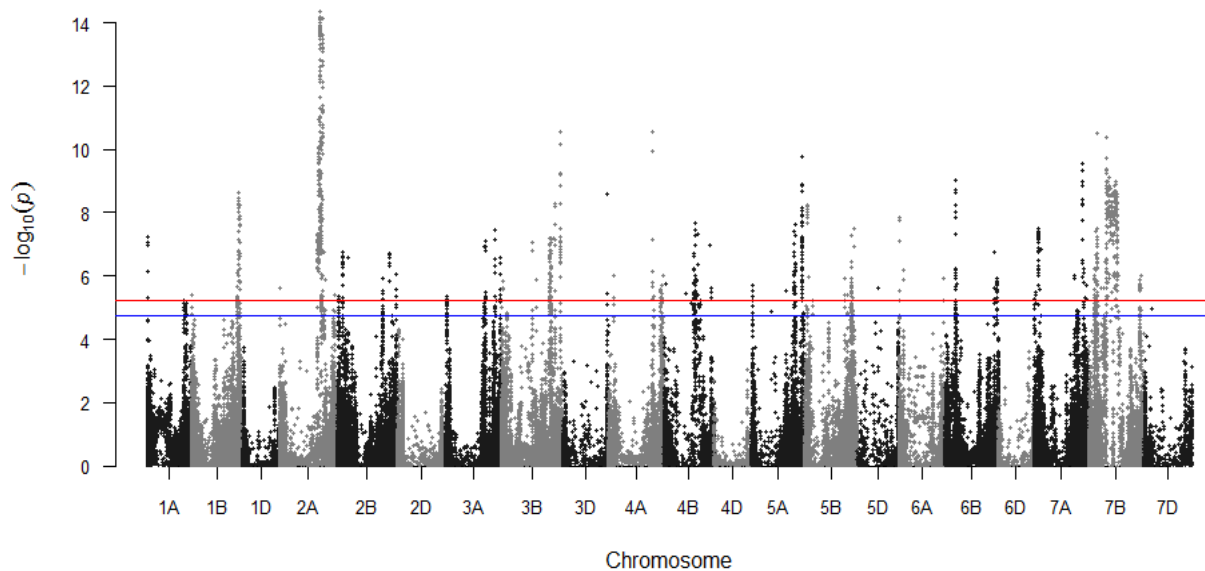


Figure S8: GWAS for heading date (HD). **A-** Manhattan plot of GWAS for heading date (HD) yielding 48 major peaks. Each point represents one of the 390,657 variants with MAF > 0.05 in 435 hexaploid wheat genotypes, with their chromosomal position indicated on the x axis. The red and blue horizontal lines show the 0.01 and 0.05 FDR significance thresholds, respectively. **B-** Manhattan Plot of the chromosome 2AL genomic region (100 Mb) where two major peaks in strong LD were detected with 34 and 35 HC genes. Among the HC genes annotated is TraesCS2A01G340400, encoding for Cry1b-2A. A single synonymous SNP was detected in the gene sequence and the distribution of the reference, late-flowering and the alternative, early-flowering alleles among winter and spring wheat genotypes is shown. According to the Wheat Expression Browser (expVIP, <http://www.wheat-expression.com/>), the gene shows high expression levels in leaves and shoot under both vegetative and reproductive stages, as well as in the spike at the reproductive stage.

A



B

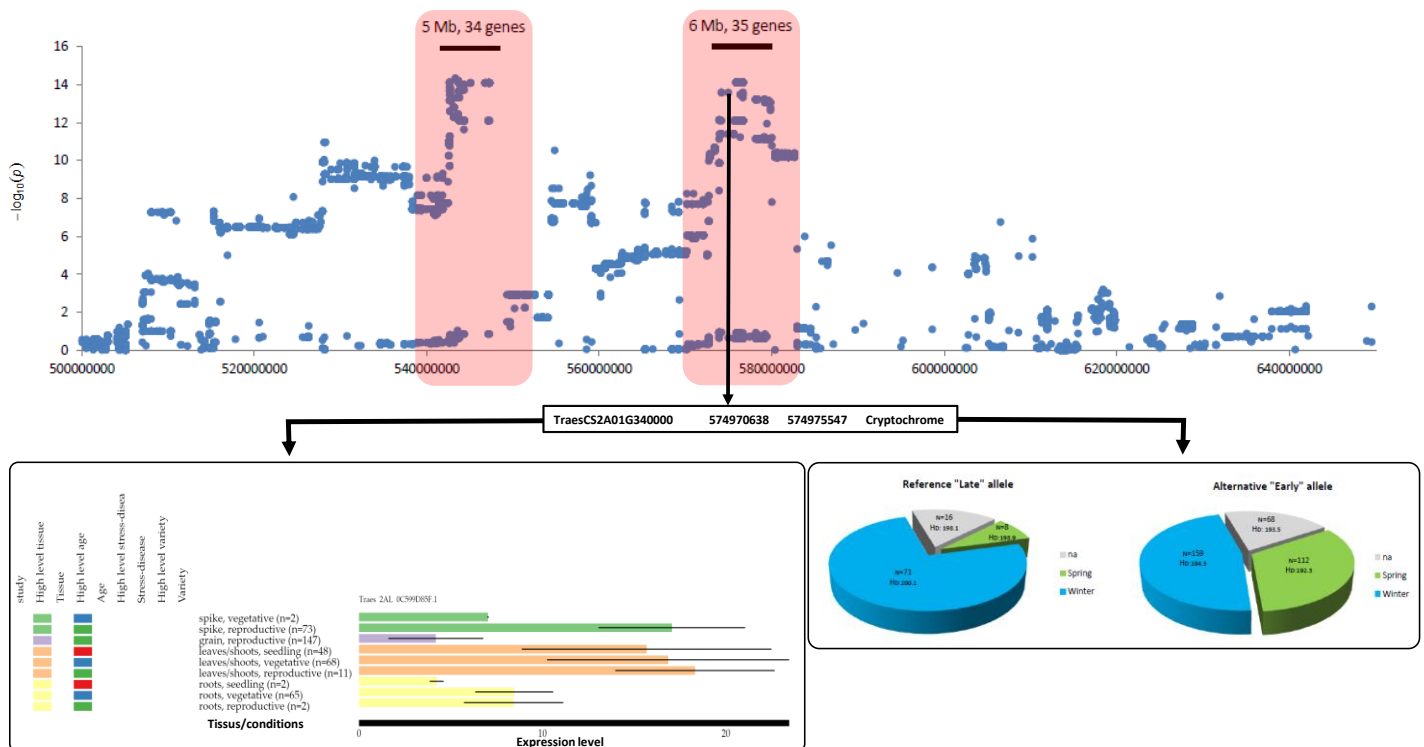


Figure S9: GWAS for plant height (PH). Manhattan plot of GWAS for plant height (PH) yielding 40 major peaks. Each point represents one of the 390,657 variants with MAF > 0.05 in 435 hexaploid wheat genotypes, with their chromosomal position indicated on the x axis. The red and blue horizontal lines show the 0.01 and 0.05 FDR significance thresholds, respectively.

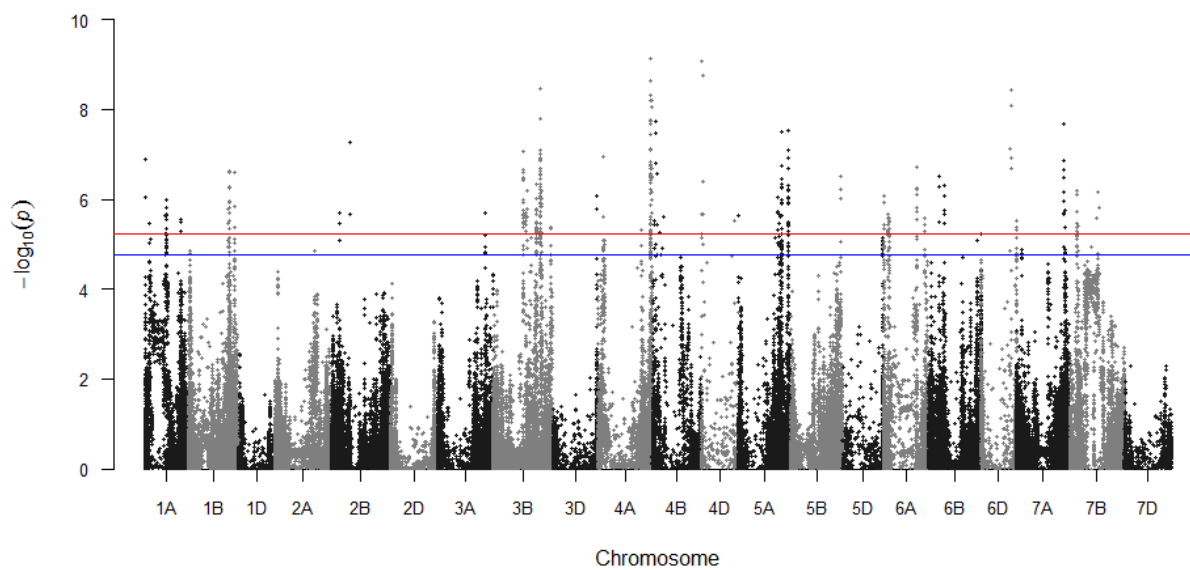


Figure S10: Inference of reticulated evolutionary scenario with phylogenetic networks. Minimum spanning tree of the phylogenetic network (see Figure 4A legend, main text), maximizing the weight of the kept edges. The resulting graph highlights the vertical evolutionary signal linking diploid and tetraploid (with the color code consistent with the evolutionary scenario in Figure 4B, main text), and hexaploid wheats (in grey).

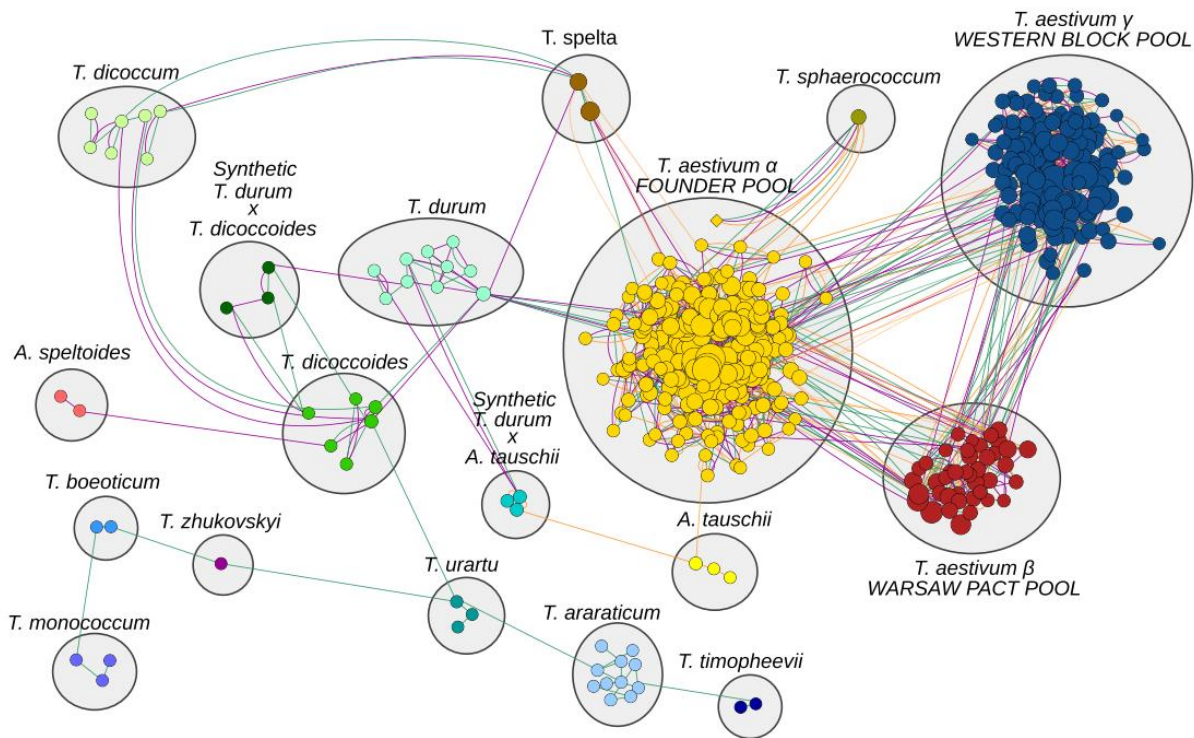
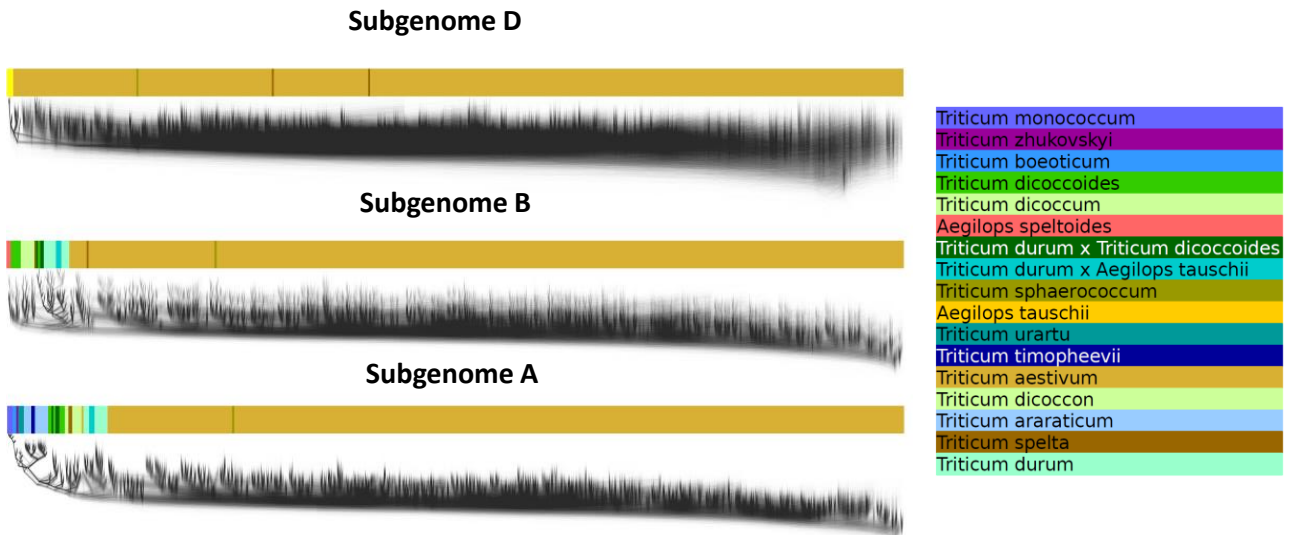


Figure S11: Wheat phylogenetic relationships. A - Cladogram for each of the 3 subgenomes (A, B and D) with the color code used for each of the investigated taxon at the right. B- Consensus of the 1,000 RRHS trees for each of the 3 subgenomes A, B and D with the color code used for each of the investigated taxon as described in panel A. Supports are shown in red, green, blue and black, respectively for support values of 100, above 79, above 49 and, under 50.

A



B

subgenome A

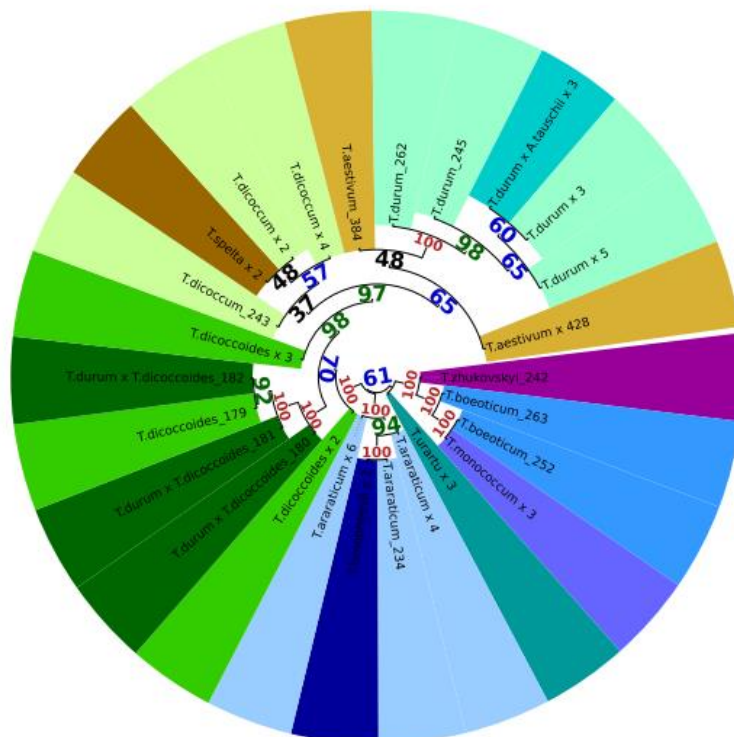


Figure S12: Inference of reticulated evolutionary scenario with ABBA-BABA test. Patterson's D and Z values were inferred using ANGSD³⁰ *T. dicoccoides* as outgroup population. Significant instances of gene flow (Z statistic > 4) are represented on a schematic and simplified tetraploid and hexaploid tree (inspired by the subgenome A consensus - concurrent tree topologies yielded a similar number of gene flows), as colored double arrows. Green, purple and blue arrows illustrate gene flow supported by, respectively, subgenome A, subgenome B, or both subgenomes. Full arrows denote a reticulation event also detected in the network-based phylogenetic approach (Figure 4, main manuscript) while dashed arrows correspond to a signal detected only with the Patterson's D analysis. Associated Z-values are written in green and purple, for, respectively, the subgenome A and subgenome B. [Sensitivity of the approach has been tested on synthetic polyploids of the same ploidy level \(ABxAB\) with F7 RIL *T. turgidum* offsprings detected as hybrids with dominant *T. dicoccoides* genotypes and multiple independent *T. durum* introgressions, illustrating the resolution gained from ABBA-BABA test.](#)

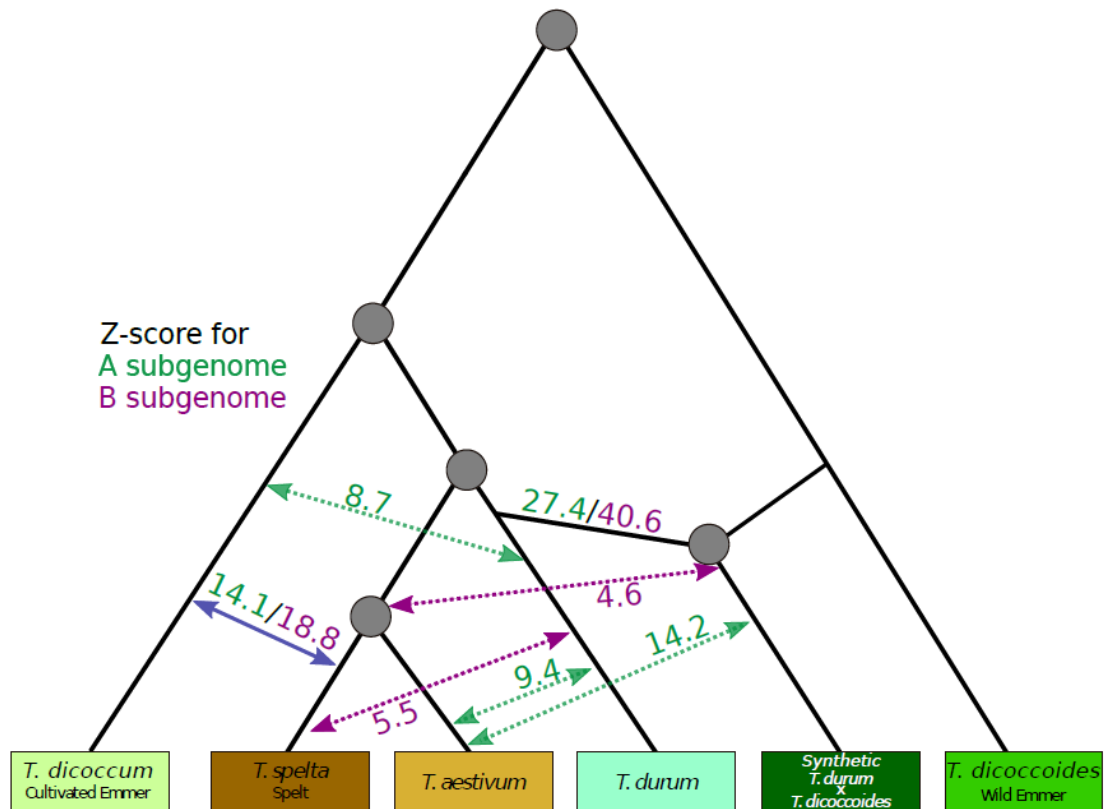
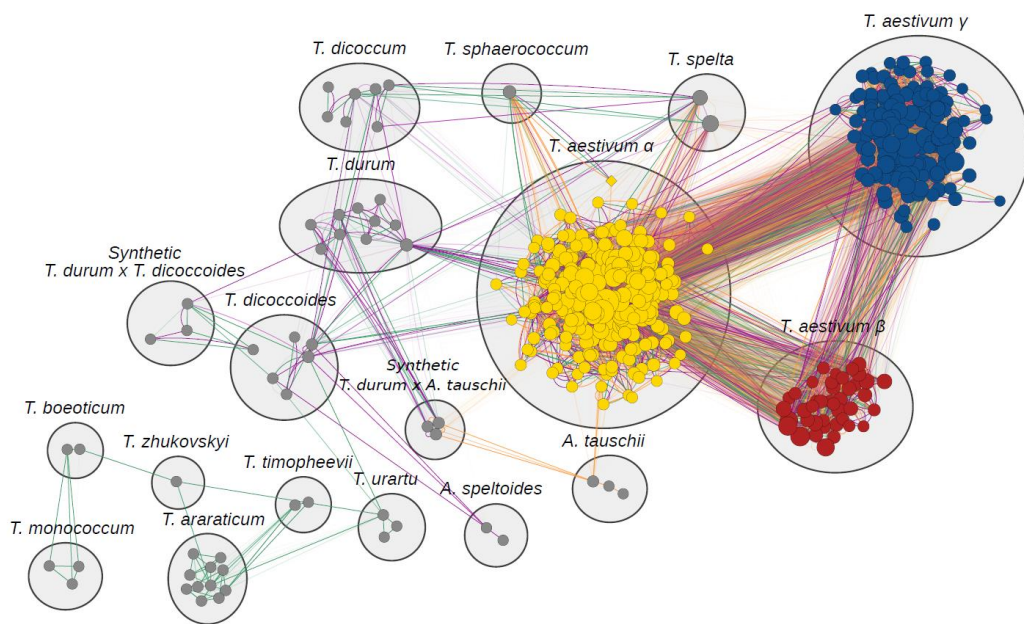
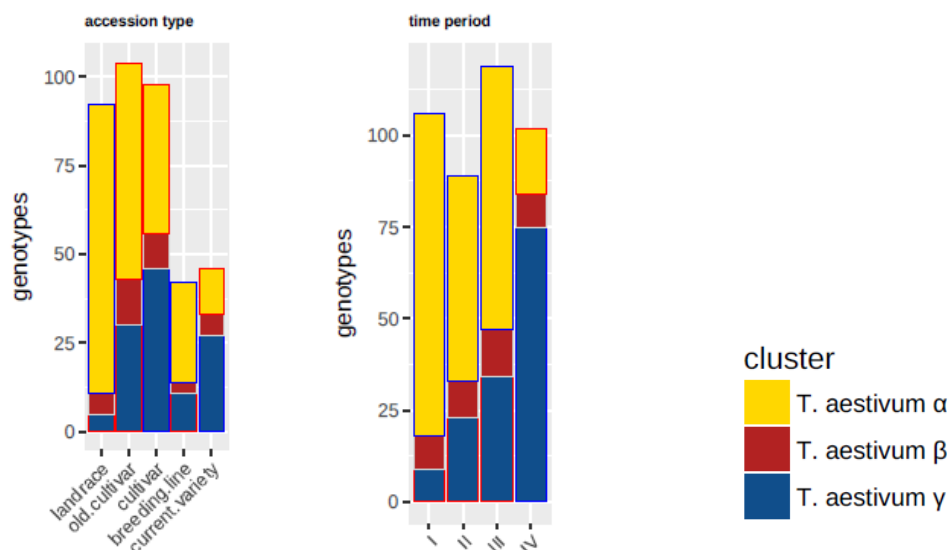


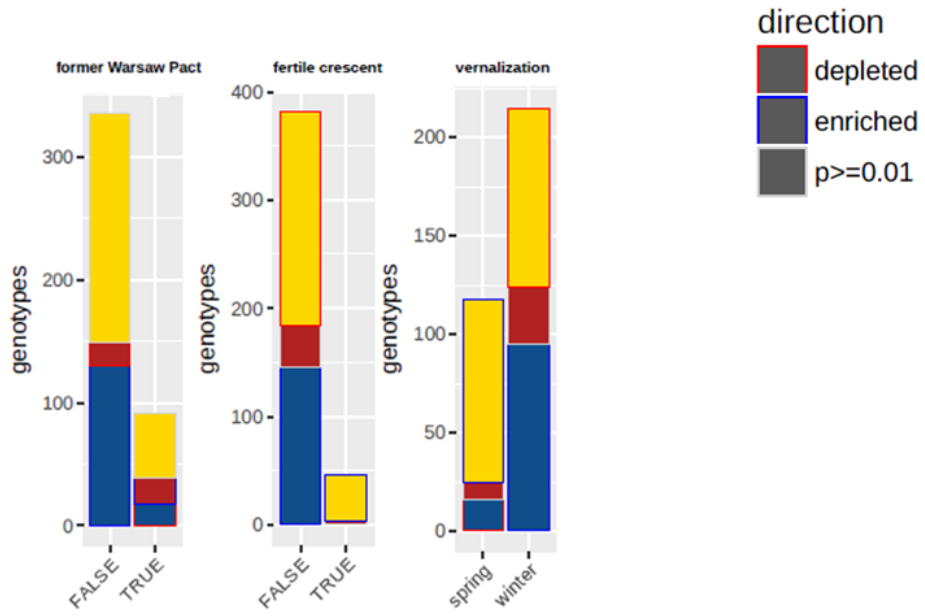
Figure S13: Network analysis of bread wheat community structure. **A-** Clustered phylogenetic consensus genotype network of 1000 maximum likelihood tree topologies inferred from repeated random haplotype samples (RRHS). Nodes represent individual genotypes and are color-coded by community cluster. Node size is proportional to the number of connections (*i.e.* node degree). Edges represent minimal evolutionary distances in the RRHS trees deduced by the minimal spanning tree (MST) algorithm and are color-coded by the respective subgenome (green: A; purple: B; orange: D). Edge transparency is proportional to the relative number of RRHS trees where the edge was an MST edge (*i.e.* edge weight). Diploid/tetraploid wheats are shown with grey circles and hexaploid genotypes in yellow, blue and red circles respectively corresponding to α , β and γ community clusters described in panel B. **B-** Stacked bar charts depicting the composition of the identified three wheat communities (α , β and γ) with respect to the type of sampled genotypes, historical groups (I to IV), affiliation to Warsaw pact countries, origin in the wheat domestication centers of the fertile crescent and growth habit pattern. Bars are color-coded by community cluster. Colors of the bar outlines are dependent of the outcome of the respective χ^2 tests depicting either significant enrichment (blue, more than expected), depletion (red, less than expected) or non-significance (grey) at 99% confidence intervals. **C-** World maps illustrating the country of origins of the communities α (top), β (center) and γ (bottom) with the color shading illuminating the number of genotypes (see legend at the right).

A



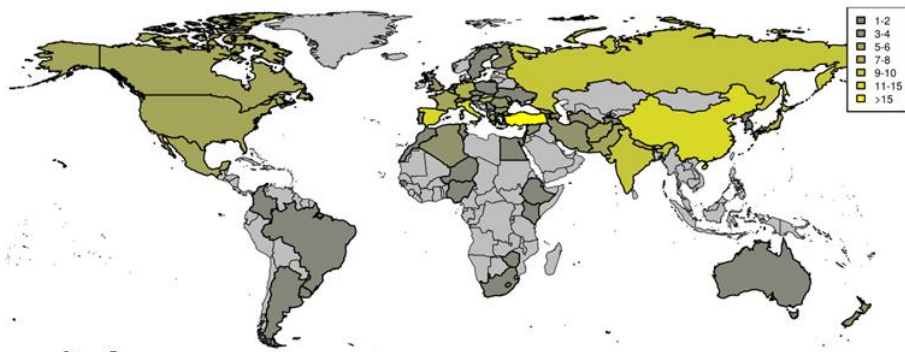
B





C

Community α



Community β



Community γ

